Aus dem

Helmholtz-Zentrum München

Comprehensive Pneumology Center (CPC)



Mechanisms of macrophage-driven fibrosis and its resolution

Dissertation

zum Erwerb des Doctor of Philosophy (Ph.D.) an der Medizinischen Fakultät der

Ludwig-Maximilians-Universität München

vorgelegt von Yue Lin

aus

Jiangxi / China

Jahr

2024

Mit Genehmigung der Medizinischen Fakultät der Ludwig-Maximilians-Universität München

Erstes Gutachten: Prof. Dr. med. Jürgen Behr

Zweites Gutachten: Dr. Yuval Rinkevich

Drittes Gutachten: Prof. Dr. Iris Helfrich

Viertes Gutachten: Prof. Dr. Susanne Lutz

Dekan: Prof. Dr. med. Thomas Gudermann

Tag der mündlichen Prüfung: 17.10.2024

Table of content

Table	e of content	3
Abstr	ract	5
List o	of figures	6
List o	of tables	7
List o	of abbreviations	8
1.	Introduction	10
1.1	Physiology and Structure of the Lung	10
1.2	Pulmonary diseases and causative factors	11
1.2.1	Environmental factors causing lung disease	11
1.2.2	Pathogenic infection causing lung disease	13
1.3	Pulmonary fibrosis	14
1.3.1	Idiopathic Pulmonary Fibrosis (IPF)	15
1.3.2	Fibrotic process in the Animal model	
1.3.3	Fibrotic phenotype in ex vivo model	18
1.4	Lung Macrophages	
1.4.1	Origins and distribution of lung macrophages	
1.4.2	Diverse functions of lung macrophage polarization	
1.5	Lung extracellular matrix	
1.5.1	Lung extracellular matrix in pulmonary fibrosis	
1.5.2	Perlecan of the lung extracellular matrix	
1.6	Hypothesis and aims	27
2.	Material and Methods	28
2.1	Materials	
2.1.1	Antibodies	
2.1.2	Primers	
2.1.3	Cell types	
2.1.42.1.5	Cell culture medium and Kits	
2.1.6	Consumables	
2.2	Cell culture methodology	
2.2.1	Mouse primary Monocyte isolation	
2.2.2	Macrophages differentiation and polarization	
2.3	scRNA-seq data analysis	
2.4	Precision-cut lung slices and in vitro culture	
2.4.1	Precision-cut lung slices assay	
2.4.2	PCLS Coculture with immune cells	
2.4.3	PCLS Coculture with Chemicals	37
2.5	Animal experiments	38
2.5.1	Approval of animal experiments	38
2.5.2	Lung bleomycin animal Model	38

Table of content

2.6	RNA analysis			
2.6.1	RNA extraction and cDNA synthesis			
2.6.2	Quantitative real-time PCR			
2.7	Histology			
2.7.1 2.7.2	Immunofluorescence			
2.7.2	Masson-trichrome stain Image Analysis			
2.7.3				
2.0 2.8.1	Protein analysis Mass spectrometry data analysis			
2.8.2	ELISA assay			
2.9	Statistical analysis			
3.	Results			
3.1	Fibrotic macromolecules accrule inward from the pleural ECM			
3.1.1	Inward egress of fibrotic macromolecules in animal models of fibrosis			
3.1.2	Inward egress of fibrotic proteins in ex vivo models	44		
3.2	Monocyte-derived macrophages adopt distinct responses signature in severe bleomycin model	46		
3.2.1	Different clusters of lung macrophages	46		
3.2.2	Aggregation of macrophage subpopulations during different stages	47		
3.3	IPF triggers fibrosis-related profiles in macrophages	49		
3.3.1	LPS/IFNγ induces macrophages to promote the diffusion of labeled fibrotic macromolecules	49		
3.3.2	Profibrotic macrophage disrupts ECM structure through Perlecan and MMP7	50		
3.4	IPF triggers self-repair regulators in macrophages	52		
3.4.1	Resolution macrophages regulate affinity for ECM and phagocytosis through secretion of Progranulin	52		
3.4.2	Prograunlin is a repair factor in the early fibrosis process	54		
3.5	Resolution macrophages in human IPF and ILD	55		
3.5.1	Human Macrophages clusters in scRNA-seq	55		
3.5.2	Distribution of human lung fibrosis and proteomic differential phenotypes	55		
3.5.3	Distribution of Profibrotic macrophages and resolution macrophages in human l samples			
4.	Discussion	58		
5.	Conclusiones and Outlook	61		
Refere	ences	62		
Ackno	Acknowledgements72			
Affidavit75				
Confir	Confirmation of congruency76			
List of publications77				

Abstract

Pulmonary fibrosis is a lung disease featured by cumulative tissue degeneration and scarring, often occurring with an elusive underlying cause. Here, we identified the functions of two macrophage subpopulations associated with pulmonary fibrosis; i.e. a profibrotic macrophage subset and a resolving macrophage subset, each of which exercise distinct functions. Using a mouse precision-cut lung slice (PCLS) explant model of fibrosis, single-cell transcriptomics, proteomics, and a mouse model of lung fibrosis, we demonstrate that pleural surfaces undergo dismantlement and diffuse inwards to form fibrosis in response to bleomycin stimulation. We determine that profibrotic and resolution macrophages are involved in regulating the different facets of this fibrotic change. We discover that profibrotic macrophages secrete matrix metallopeptidase to promote surface dismantlement leading to fibrotic accrual within lungs. We determined that resolution macrophages secrete the anti-inflammatory factor progranulin to activate lung selfrepair function and enhance phagocytosis and clearance of the transferred fibrotic components. The elucidation of the mechanisms underlying the function of profibrotic and repair macrophages in lung fibrosis offers a novel framework for comprehending and therapeutically addressing pulmonary fibrotic conditions.

List of figures

Figure 1.1 SEM image of the parenchyma of the human lung	10
Figure 1.2 Clinical treatment of pneumoconiosis.	11
Figure 1.3 Pathogenic mechanisms resulting from cigarette smoke exposure	in alveolar
macrophages	12
Figure 1.4 Genome-wide significant variants linked with COVID-19.	14
Figure 1.5 A proposed pathogenetic model of idiopathic pulmonary fibrosis	16
Figure 1.6 Representative tissue sections	18
Figure1.7 Immunofluorescence (IF) staining of FN1	19
Figure 1.8 Functions of different macrophages during tissue development	20
Figure 1.9 Schematic map illustrating macrophage clusters	23
Figure 1.10 Schematic of the perlecan	26
Figure 3.1 Pleural layer ECM is accompanied by inward movement of fibrosis	44
Figure 3.2 In vitro pulmonary fibrotic 3D model	45
Figure 3.3 fibrotic markers signature in PCLS model.	45
Figure 3.4 two macrophages subcluster in mouse IPF scRNA-seq	47
Figure 3.5 Profibrotic and resolution macrophage stages in the fibrosis process	48
Figure 3.6 LPS/IFNγ-induced and IL4/M-CSF activated macrophages play different ro	le in fibrotic
matrix movement	50
Figure 3.7 Effect of Profibrotic macrophage on lung perlecan	51
Figure 3.8 The role of resolution macrophages in pulmonary fibrosis	53
Figure 3.9 Progranulin regulates early pulmonary fibrosis levels	54
Figure 3.10 Macrophage population in human IPF	55
Figure 3.11 Distribution of human pleural layer ECM in IPF lesions	56
Figure 3.11 marker signals in human IPF	57
Figure 5.1 Revised model of pulmonary fibrosis	61

List of tables

List of tables

Table 1 Primary antibodies applied in histology staining	28
Table 2 Secondary antibodies applied in histology staining	29
Table 3 Primers used for qPCR experiments	29
Table 4 Cell types	30
Table 5 Medium and Chemicals.	31
Table 6 Chemical lists	31
Table 7 Consumables	33
Table 8 Chemicals for the targets	

List of abbreviations

ACTA2/ a-SMA α-smooth muscle actin

AEC2 Type 2 alveolar epithelial cells

COL1A1 Collagen 1

CTGF Connective tissue growth factor

COPD Chronic obstructive pulmonary disease

CPF Cystic pulmonary fibrosis

DHFR Dihydrofolate reductase

EMT Epithelial-mesenchymal transition

ECM Extracellular matrix

FN1 Fibronectin 1

FGF Fibroblast growth factor

FGF Fibroblast growth factor

GM-CSF Granulocyte-macrophage colony-stimulating factor

GRN Progranulin

HSCs Hematopoietic stem cells

HSPG2 Perlecan

IL4 Interleukin-4

IFNy Interferon-y

I.T. Intratracheal instillation

ILD Interstitial lung disease

IPF Idiopathic pulmonary fibrosis

LPS Lipopolysaccharide

LDH Lactate dehydrogenase

M0 Inactivated tissue-resident macrophages

M1 Classically activated macrophages

M2 Alternatively activated macrophages

MMP7 Matrix metallopeptidase 7

MMP12 Matrix metalloproteinase12

M-CSF Macrophage colony-stimulating factor

List of abbreviations

O.A. Oropharyngeal administration

pMacs Pre-macrophages

PCLS Precision cut lung slices

PDGFR Platelet derived growth factor receptors

ROI Reactive oxygen intermediates

ROS Reactive oxygen species

TIMP1 Tissue inhibitor of metalloproteinases

TGF-β1 Transforming growth factor β1

TNF- α , Tumor necrosis factor- α

UIP Usual interstitial pneumonia

VEGFR Vascular endothelial growth factor receptors

EMPs Yolk sac erythro-myeloid progenitors

1. Introduction

1.1 Physiology and Structure of the Lung

Lungs are vital respiratory organs of the human body and are located in the chest cavity with five lobes, three on the right and two on the left. In the center of the lungs are the heart, large blood vessels, organs and esophagus. The diaphragm at the base of the lungs separates the chest and abdominal cavities, which facilitates breathing movement. The lungs consist of bronchi, bronchioles, alveolar ducts and a large number of alveoli. After being inhaled from the nose and mouth, air traverses the pharynx, trachea and progressively into more refined bronchi, bronchioles and reaches the alveoli space, then it is exchanged for carbon dioxide and oxygen gases in the alveoli. The thickness of the respiratory membrane is less than 1 micrometer, and the higher permeability contributes to rapid gas exchange (Fig.1.1)(Weibel, 2017).

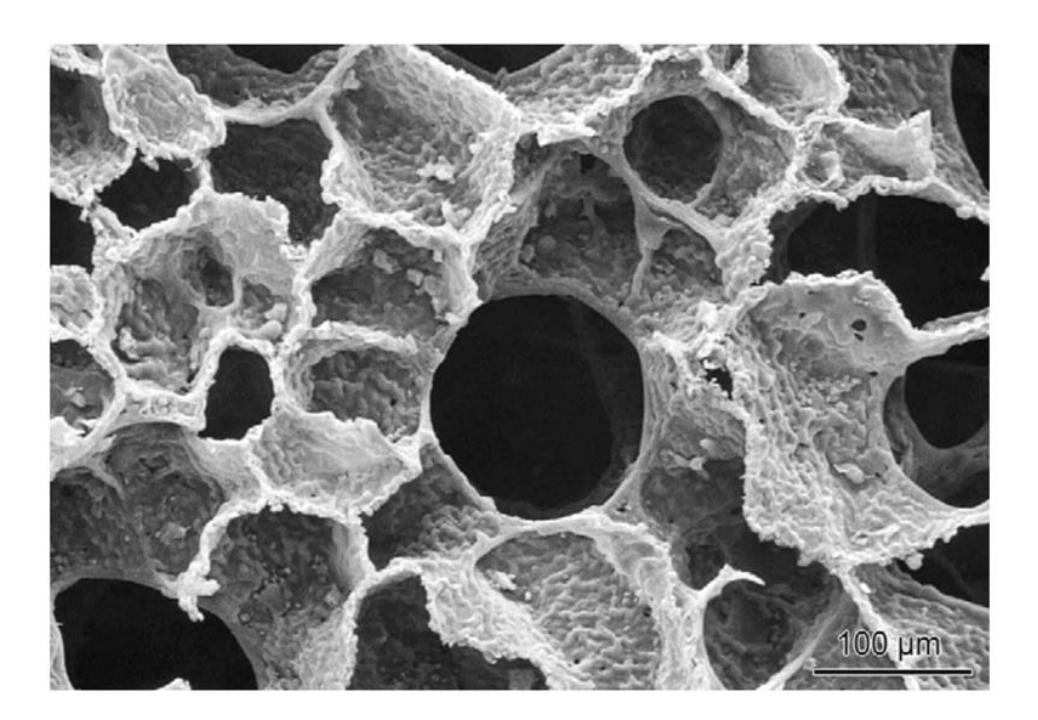


Figure 1.1 SEM image of the parenchyma of the human lung

SEM image shows an alveolar duct surrounded by narrow septa separating the alveoli (Murray, 2010; Weibel, 2009).

1.2 Pulmonary diseases and causative factors

Due to innovations in modern medical technology, our understanding of human pulmonary diseases has accumulated more theoretical knowledge and diagnostic techniques. Based on extensive disease statistics, pulmonary diseases are health concerns with a relatively high incidence, characterized by weak treatment and self-repair capabilities. Various causative factors can lead to different degrees of lung damage.

1.2.1 Environmental factors causing lung disease

Pulmonary injuries associated with environmental pollution often result from airborne particulates or chemicals, causing chronic conditions such as asthma and bronchitis. Specific chemicals, such as silica dust, asbestos and coal dust, can also lead to severe pneumoconiosis (Hanson & Kasik, 1977). The diagnosis of common pneumoconiosis can be made by looking at the lung structures on histologic slides to see if there is a predominantly rounded or irregular cloudy mass distributed in various dimensions of lung lobes, where immune cells are activated and recruited, and also in the context of the patient's occupational characteristics to determine environmentally-specific impacts, which, in severe cases, may lead to lung fibrosis and require lung transplantation surgery (Fig.1.2).

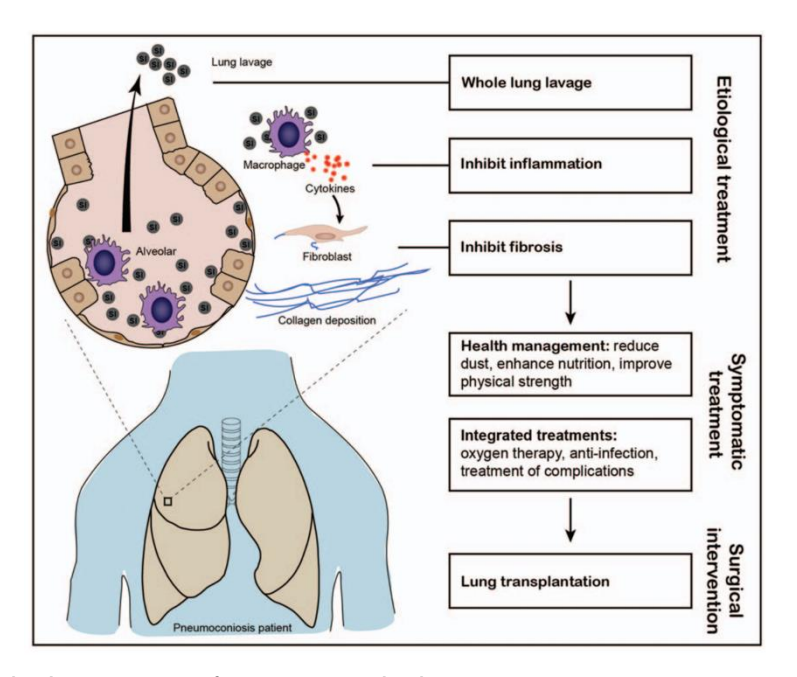


Figure 1.2 Clinical treatment of pneumoconiosis.

SI: Silica (Qi et al., 2021).

Factors related to self, such as smoking, genetic mutations, aging, and immune system dysregulation, increase the risk of disease. Cigarette smoking, in particular, stands out as a prominent causative factor in a substantial proportion of lung cancer cases (Adams et al., 2023; Malhotra et al., 2016), chronic obstructive pulmonary disease (COPD) (Christenson et al., 2022; Hou et al., 2019), and other respiratory disorders. Smoking can greatly influence the activation of macrophages, such as regulating the secretion of reactive oxygen species (ROS), hindering the phagocytosis function of macrophages, increasing the release of ferritin, etc., and pulmonary immune cell homeostasis (Fig.1.3). Being broken creates antecedent conditions for the occurrence of disease (Lugg et al., 2022).

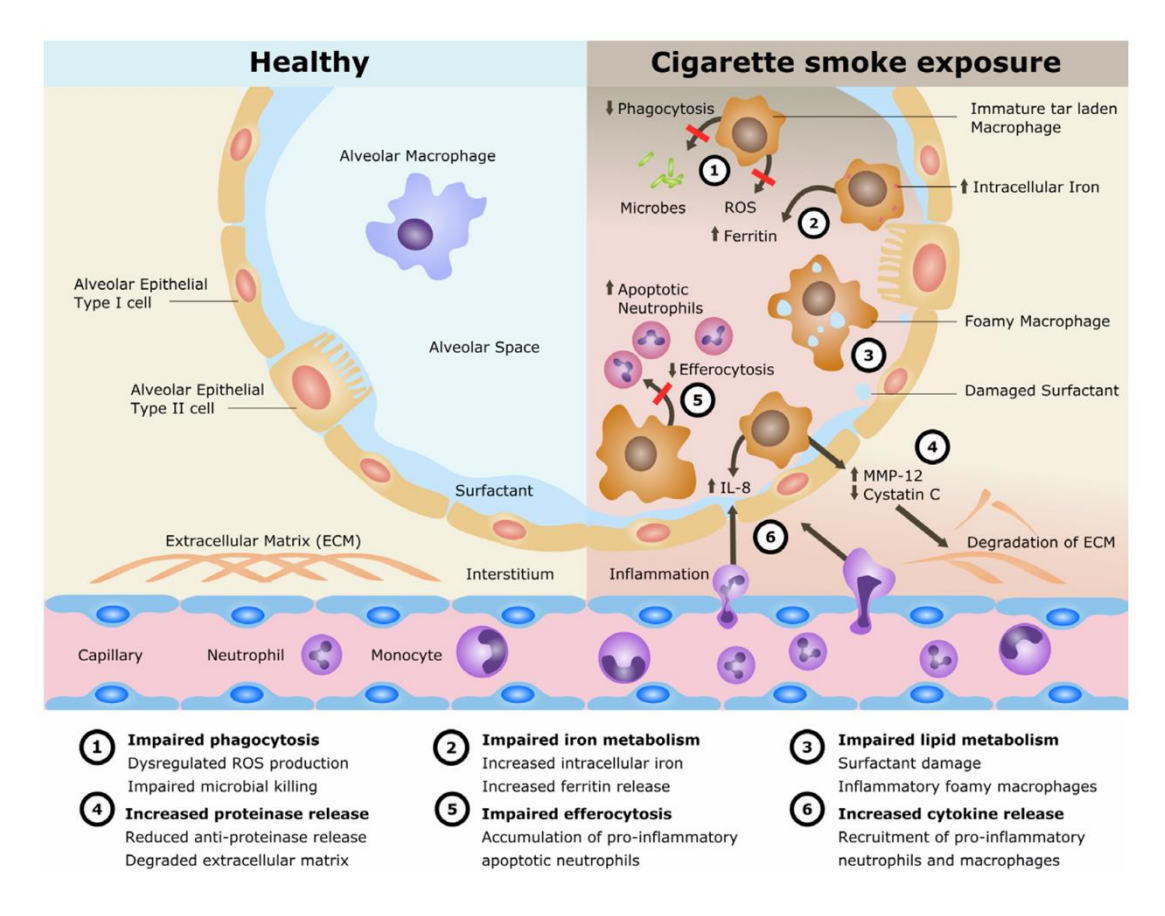


Figure 1.3 Pathogenic mechanisms resulting from cigarette smoke exposure in alveolar macrophages.

Six major functional pathways (Lugg et al., 2022).

1.2.2 Pathogenic infection causing lung disease

In some cases, lung diseases are due to external infections, such as bacteria (Curran et al., 2018), viruses (Sefik et al., 2022), and fungi (Curran et al., 2018). All three can cause varying degrees of lung infection. Bacterial infections can lead to pneumonia, bronchitis and other respiratory infections. Antibiotics can be used, but attention needs to be paid to bacterial resistance. Pulmonary fungal infections are usually caused by inhalation or exposure to fungal spores and may be treated with antifungal medications (such as fluconazole, itraconazole, etc.). Viral infections often cause respiratory symptoms such as sore throat, cough, flu-like symptoms, pneumonia, etc. Viral infections can also cause systemic symptoms such as fever, fatigue and headache. Some viral infections can be prevented by vaccines, but not all viruses have effective vaccines. The novel coronavirus, which began spreading globally at the end of 2019 and continues to mutate, has resulted in recurrent cross-infections affecting human lungs. Despite the use of inactivated vaccines and mRNA vaccines, the virus cannot be completely eradicated, and its impact on human health will persist. It is evident that the causative factors of pulmonary diseases are multifaceted, and preventive measures and early health checks can help reduce the incidence and severity of these diseases.

A study analyzing the effect of genetic factors on the development and spread of COVID-19 disease in 219,692 cases identified 79 different genome-wide significant loci involved in the responding pathways activated by virus. The severity loci were matched to the type I interferon pathway (Fig.1.4), while the susceptibility loci were differentially matched to the viral entry and airway defense pathways, except for two severity loci, TMPRSS2 and MUC5B (Initiative, 2023). Most patients with acute SARS-CoV-2 infections recover, but about 10-20% of them turn into chronic infections that can even be fatal. High levels of IL-1β and IL-18 correlate with the severity of COVID-19 infection in patients, and it was found that SARS-CoV-2 infection of human lung macrophages activates inflammatory vesicles and initiates an inflammatory cascade that leads to cellular pyroptosis and facilitates downstream type I IFN responses. This demonstrates that chronic inflammation in the lungs associated with the type I interferon pathway will further impair lung tissue function (Sefik et al., 2022).

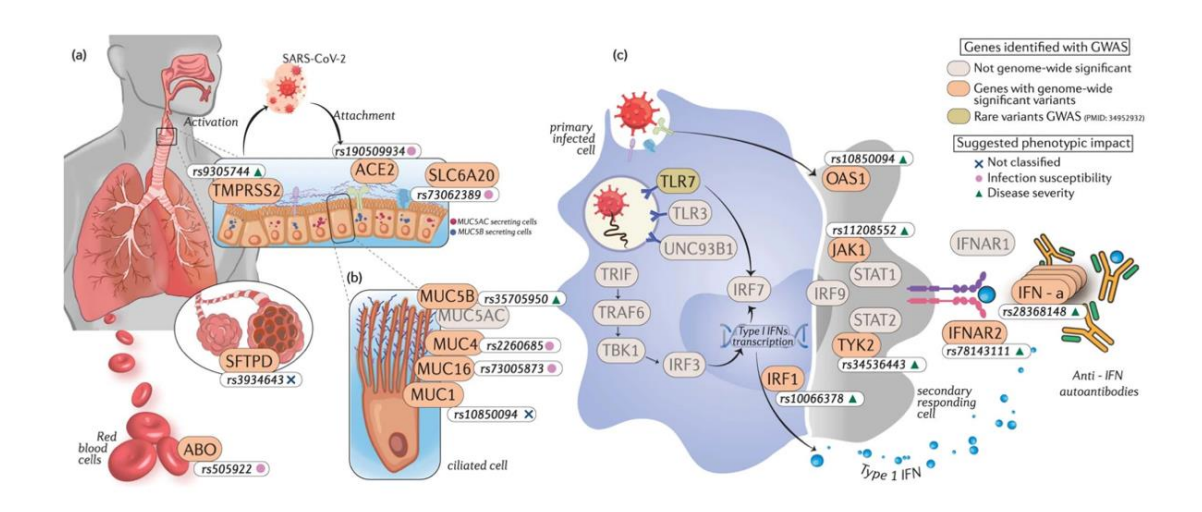


Figure 1.4 Genome-wide significant variants linked with COVID-19.

Annotated genes (illustrated in peach boxes) are enriched in different pathways (a) viral entry and innate immunity. (b) defense against entry in airway mucus. (c) type I interferon response (Initiative, 2023).

1.3 Pulmonary fibrosis

Pulmonary fibrosis is a lung interstitial fibrotic injury disease. It is mainly characterized by massive proliferation of fibroblasts, accumulation of extracellular matrix, recruitment of immune cells and destruction of tissue structure (Martinez et al., 2017). It develops from local to diffuse interstitial pulmonary fibrosis, and ultimately restricts lung function, causing most patients to die from respiratory failure and related complications. However, pulmonary fibrosis is often not a separate disease. It is formed by the end-stage changes of a lung disease. The late stages of many lung damage diseases are often accompanied by symptoms such as pulmonary fibrosis and breathing disorders (King et al., 2011). In general, alveolar inflammation, diffuse lung parenchyma and interstitial fibrosis are the main pathological features of interstitial lung disease (ILD), which is divided into two types, secondary interstitial lung disease and idiopathic interstitial pulmonary disease(Kalchiem-Dekel et al., 2018). The causes of the first type of diseases are relatively clear and are mainly related to environmental factors, such as pneumoconiosis, silicosis, asbestosis, radiation-induced pulmonary fibrosis, and drug induced pulmonary interstitium. The cause of the second type of disease is unclear, which is mainly idiopathic pulmonary fibrosis (IPF), also includes cystic pulmonary fibrosis (CPF) and autoimmune interstitial pneumonia with pneumonia autoimmune features (Abuserewa et al., 2021). Because of its complex pathogenesis, there is still a lack of early diagnostic indicators and effective treatments. Therefore, paying attention to the causative factors and the regulation of lung fibrosis by the immune system will help to further explore potential treatment strategies and targets for this disease.

1.3.1 Idiopathic Pulmonary Fibrosis (IPF)

IPF is characterized by ongoing fibrosis and scarring of lung tissue, leading to dyspnea and reduced lung function (Richeldi et al., 2017). The challenge with IPF lies in the uncertainty of the etiology and the lack of initial diagnostic indicators, as well as in the fact that some studies suggest that inflammatory and fibrotic processes are heavily involved in lung injury, and that aging, genetics, and chronic injuries also influence the severity of the disease. The existing diagnosis of the disease is usually based on high-resolution CT to determine whether it is generalized usual interstitial pneumonia (UIP) and of unknown etiology (Mei et al., 2021; Thiessen et al., 2019). The lesions mainly manifest as "honeycombing" of subpleural cystic cavities or patchy fibrosis of the lung parenchyma, traction bronchiectasis, and thickening of the surrounding alveolar septa. The lesions of IPF spread inward from the pleural layer at the bottom and outer edges of the lungs, gradually losing lung tissue and limiting gas exchange. Patients who are diagnosed typically show signs of dyspnea, dry cough, fatigue, and decreased strength, but the average life expectancy after diagnosis is only 3 years (Martinez et al., 2017).

The histological features of IPF are over-deposition of extracellular matrix proteins, the presence of fibroblastic foci, and areas of fibrosis immediately adjacent to areas of normal lung parenchyma (Natsuizaka et al., 2014; Richeldi et al., 2014). Alveolar epithelial cells undergo aging and damage, and studies have found that in areas where fibrosis occurs, AEC2 cells are undergoing apoptosis (Mulugeta et al., 2015) (Fig.1.5). Abnormal activation of epithelial cells can secrete pro-inflammatory and pro-fibrotic factors, including fibroblast growth factor (FGF), chemokines, connective tissue growth factor (CTGF), etc. These mediators have the capacity to stimulate the migration, proliferation, and activation of fibroblasts and myofibroblasts. These cells can continue to secrete extracellular matrix components and aggregate abnormally to form scar tissue, thereby destroying the lung tissue structure (Martinez et al., 2017).

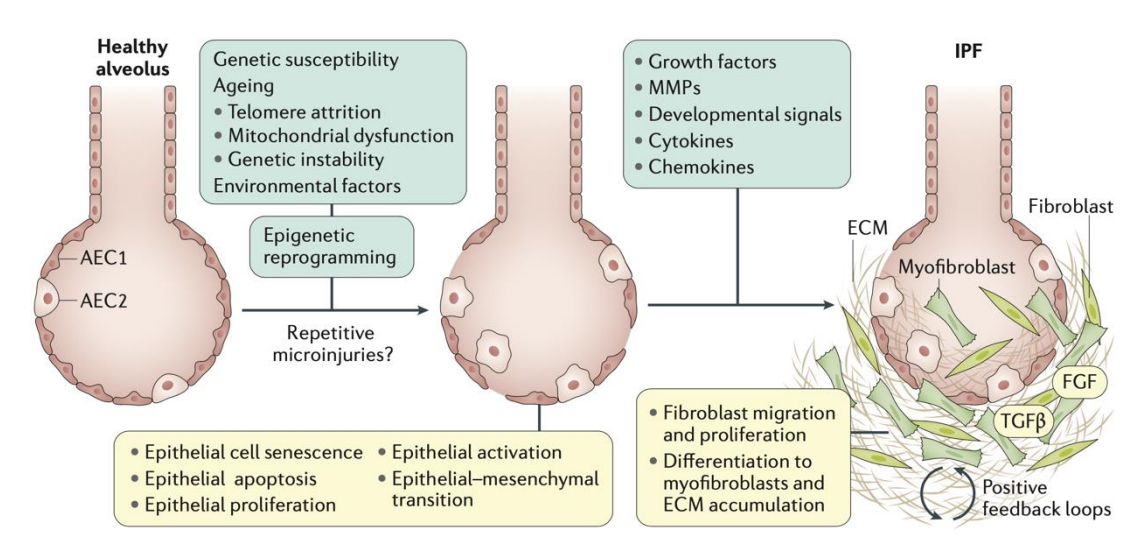


Figure 1.5 A proposed pathogenetic model of idiopathic pulmonary fibrosis (Martinez et al., 2017).

Due to the lack of medications to treat irreversible lung damage, the current treatment approach for this disease is to slow down the fibrosis and improve the patient's quality of life, such as by using a ventilator for oxygenation, etc (Eaton et al., 2004). Currently, there are only two antifibrotic drugs on the market, Nintedanib and Pirfenidone, which do not share the same therapeutic principle. Nintedanib is a multi-targeted tyrosine kinase inhibitor, which works by inhibiting a variety of receptor tyrosine kinases (Martinez et al., 2017; Wollin et al., 2015). Pirfenidone is thought to have antioxidant and anti-inflammatory effects, and it slows the process of pulmonary fibrosis by inhibiting collagen synthesis and reducing oxidative stress (Lancaster et al., 2017; Solomon et al., 2023). The choice between the two drugs often depends on the patient's specific situation and drug tolerance, there are also studies trying to combine the two drugs for treatment (Flaherty et al., 2018; Vancheri et al., 2018). Significant research effort is also devoted to finding more improved drugs, such as Pentraxin 2. Some studies have shown that intravenous injection of human recombinant Pentraxin 2 into IPF patients slowed down the decline of lung function compared with the control groups (Murray et al., 2011; Raghu et al., 2018). Pentraxin 2 is a serum amyloid protein whose function is to inhibit pulmonary fibrosis and inflammatory responses by inhibiting the differentiation of macrophages and fibrocytes. It can also inhibit the TGF-β1 that promotes the formation of connective tissue (Abuserewa et al., 2021). Another potential drug is Pamrevlumab (FG-3019), it shows the decline in FVC, comparing with Pirfenidone and Nintedanib treatments (Di Martino et al., 2021). As a large number of studies delve into the etiology and formation process of IPF, more potential target drugs will be tested to provide more targeted options for future clinical treatments.

1.3.2 Fibrotic process in the Animal model

According to existing reports of drug-induced interstitial lung diseases, animal models of pulmonary fibrosis induced by drugs such as Methotrexate, Amiodarone, and Bleomycin have provided a research basis and direction for a large number of studies. The three drugs function through different pathogenic mechanisms. Amiodarone is a widely used antiarrhythmic drug, but it has high pulmonary toxicity and can induce intracellular phospholipid accumulation in AEC2 and alveolar macrophages, which in turn affects late endosomes and lysosomes (Dharmarajan et al., 2017; Li et al., 2022). Methotrexate is a folate antagonist that is widely used in autoimmune diseases such as leukemia and solid tumors, such as rheumatoid arthritis. Methotrexate achieves cytotoxicity by inhibiting dihydrofolate reductase (DHFR), thereby disrupting the folate cycle and affecting DNA synthesis. It has pulmonary toxicity by promoting the epithelial-mesenchymal transition (EMT) process of AEC2, leading to acute interstitial pneumonia and even pulmonary fibrosis (Abdalhameid et al., 2023; Fragoulis et al., 2019). Bleomycin is a water-soluble glycopeptide antibiotic that inhibits DNA metabolism and is used as an antineoplastic agent. However, it can diffuse into cells through the glycosaminoglycan chains in proteoglycans and induce DNA damage to cause lung tissue damage. In particular, the bleomycin-ANXA2-YWHA-TFEB complex can induce autophagy dysfunction in AECs (Della Latta et al., 2015; Liu et al., 2017).

The bleomycin-induced pulmonary fibrosis mouse model has been most widely used to study the pathogenesis of IPF. According to the results of a large number of studies, it has been found that a single administration of bleomycin to the mouse airway can be achieved by two commonly used methods, intratracheal instillation (I.T.) and oropharyngeal administration (O.A.) (Jenkins et al., 2017). Early day0 to day3 shows lung tissue damage and edema, mainly damage to alveolar epithelium and capillary endothelial cells. From the 3rd to the 7th day, the inflammatory reaction and type II alveolar epithelial hyperplasia recruit inflammatory cells to infiltrate the alveoli, first dominated by neutrophils, and then macrophages proliferate in large numbers. Between days 7 and 14, inflammatory cells are recruited and activated, and chemokines and growth factors are expressed in large quantities (Francois et al., 2015; Nagao et al., 2014), they are involved in the regulation of mesenchymal cells, inflammatory cells and epithelial cells. From the 14th to the 21st day, the inflammation level decreased, but the lesions showed a large number of proliferation of collagen fibers, elastic fibers and smooth muscle bundles, and

the lesions expanded in sheets. After day 28, fibrosis levels gradually decreased (Fig.1.6). On day 56, it was observed that the lung organs were almost completely repaired, and a large amount of collagen deposition was removed (Duitman JanWillem, 2018; Schiller et al., 2015).

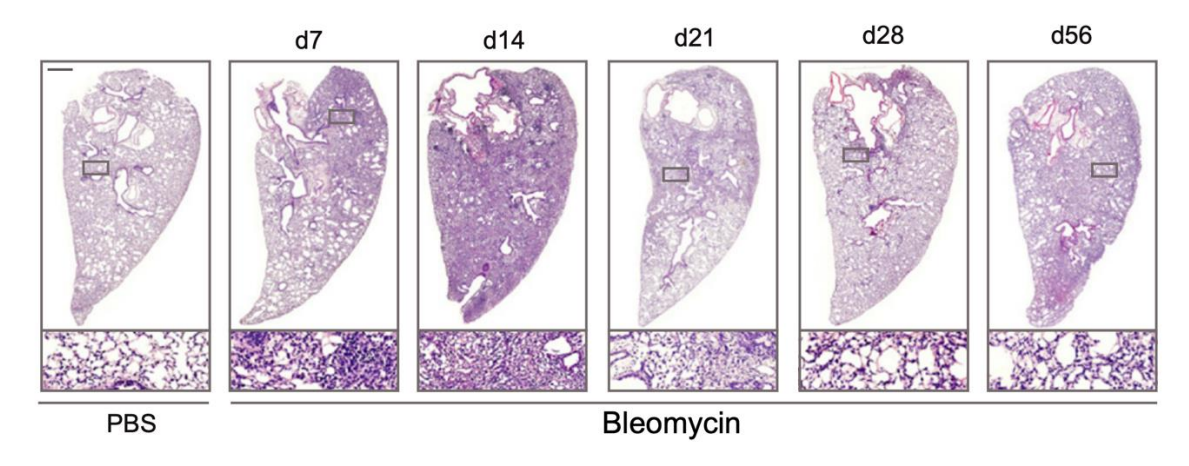


Figure 1.6 Representative tissue sections

The images indicated experimental conditions and time points were analyzed using hematoxylin and eosin stain (H&E) (Schiller et al., 2015).

1.3.3 Fibrotic phenotype in ex vivo model

Based on the observation of animal pulmonary fibrosis models and human lung tissue lesions, a large number of cells and relevant cytokines related to the formation of lesions were shown to be main regulators of pulmonary fibrosis (Agostini & Gurrieri, 2006). Targeted testing of a variety of specific drugs has been shown to slow the progression of this disease, but there is still a lack of specific target drugs that can prevent or reverse the development of IPF. Lung tissue *ex vivo* models are widely used for chemical screening, among that PCLS are a model suitable for both mouse and human lung samples, can be stably cultured *in vitro*, and can develop pulmonary fibrosis through drug stimulation (Henjakovic et al., 2008; Lauenstein et al., 2014). Studies have demonstrated that precision-cut lung slices (PCLS) retain functionality even when exposed to a mixture of profibrotic elements (TGF-β, TNF-α, PDGF-AB, and LPA). Furthermore, genes and proteins associated with fibrosis (including FN1, CTGF, MMP7, ACTA2, SERPINE1 and COL1A1) are swiftly upregulated in response. (Fig.1.7), forming a phenotype of excessive extracellular matrix deposition (Alsafadi et al., 2017).

Bleomycin treatment of PCLS has also been shown to form a fibrosis phenotype in vitro. PCLS under this treatment highly expressed fibrotic genes such as ACTA2, COL1A1, FN1, MMP12 and TIMP1 (Cedilak et al., 2019; Zhou et al., 2021). Based on the PCLS

in vitro model, some studies have observed that Distal tissue repair pathways can be activated within diseased tissues. (Uhl et al., 2015). Precision cut lung slices (PCLS) could spatially retain the original state of the lung microenvironment, which is conducive to simulating and observing the dynamic changes in the occurrence and progression of lesions. In a short period of time, PCLS can be used for testing the effects of multiple drugs on pulmonary fibrosis, which will provide more potential specific targeted drugs for early diagnosis and treatment.

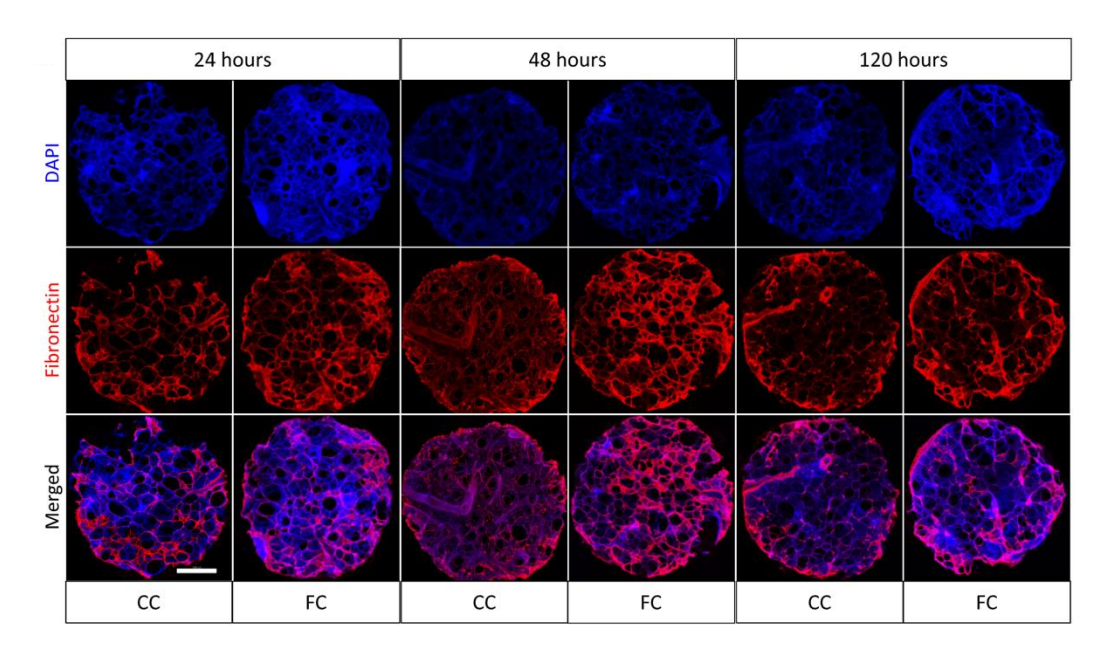


Figure 1.7 Immunofluorescence (IF) staining of FN1.

Scale bar=1mm (Alsafadi et al., 2017).

1.4 Lung Macrophages

1.4.1 Origins and distribution of lung macrophages

Macrophages are omnipresent cells found in all tissues and are renowned for their remarkable plasticity within the hematopoietic system. They play pivotal roles in organogenesis, tissue homeostasis, repair, and immune surveillance. Conventionally, tissue-resident macrophages originate from HSCs through circulating monocyte precursors. Their principal role involves safeguarding organs against infections. But in recent years, with the development of novel fate-mapping mouse models that can longitudinally track macrophages from their progenitor state to their mature cellular state within the organs they inhabit, the derivation of new research methods has revealed a new chapter in macrophage biology (Jenkins & Allen, 2021). Studies have shown that resident macrophage populations exist in certain tissues during the embryonic stage before HSC development

(Fig.1.8a). Beginning on day 8.5 of mouse embryonic development, Yolk sac erythromyeloid progenitors (EMPs) regulate the embryonic development by generating premacrophages (pMacs) in the early stages, which are dispersed throughout different embryonic tissues starting from E9.0. These pMacs subsequently undergo differentiation into tissue -specific macrophages (Dick et al., 2022; Gomez Perdiguero et al., 2015; Mass et al., 2016; Mass et al., 2023). They have different life cycles (Fig.1.8b), with shorter-lived cells requiring constant supply from bone marrow HSCs (Perdiguero & Geissmann, 2016; Yona et al., 2013), such as intestinal macrophages, which are rapidly replaced after birth (Bain et al., 2014). HSC-derived cells are difficult to replace long-lived tissue macrophages (Kupffer cells, microglia, Langerhans cells) in steady state (Ginhoux et al., 2010; Hoeffel et al., 2012; Lahmar et al., 2016; Schulz et al., 2012). There are also cases that are gradually replaced throughout life, such as alveolar giant cells (Gomez Perdiguero et al., 2015) and cardiac macrophages (Epelman, Lavine, Beaudin, et al., 2014; Epelman, Lavine, & Randolph, 2014; Molawi et al., 2014).

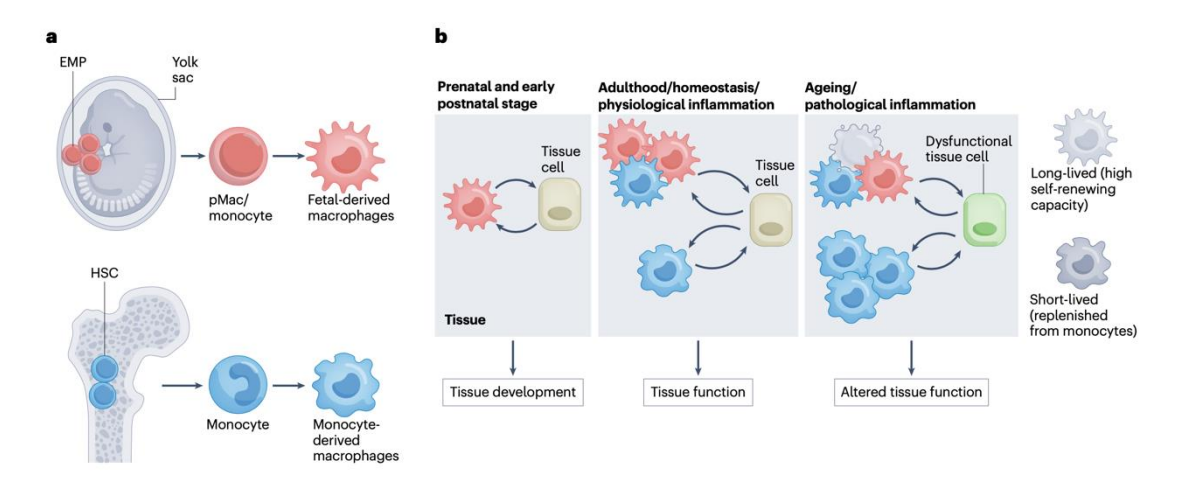


Figure 1.8 Functions of different macrophages during tissue development

a. Diverse developmental trajectories of tissue-resident macrophages. b. Macrophages derived from both erythromyeloid progenitors (EMPs) and hematopoietic stem cells (HSCs) participate in tissue function through intricate cell-cell communication with specialized tissue cells. (Mass et al., 2023).

The lung organ has its own unique tissue structure, which is mainly composed of bronchi, small bronchi, alveolar ducts and alveoli. In the steady-state lung organ, multiple distinct macrophage populations are identified based on their anatomical locations, including the alveolar macrophage population and two to three interstitial macrophage populations. (Aegerter et al., 2022). The alveoli serve as the main site for gas exchange, and alveolar

macrophages are tightly attached to epithelial cells and directly exposed to the air. These macrophages serve as guardians of the alveolar microenvironment, performing phagocytosis of cells and pathogenic debris, as well as clearing mucus material within the alveoli, thereby contributing to alveolar homeostasis maintenance. Macrophages originate during embryonic development, and their ongoing development and maintenance are contingent upon the presence of GM-CSF, which is generated by specific epithelial cells (Guilliams et al., 2013), and have a high self-renewal capacity (Liu et al., 2019; Mass et al., 2016; Yona et al., 2013). The number of interstitial macrophages is smaller than that of alveolar macrophages, and their development is heavily dependent on steady-state CSF1R signaling. They commonly can produce IL-10 signals, but their ability to present antigens is different (Bain & MacDonald, 2022; Ural et al., 2020). They can mainly be subdivided into LYVE1highMHCIIlow and LYVE1lowMHCIIhigh subpopulations, or grouped based on TIM4, FOLR2, LYVE1, CCR2 and MHCII expression. LYVE1^{low}MHCII^{high} macrophages exhibit high expression levels of pro-inflammatory factors, predominantly localized around nerve bundles or nerve terminals. (Ural et al., 2020). LYVE1highMHCIIlow interstitial macrophages are located proximal to blood vessels and express signaling molecules such as Tgfb2, Plaur and Fcna to participate in the immune regulatory process (Chakarov et al., 2019). Pulmonary macrophages perform their own guard functions in different locations, and support homeostasis of the lung environment by responding to changes and challenges in external stimuli.

1.4.2 Diverse functions of lung macrophage polarization

Macrophages in lung tissue can defend against foreign invasion and remove apoptotic cells, tumor cells, etc. through phagocytosis to maintain internal balance (Gordon, 2003; Varin & Gordon, 2009). They are highly plastic immune cells, and diverse environmental signals can stimulate them to activate specific functions through phenotypic polarization (O'Shea & Paul, 2010). Pulmonary macrophages are classified into two main cell types: classically activated macrophages and alternatively activated macrophages. Activated macrophages can regulate immune responses through various signals such as cytokines and chemokines, which supports communication with additional functional cells such as T cells and fibroblasts (Arora et al., 2018; Stout & Suttles, 2005). Multifunctional lung macrophages can directly or indirectly participate in regulating more tissue microenvironment immune responses and tissue reconstruction processes (Biswas & Mantovani, 2010).

Macrophage polarization is a rapid and reversible process that allows it to adjust to changes in the microenvironment. Different stimuli can polarize tissue-resident macrophages (M0), and LPS/IFNy induces classically activated M1 macrophages (Tarique et

al., 2015). The LPS on the outer membrane of Gram-negative bacteria facilitates their recognition by cell surface receptor complexes, mediated by LPS-binding proteins (Guha & Mackman, 2001). Interferon-gamma (IFN-y) is produced by a diverse array of immune cells within the body, including T helper 1 cells, CD8+ lymphocytes, NK cells, B cells and APCs. Subsequently, IFN-y binds to its receptor, IFNGR, upon absorption. The specific binding of IFNGR initiates a cascade of signaling events, JAK (JAK/STAT pathway) is activated to facilitate the dimerization and translocation of STAT1. STAT1 activats M1related genes to transcribe, also increase the expression of proinflammatory factors (Senga et al., 2001). Therefore, M1 macrophages are characterized by enhancing proinflammatory factors to secret (Fig.1.9) and increasing reactive oxygen intermediates (ROI) and iNOS-dependent production of reactive nitrogen intermediates (RNI), which in turn enhance antigen presentation capacity (Murray et al., 2014). According to studies, pro-inflammatory macrophages can release cytokines to damage tissue structures (Saarialho-Kere et al., 1999; Yang et al., 2020). Previous investigations have demonstrated that under inflammatory conditions, lipopolysaccharides (LPS) can induce and activate macrophages to significantly upregulate the expression of matrix metalloproteinase 7 (MMP7). The role of MMP7 entails the degradation of various macromolecules within the extracellular matrix, including gelatins, fibronectin, and proteoglycan (Vandenbroucke et al., 2014; Yu & Woessner, 2000). In idiopathic pulmonary fibrosis (IPF), MMP7, as a validated biomarker of disease severity, can promote fibrosis and inflammation (Bauer et al., 2017; Lev et al., 2014; Xiao et al., 2022). These evidences indicate during pulmonary fibrosis, macrophages may participate in the regulation of immunity and fibrosis by directly acting on lung ECM through MMP7.

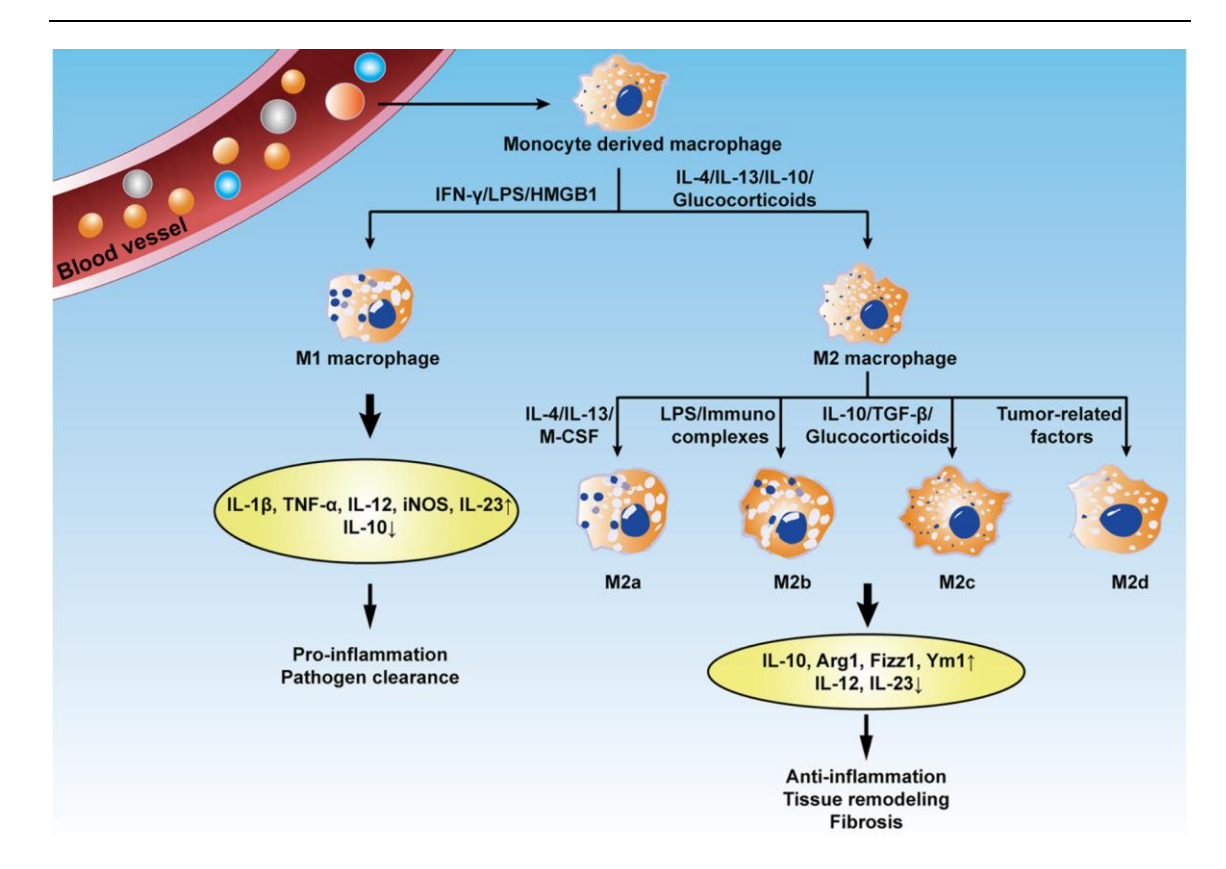


Figure 1.9 Schematic map illustrating macrophage clusters.

The M1 like exhibits proinflammatory characteristics. The M2a is activated by IL-4 and IL-13. The M2b and M2c are predominantly regulating the Anti-inflammation and Fibrosis process. (Zhang et al., 2018)

Alternatively activated macrophages have many stimulatory factors, for example IL-4 and M-CSF (Zhang et al., 2018). The function of M2 macrophages is mainly to regulate inflammation levels and Th2 immunity, support angiogenesis, tissue remodels, repairs damaged tissue, removes debris, and promote tumor development (Bosurgi et al., 2017). These macrophages can directly participate in regulating the remodeling of the extracellular matrix, such as by overexpressing Stabilin-1, which is a receptor that binds to the matrix protein SPARC to mediate clearance. Based on gene expression profiles, M2 like macrophages are defined into four subtypes: M2a, M2b, M2c, and M2d (Fig. 1.9). Stimulation with macrophage colony-stimulating factor (M-CSF), IL-13, and IL-4 prompts M2 to upregulate scavenger and mannose receptors, the interleukin-1 receptor antagonist, and express elevated levels of interleukin-10 (IL-10), CCL17, CCL18, and CCL22. These factors play pivotal roles in modulating anti-inflammatory responses, tissue remodeling, and fibrosis processes (Arora et al., 2018).

Nevertheless, there are no specific surface markers that differentiate subpopulation of M2, which are shown low expression of CD86, MHCII, and iNOS2 but high expression of Arg1, Ym1/2, Fizz1, and CD206 (Raes et al., 2002). CD206 is a marker of alveolar macrophages, participates in regulating the phagocytosis of M2, and can increase the engulfment of pathogens debris and apoptotic cells (Desch et al., 2016; Hong et al., 2014). IL4 can activate two downstream signaling pathways, JAK1/STAT6 and PI3K/AKT, to induce M2 activity. Studies have shown that M2 macrophages can generate profibrotic factors like TGF-β and PDGF after activation to promote continued activation of fibroblasts and rapid proliferation of myofibroblasts. However, there are also results showing that the anti-fibrotic drug nintedanib can increase IL-4 signaling in macrophages by inhibiting the CSF1 receptor, thereby promoting a tissue repair phenotype (Watson et al., 2023). Therefore, classification based on M2 limits the possibility of functional classification of macrophages. As highly plastic immune cells, macrophages can dynamically switch functional states according to changes in the microenvironment and stimuli. Studies have shown that Progranulin can inhibit M1 polarization and promote M2 polarization to repair lung injury models (Chen et al., 2020). Therefore, further subdividing the functions of M1 and M2 macrophages has important clinical therapeutic and diagnostic significance for the study of pulmonary fibrosis.

1.5 Lung extracellular matrix

The extracellular matrix (ECM) is the basic structure of the lung tissue environment and consists of the basement membrane and interstitial space. It consists of fibrin, glycoprotein and proteoglycan complexes that constitute the non-cellular part of the tissue, and its specific composition changes according to the dynamic microenvironment. The basement membrane in lung tissue is a thin and specialized ECM layer that underlies all epithelial and endothelial cells, while the interstitial space forms the lung parenchymal structure (White, 2015).

1.5.1 Lung extracellular matrix in pulmonary fibrosis

The lung extracellular matrix contains abundant fibrillar proteins and elastin, crucial for determining the tensile strength and elastic recoil of the lung tissue. (Senior et al., 1975; Shifren & Mecham, 2006), so these proteins can affect the stiffness of the ECM. When tissue is damaged, the body normally recruits highly differentiated myofibroblasts to produce ECM proteins. After completing the repair mission, the body initiates apoptosis and is quickly eliminated. However, in IPF, myofibroblasts are resistant to apoptosis, and their persistence leads to excessive scarring (Upagupta et al., 2018) and subsequent

damage to the alveolar structure. Therefore, the communication between cells and extracellular matrix may be one of the potential mechanisms triggering the pathogenesis of IPF.

The ECM is composed of more than 300 proteins. With the highly dynamic changes in the ECM structure, ECM proteins are constantly secreted and degraded. In IPF, the remodeling of the ECM directly leads to the imbalance of protein composition, excessive deposition of proteoglycans, collagen, elastin, and fibronectin, thereby increasing the stiffness of the matrix. Studies have shown that this process can activate the mechanosensitive Hippo pathway effector Yes-associated protein 1 (YAP) (DuFort et al., 2011). Other mechanosensitive pathways also interact with the YAP signaling pathway. For example, the signal generated by Notch mechanotransduction forms a positive feedback with YAP signal. This feedback loop can be inhibited by Wnt/β-catenin signaling (Kim et al., 2017). ECM remodeling can also affect FAK, ROCK/RhoA, and actin cytoskeletal rearrangements (Duscher et al., 2014). Not only that, but direct interactions between cells and ECM such as epithelial stress, activated macrophages, and fibroblasts can affect the fiber remodeling process. Therefore, in IPF disease, cell-ECM interaction is an indispensable part of in-depth study of pulmonary fibrosis.

1.5.2 Perlecan of the lung extracellular matrix

A kind of HS proteoglycan is ubiquitous in the extracellular matrix and most cells. Most of this perlecan is synthesized by cells and is considered to be one of the important components of the basement membrane (Lord et al., 2018). Human perlecan protein contains five different and conserved structural domains (Fig 1.10). Glycosaminoglycans attached to the N-terminal and C-terminal domains can exert tissue-specific activity. The five conserved domains perform different functions. Domain I interacts with PDGF, BMP2, HGF, FGF2 and GM-CSF respectively through HS. Angiopoietin-3, and activin A to act as co-receptors in cell signaling that transmit growth factors and receptor activation (Melrose, 2020; Whitelock et al., 2008). Domain II has four LDL receptor type A domains, that are involved in the regulation of Wnt/calcium signaling pathways in vascular atherogenic lipid internalization (Hayes et al., 2022). Domain III consists of 3 tandem laminin B domains and 3 laminin-type epidermal growth factor (EGF) domains consisting of 4 disulfide bonds, capable of binding the FGF growth factor binding proteins, FGF7 and FGF18 (Mongiat et al., 2000; Smith et al., 2007). Base Membrane domain IV has the longest amino acid sequence. This recombinant domain can produce high affinity interactions with fibronectin, nidogen-1, fibulin-2 and type IV collagen. This domain acts on the basement membrane through these interactions. Studies have shown that domain

IV is sensitive to the action of proteolytic enzymes (Martinez et al., 2019). Domain V of the basement membrane, which contains 3 laminin G (LG) and 2 pairs of proteins released by cathepsin L proteolysis, may act as a functional proteoglycan and may have different action properties than the core properties of the intact basement membrane protein. Tolloid-like MMPs can further hydrolyze domain V releasing the LG3 module (Gubbiotti et al., 2017). The different functions of these conserved domains imply that Perlecan can be a potentially important target in the process of pulmonary fibrosis.

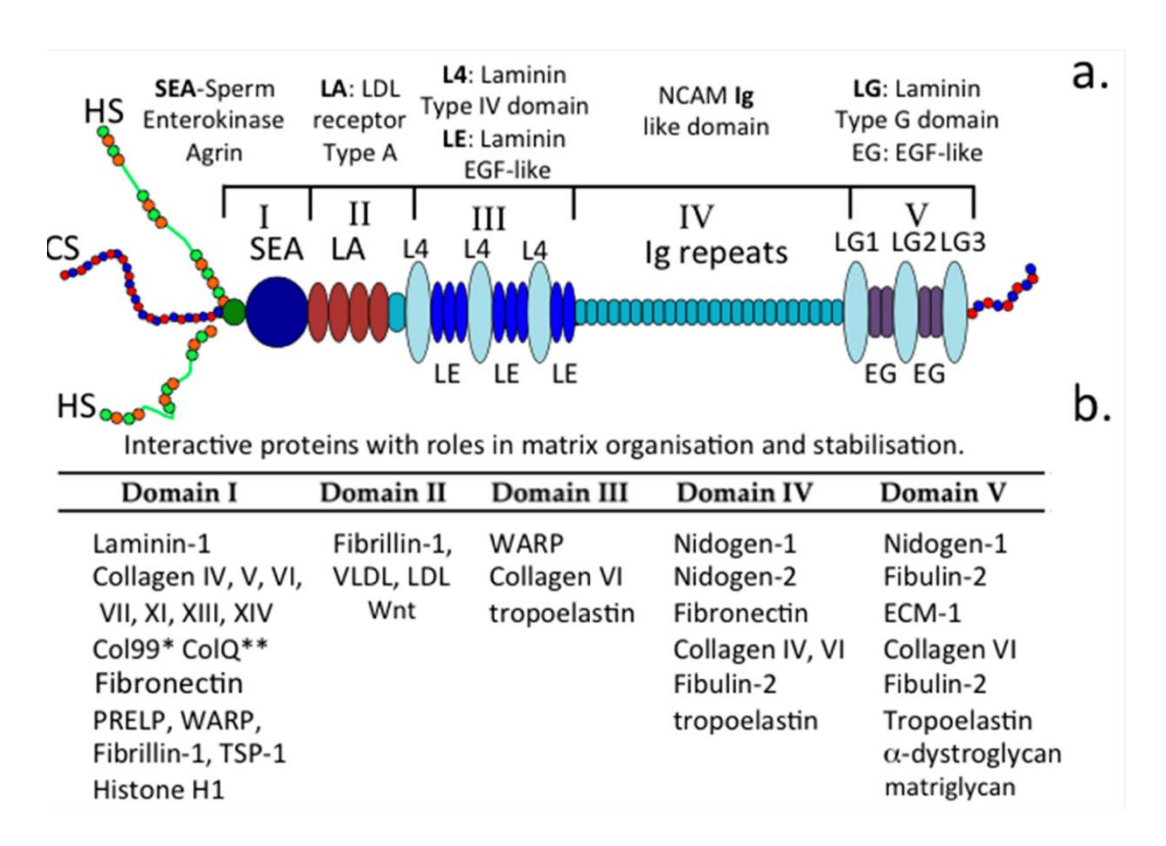


Figure 1.10 Schematic of the perlecan.

its five modular domains (a). and their interactive ligands (b).

1.6 Hypothesis and aims

During pulmonary fibrosis, alveoli and distal bronchioles are the onset of lesions, and a large amount of collagen and parenchymal structures form leading to scarring of the lungs. According to our preliminary observations, we found that the ECM in the pleural layer moved inward to become part of the fibrosis during the fibrosis process. In order to explore the mechanism of this phenomenon, we noticed that a large number of immune cells appeared around this lesion. Among them, macrophages, as one of the major immune cells, can regulate the lung microenvironment through intercellular communication and secretion of cytokines, and they can also act directly on the damaged structures of the lung. However, the existing functional typing of macrophages is not clear. In recent years, it has been found that macrophages are highly plastic and diverse, and macrophages can define different functional subpopulations based on different gene markers. Thus, we identified two macrophage subpopulations based on single-cell sequencing results of pulmonary fibrosis, identified two subpopulations of macrophages based on significantly different cell markers, tracked the changes of the two subpopulations during fibrosis, and defined them as profibrotic and resolution macrophages based on their functions. We designed fibrotic PCLS in vitro experiments to investigate the mechanism of action of different macrophages on the dynamic migration of ECM.

The hypothesis of this study is that, during fibrosis, profibrotic macrophages secrete MMP7 to break the lung ECM structure perlecan to promote inward migration of fibers. In contrast, resolution macrophages secrete the anti-inflammatory factor progranulin to enhance phagocytosis and clearance of ECM perlecan.

We set 5 following plans:

- 1. Tracking the dynamics of fibrosis in the pleural ECM layer
- 2. Analysis of profibrotic macrophages and resolution macrophage in relation to fibrosis based on single-cell data
- 3. Studying the direct effect of profibrotic macrophages on lung fibrosis
- 4. Studying the role of resolution macrophage on fibrosis
- 5. Analyzing human lung single cell RNA data to uncover the fucntions of the two macrophage types in lung fibrosis

2. Material and Methods

2.1 Materials

2.1.1 Antibodies

Table 1 Primary antibodies applied in histology staining.

Antigen	Host Species	Dilution	Manufacturer	Ref No.	Application
a-SMA	Goat	1:200	Abcam	ab21027	IF
CD206	Goat	1:500	R und D Systems	AF2535	IF
CD80	Rabbit	1:200	Abcam	ab134120	IF
GRN	Sheep	1:500	Bio-Techne	AF2557	IF, WB
MMP7	Rabbit	1:200	Proteintech	10374-2- AP	IF, WB
YAP	Rabbit	1:200	Abcam	ab205270	IF
PSMAD2	Rabbit	1:200	Cell Signaling	18338S	IF
Col1	Rabbit	1:200	Biomol	E-AB- 36387.20	IF
Col4	Rabbit	1:200	Abcam	ab6586	IF
LGMN	Rabbit	1:200	Tebu-Bio	126144- 61944-100	IF
MARCO	Rabbit	1:200	Abcam	ab259264	IF
Perlecan (A76)	Mouse	1:500	Abcam	ab26265	IF, WB
Perlecan (7B5)	Mouse	1:500	Life Technologies	134400	IF, WB
Perlecan (A74)	Mouse	1:500	Abcam	ab23418	IF, WB
Perlecan (5D7-2E4)	Mouse	1:500	Life Technologies	MABT12	IF, WB
Perlecan (A7L6)	Rat	1:500	Abcam	ab2501	IF, WB

Table 2 Secondary antibodies applied in histology staining.

Antigen	Dilution	Manufacturer	Ref No.	Application
Alexa Fluor 647 Donkey Anti- Rabbit Antibody	1:500	Life Technologies	A31573	IF
Alexa Fluor 594 Donkey Anti- Rat Antibody	1:500	Life Technologies	A31573	IF
Alexa Fluor 647 Goat anti- Mouse Antibody	1:500	Life Technologies	A21235	IF
Alexa Fluor 647 Donkey anti- Goat Antibody	1:500	Life Technologies	A21447	IF
Alexa Fluor 647 Donkey anti- Sheep Antibody	1:500	Life Technologies	A21448	IF
Alexa Fluor 568 Donkey anti- Rabbit Antibody	1:500	Life Technologies	A10042	IF
ScanLater™ assay kit, Goat Anti-Rabbit IgG Antibody	1:5000	VWR /Molecular Device	10048- 858	WB
ScanLater EU-LAB, Anti- Mouse IgG Antibody	1:5000	VWR /Molecular Device	MLDVR82 08	WB
Donkey Anti-Sheep HRPAnti- body	1:10000	Abcam	ab195176	WB

2.1.2 Primers

 Table 3 Primers used for qPCR experiments.

Gene	Species	Sequence 5'-3'
GAPDH	Mouse	F:AGGTCGGTGTGAACGGATTTG
		R:TGTAGACCATGTAGTTGAGGTCA
Progranulin	Mouse	F:ATGTGGGTCCTGATGAGCTG
		R:GCTCGTTATTCTAGGCCATGTG
MMP7	Mouse	F:CTGCCACTGTCCCAGGAAG
		R:GGGAGAGTTTTCCAGTCATGG
LGMN	Mouse	F:TGGACGATCCCGAGGATGG
		R:GTGGATGATCTGGTAGGCGT
Marco	Mouse	F:ACAGAGCCGATTTTGACCAAG

R:CAGCAGTGCAGTACCTGCC MMP2 Mouse F:CAAGTTCCCCGGCGATGTC R:TTCTGGTCAAGGTCACCTGTC R:TTCTGGTCAAGGTCACCTGTC MMp9 Mouse F:CTGGACAGCCAGACACTAAAG R:CTCGCGGCAAGTCTTCAGAG JAK1 Mouse F:CTCTCTGTCACAACCTCTTCGC R:TTGGTAAAGTAGAACCTCATGCG JAK2 Mouse F:TTGTGGTATTACGCCTGTGTATC R:ATGCCTGGTTGACTCGTCTAT STAT1 Mouse F:CGGAGTCGGAGGCCCTAAT R:ACAGCAGGTGCTTCTTAATGAG STAT6 Mouse F:CTCTGTGGGGCCTAATTTCCA R:CATCTGAACCGACCAGGAACT PI3K Mouse F:GCAGAGGGCTACCAGTACAGA R:CTGAATCCAAGTGCCACTAAGG IL1 Mouse F:GCAACTGTTCCTGAACTCAACT R:ATCTTTTGGGGTCCGTCAACT R:GCCGATGATCTCTCAACTGAT IL4 Mouse F:GGTCTCAACCCCCAGCTAGT R:GCCGATGATCTCTCAAGTGAT IL4R Mouse F:CCCAACGGGACCACTGATG R:CTGTTGTTCAGACTCCCC R:CTGTTGTTCAGACTCCCCT ATAC Mouse F:CCCAACTGGGACCACATGG R:TACATGCGGGGGACCACTGAAG R:TACATGCGGGGGGACATTGAAG			
R:TTCTGGTCAAGGTCACCTGTC MMp9 Mouse F:CTGGACAGCCAGACACTAAAG R:CTCGCGGCAAGTCTTCAGAG JAK1 Mouse F:CTCTCTGTCACAACCTCTTCGC R:TTGGTAAAGTAGAACCTCATGCG JAK2 Mouse F:TTGTGGTATTACGCCTGTGTATC R:ATGCCTGGTTGACTCGTCTAT STAT1 Mouse F:CGGAGTCGGAGGCCCTAAT R:ACAGCAGGTGCTTCTTAATGAG STAT6 Mouse F:CTCTGTGGGGCCTAATTTCCA R:CATCTGAACCGACCAGGAACT PI3K Mouse F:GCAGAGGGCTACCAGTACAGA R:CTGAATCCAAGTGCCACTAAGG IL1 Mouse F:GCAACTGTTCCTGAACTCAACT R:ATCTTTTGGGGTCCGTCAACT R:GCCGATGATCCTCAACT R:GCCGATGATCCTCAAGTGAT IL4 Mouse F:GCTCTGCATCCCCAGCTAGT R:GCCGATGATCTCTCTCAAGTGAT IL4R Mouse F:TCTGCATCCCGTTGTTTTGC R:GCACCTGTGCATCCTGAATG IL6 Mouse F:CCCAACAGGGACCACTGG IL6 Mouse F:CCCAACTGGGACCACTGG			R:CAGCAGTGCAGTACCTGCC
MMp9 Mouse F:CTGGACAGCCAGACACTAAAG R:CTCGCGGCAAGTCTTCAGAG JAK1 Mouse F:CTCTCTGTCACAACCTCTTCGC R:TTGGTAAAGTAGAACCTCATGCG JAK2 Mouse F:TTGTGGTATTACGCCTGTGTATC R:ATGCCTGGTTGACTCGTCTAT STAT1 Mouse F:CGGAGTCGGAGGCCCTAAT R:ACAGCAGGTGCTTCTTAATGAG STAT6 Mouse F:CTCTGTGGGGCCTAATTTCCA R:CATCTGAACCGACCAGGAACT PI3K Mouse F:GCAGAGGGCTACCAGTACAGA R:CTGAATCCAAGTGCCACTAAGG IL1 Mouse F:GCAACTGTTCCTGAACTCAACT R:ATCTTTTGGGGTCCGTCAACT R:GCCGATGATCCTCAACT R:GCCGATGATCCTCAAGTGAT IL4R Mouse F:TCTGCATCCCGTTGTTTTGC R:GCACCTGTGCATCCTGAATG IL6 Mouse F:CCAAGAGGTGATCTCCC R:CTGTTGTTCAGACTCTCCC R:CTGTTGTTCAGACTCTCCCT ATAC Mouse F:CCCAACTGGGACCACATGG	MMP2	Mouse	F:CAAGTTCCCCGGCGATGTC
R:CTCGCGGCAAGTCTTCAGAG JAK1 Mouse F:CTCTCTGTCACAACCTCTTCGC R:TTGGTAAAGTAGAACCTCATGCG R:TTGGTAAAGTAGAACCTCATGCG R:ATGCCTGGTTATC R:ATGCCTGGTTGACTCATT STAT1 Mouse F:CGGAGTCGGAGGCCCTAAT R:ACAGCAGGTGCTTCTTAATGAG STAT6 Mouse F:CTCTGTGGGGCCTAATTTCCA R:CATCTGAACCGACCAGGAACT PI3K Mouse F:GCAGAGGGCTACCAGTACAGA R:CTGAATCCAAGTGCCACTAAGG IL1 Mouse F:GCAACTGTTCCTGAACTCAACT R:ATCTTTTGGGGTCCGTCAACT IL4 Mouse F:GGTCTCAACCCCCAGCTAGT R:GCCGATGATCTCTCAAGTGAT IL4R Mouse F:TCTGCATCCCGTTGTTTTGC R:GCACCTGTGCATCCTGAATG IL6 Mouse F:CCAAGAGGTGATCCCCC R:CTGTTGTTCAGACTCCCCT ATAC Mouse F:CCCAACTGGGACCACATGG			R:TTCTGGTCAAGGTCACCTGTC
JAK1 Mouse F:CTCTCTGTCACAACCTCTTCGC R:TTGGTAAAGTAGAACCTCATGCG JAK2 Mouse F:TTGTGGTATTACGCCTGTGTATC R:ATGCCTGGTTGACTCGTCTAT STAT1 Mouse F:CGGAGTCGGAGGCCCTAAT R:ACAGCAGGTGCTTCTTAATGAG STAT6 Mouse F:CTCTGTGGGGCCTAATTTCCA R:CATCTGAACCGACCAGGAACT PI3K Mouse F:GCAACTGTTCCTGAACTCAACT R:ATCTTTTGGGGTCCGTCAACT R:ATCTTTTTGGGGTCCGTCAACT R:ATCTTTTTGGGGTCCGTCAACT R:GCCGATGATCCCAGCTAGT R:GCCGATGATCTCTCAAGTGAT IL4 Mouse F:GGTCTCAACCCCCAGCTAGT R:GCCGATGATCCTCAACT R:GCCGATGATCCTGAATG IL6 Mouse F:CCCAAGAGGTGACTCCCCT ATAC Mouse F:CCCAACTGGGACCACATGG	ММр9	Mouse	F:CTGGACAGCCAGACACTAAAG
R:TTGGTAAAGTAGAACCTCATGCG JAK2 Mouse F:TTGTGGTATTACGCCTGTGTATC R:ATGCCTGGTTGACTCGTCTAT STAT1 Mouse F:CGGAGTCGGAGGCCCTAAT R:ACAGCAGGTGCTTCTTAATGAG STAT6 Mouse F:CTCTGTGGGGCCTAATTTCCA R:CATCTGAACCGACCAGGAACT PI3K Mouse F:GCAGAGGGCTACCAGTACAGA R:CTGAATCCAAGTGCCACTAAGG IL1 Mouse F:GCAACTGTTCCTGAACTCAACT R:ATCTTTTGGGGTCCGTCAACT IL4 Mouse F:GGTCTCAACCCCCAGCTAGT R:GCCGATGATCTCTCAAGTGAT IL4R Mouse F:TCTGCATCCCGTTGTTTTGC R:GCCACTGTGCATCCCGTTGTTTTGC R:GCCACTGTGCATCCCGAGTGATG IL6 Mouse F:CCCAAGAGGTGACTCCCCT ATAC Mouse F:CCCAACTGGGACCACATGG			R:CTCGCGGCAAGTCTTCAGAG
JAK2 Mouse F:TTGTGGTATTACGCCTGTGTATC R:ATGCCTGGTTGACTCGTCTAT F:CGGAGTCGGAGGCCCTAAT R:ACAGCAGGTGCTTCTTAATGAG STAT6 Mouse F:CTCTGTGGGGCCTAATTTCCA R:CATCTGAACCGACCAGGAACT PI3K Mouse F:GCAGAGGGCTACCAGTACAGA R:CTGAATCCAAGTGCCACTAAGG IL1 Mouse F:GCAACTGTTCCTGAACTCAACT R:ATCTTTTGGGGTCCGTCAACT R:ATCTTTTGGGGTCCGTCAACT IL4 Mouse F:GGTCTCAACCCCCAGCTAGT R:GCCGATGATCTCTCTCAAGTGAT IL4R Mouse F:TCTGCATCCCGTTGTTTTGC R:GCACCTGTGCATCCTGAATG IL6 Mouse F:CCCAAGAGGTGAGTGCTTCCC R:CTGTTGTTCAGACTCTCCCT ATAC Mouse F:CCCAACTGGGACCACATGG	JAK1	Mouse	F:CTCTCTGTCACAACCTCTTCGC
R:ATGCCTGGTTGACTCGTCTAT STAT1 Mouse F:CGGAGTCGGAGGCCCTAAT R:ACAGCAGGTGCTTCTTAATGAG STAT6 Mouse F:CTCTGTGGGGCCTAATTTCCA R:CATCTGAACCGACCAGGAACT PI3K Mouse F:GCAGAGGGCTACCAGTACAGA R:CTGAATCCAAGTGCCACTAAGG IL1 Mouse F:GCAACTGTTCCTGAACTCAACT R:ATCTTTTGGGGTCCGTCAACT IL4 Mouse F:GGTCTCAACCCCCAGCTAGT R:GCCGATGATCTCTCAAGTGAT IL4R Mouse F:TCTGCATCCCGTTGTTTTGC R:GCACCTGTGCATCCTGAATG IL6 Mouse F:CCCAAGAGGTGAGTGCTTCCC R:CTGTTGTTCAGACTCTCCCT ATAC Mouse F:CCCAACTGGGACCACATGG			R:TTGGTAAAGTAGAACCTCATGCG
STAT1 Mouse F:CGGAGTCGGAGGCCCTAAT R:ACAGCAGGTGCTTCTTAATGAG STAT6 Mouse F:CTCTGTGGGGCCTAATTTCCA R:CATCTGAACCGACCAGGAACT PI3K Mouse F:GCAGAGGGCTACCAGTACAGA R:CTGAATCCAAGTGCCACTAAGG IL1 Mouse F:GCAACTGTTCCTGAACTCAACT R:ATCTTTTGGGGTCCGTCAACT R:GCCGATGATCTCTCAAGTGAT IL4 Mouse F:TCTGCATCCCAGTTATTTGC R:GCCGATGATCTCTCTCAAGTGAT IL4R Mouse F:TCTGCATCCCGTTGTTTTGC R:GCACCTGTGCATCCTGAATG IL6 Mouse F:CCAAGAGGTGAGTGCTTCCC R:CTGTTGTTCAGACTCCCTT ATAC Mouse F:CCCAACTGGGACCACATGG	JAK2	Mouse	F:TTGTGGTATTACGCCTGTGTATC
R:ACAGCAGGTGCTTCTTAATGAG STAT6 Mouse F:CTCTGTGGGGCCTAATTTCCA R:CATCTGAACCGACCAGGAACT PI3K Mouse F:GCAGAGGGCTACCAGTACAGA R:CTGAATCCAAGTGCCACTAAGG IL1 Mouse F:GCAACTGTTCCTGAACTCAACT R:ATCTTTTGGGGTCCGTCAACT R:GCCGATGATCTCTCAAGTGAT IL4R Mouse F:TCTGCATCCCGTTGTTTTGC R:GCACCTGTGCATCCTGAATG IL6 Mouse F:CCAAGAGGTGAGTGCTTCCC R:CTGTTGTTCAGACTCCCT ATAC Mouse F:CCCAACTGGGACCACATGG			R:ATGCCTGGTTGACTCGTCTAT
STAT6 Mouse F:CTCTGTGGGGCCTAATTTCCA R:CATCTGAACCGACCAGGAACT PI3K Mouse F:GCAGAGGGCTACCAGTACAGA R:CTGAATCCAAGTGCCACTAAGG IL1 Mouse F:GCAACTGTTCCTGAACTCAACT R:ATCTTTTGGGGTCCGTCAACT R:GCCGATGATCTCTCAAGTGAT IL4R Mouse F:TCTGCATCCCGTTGTTTTGC R:GCACCTGTGCATCCTGAATG IL6A Mouse F:CCAAGAGGTGAGTGCTTCCC R:CTGTTGTTCAGACTCCCT ATAC Mouse F:CCCAACTGGGACCACATGG	STAT1	Mouse	F:CGGAGTCGGAGGCCCTAAT
PI3K Mouse F:GCAGAGGGCTACCAGTACAGA R:CTGAATCCAAGTGCCACTAAGG IL1 Mouse F:GCAACTGTTCCTGAACTCAACT R:ATCTTTTGGGGTCCGTCAACT IL4 Mouse F:GGTCTCAACCCCCAGCTAGT R:GCCGATGATCTCTCAAGTGAT IL4R Mouse F:TCTGCATCCCGTTGTTTTGC R:GCACCTGTGCATCCTGAATG IL6 Mouse F:CCAAGAGGTGAGTGCTTCCC R:CTGTTGTTCAGACTCCCTT			R:ACAGCAGGTGCTTCTTAATGAG
PI3K Mouse F:GCAGAGGGCTACCAGTACAGA R:CTGAATCCAAGTGCCACTAAGG IL1 Mouse F:GCAACTGTTCCTGAACTCAACT R:ATCTTTTGGGGTCCGTCAACT R:GCCGATGATCTCTCAAGT R:GCCGATGATCTCTCAAGTGAT R:GCCGATGATCTCTCTCAAGTGAT R:GCACCTGTGCATCCCGTTGTTTTGC R:GCACCTGTGCATCCTGAATG IL6 Mouse F:CCAAGAGGTGAGTGCTTCCC R:CTGTTGTTCAGACTCTCCT ATAC Mouse F:CCCAACTGGGACCACATGG	STAT6	Mouse	F:CTCTGTGGGGCCTAATTTCCA
R:CTGAATCCAAGTGCCACTAAGG IL1 Mouse F:GCAACTGTTCCTGAACTCAACT R:ATCTTTTGGGGTCCGTCAACT IL4 Mouse F:GGTCTCAACCCCCAGCTAGT R:GCCGATGATCTCTCTCAAGTGAT IL4R Mouse F:TCTGCATCCCGTTGTTTTGC R:GCACCTGTGCATCCTGAATG IL6 Mouse F:CCAAGAGGTGAGTGCTTCCC R:CTGTTGTTCAGACTCCCT ATAC Mouse F:CCCAACTGGGACCACATGG			R:CATCTGAACCGACCAGGAACT
IL1 Mouse F:GCAACTGTTCCTGAACTCAACT R:ATCTTTTGGGGTCCGTCAACT IL4 Mouse F:GGTCTCAACCCCCAGCTAGT R:GCCGATGATCTCTCTCAAGTGAT IL4R Mouse F:TCTGCATCCCGTTGTTTTGC R:GCACCTGTGCATCCTGAATG IL6 Mouse F:CCAAGAGGTGAGTGCTTCCC R:CTGTTGTTCAGACTCTCCCT ATAC Mouse F:CCCAACTGGGACCACATGG	PI3K	Mouse	F:GCAGAGGGCTACCAGTACAGA
R:ATCTTTTGGGGTCCGTCAACT IL4 Mouse F:GGTCTCAACCCCCAGCTAGT R:GCCGATGATCTCTCTCAAGTGAT IL4R Mouse F:TCTGCATCCCGTTGTTTTGC R:GCACCTGTGCATCCTGAATG IL6 Mouse F:CCAAGAGGTGAGTGCTTCCC R:CTGTTGTTCAGACTCTCCCT ATAC Mouse F:CCCAACTGGGACCACATGG			R:CTGAATCCAAGTGCCACTAAGG
IL4 Mouse F:GGTCTCAACCCCCAGCTAGT R:GCCGATGATCTCTCTCAAGTGAT IL4R Mouse F:TCTGCATCCCGTTGTTTTGC R:GCACCTGTGCATCCTGAATG IL6 Mouse F:CCAAGAGGTGAGTGCTTCCC R:CTGTTGTTCAGACTCTCCCT ATAC Mouse F:CCCAACTGGGACCACATGG	IL1	Mouse	F:GCAACTGTTCCTGAACTCAACT
R:GCCGATGATCTCTCAAGTGAT IL4R Mouse F:TCTGCATCCCGTTGTTTTGC R:GCACCTGTGCATCCTGAATG IL6 Mouse F:CCAAGAGGTGAGTGCTTCCC R:CTGTTGTTCAGACTCTCCCT ATAC Mouse F:CCCAACTGGGACCACATGG			R:ATCTTTTGGGGTCCGTCAACT
IL4R Mouse F:TCTGCATCCCGTTGTTTTGC R:GCACCTGTGCATCCTGAATG IL6 Mouse F:CCAAGAGGTGAGTGCTTCCC R:CTGTTGTTCAGACTCTCTCCCT ATAC Mouse F:CCCAACTGGGACCACATGG	IL4	Mouse	F:GGTCTCAACCCCCAGCTAGT
R:GCACCTGTGCATCCTGAATG IL6 Mouse F:CCAAGAGGTGAGTGCTTCCC R:CTGTTGTTCAGACTCTCTCCCT ATAC Mouse F:CCCAACTGGGACCACATGG			R:GCCGATGATCTCTCTCAAGTGAT
IL6 Mouse F:CCAAGAGGTGAGTGCTTCCC R:CTGTTGTTCAGACTCTCTCCCT ATAC Mouse F:CCCAACTGGGACCACATGG	IL4R	Mouse	F:TCTGCATCCCGTTGTTTTGC
R:CTGTTGTTCAGACTCTCCCT ATAC Mouse F:CCCAACTGGGACCACATGG			R:GCACCTGTGCATCCTGAATG
ATAC Mouse F:CCCAACTGGGACCACATGG	IL6	Mouse	F:CCAAGAGGTGAGTGCTTCCC
			R:CTGTTGTTCAGACTCTCTCCCT
R:TACATGCGGGGACATTGAAG	ATAC	Mouse	F:CCCAACTGGGACCACATGG
			R:TACATGCGGGGGACATTGAAG

2.1.3 Cell types

Table 4 Cell types.

NIH3T3/Cas9	Mouse embryonic fibroblasts	NIH Swiss, Embryo
Monocytes	Mouse Primary Monocytes	Mouse Bone marrow
Macrophages	Mouse Primary Macrophages	Mouse Bone marrow

2.1.4 Cell culture medium and Kits

Table 5 Medium and Chemicals.

Medium, Chemicals	Source	Ref No.
RPMI 1640	GIBCO	21875034
Phenol red-free RPMI1640	GIBCO	11835030
Fetal Bovine Serum	Life Technologies	10500064
Sodium pyruvate	Sigma	S8636
M-CSF	Peprotech	315-02-10
IFN-gamma	Peprotech	315-05-100
GM-CSF	R And D Systems	415-ML-020/CF
LPS	Sigma Aldrich	L8274
IL4	Peprotech	214-14-20
Pen-Strep	Gibco	15140122
Amphotericin B	Sigma	A2942
MACS Monocyte Isolation kit	Miltenyi Biotec	130-100-629
Red Cell Lysis Solution	Miltenyi Biotec	130-094-183
RNeasy	Qiagen	74104

2.1.5 Chemicals

Table 6 Chemical lists

Product	Manufacturer
Bleomycin	Sigma-Aldrich
Bovine serum albumin (BSA)	Sigma-Aldrich
4% paraformaldehyde (PFA)	VWR International
DAPI staining	Becton Dickinson

Material and Methods

Fluorescent-G Mounting Medium Invitrogen

Isopropanol Roth Carl Roth Sonderaktion

Phalloidin Alexa Fluor 647 Biomol

Recombinant mouse TGF-β1 protein R&D Systems

Triton X-100 Sigma

Trypsin EDTA 0.25% Life Technologies

DPBS Life Technologies

GM6001 Sigma-Aldrich

Heparan Sulfate Medchemexpress

Chlorate Sigma-Aldrich

Isofraxidin Sigma-Aldrich Chemie

Anti-CD47 Blocking Antibody Biozol Diagnostica

Recombinant Progranulin protein Enzo Life Sciences

Gliotoxin Cay11433-1

Vorinostat LC-V-8477_250mg

D(+)-Trehalose Dihydrat Carl Roth

NHS-ester dye Life Technologies

Micro Particles Sigma-Aldrich

rmEndorepellin Bio-Techne

Collagenase Type I Th Geyer

Dnase I, Grade Ii Sigma-Aldrich Chemistry

Liberase Tm Research Grade 10 Mg Sigma-Aldrich Chemistry

RR-11a Biozol Diagnostica

Clodronate liposomes & control liposomes Liposoma BV

Paraformaldehyde, 16% w/v aq. VWR International

Cytochalasin D Th Geyer.

Nintedanib esylate Santa Cruz

Pirfenidone Santa Cruz

Sucrose Santa Cruz

Agarose, low gelling temperature Sigma-Aldrich Chemie

Sulfosuccinimidyl oleate sodium MCE

Ointment Bayer

Gelatine Sigma

Triton X-100 Sigma

Material and Methods

Thimerosal	Sigma
HSPG2 ELISA kit	Biozol
Progranulin ELISA kit	Life technologies

2.1.6 Consumables

Table 7 Consumables

Product	Manufacturer
6/12/24/48 well plates	e.biss Lagermaterial
μ-Plate 24 Well Black	Ibidi
Cell culture dishes	Neolab
Cell culture flasks	Schubert und Weiss
Falcon tubes 15ml/50ml	Falcon
Filter pipet tips	Sigma
Cell strainer, nylon 100,70,40µm	Falcon
26G needle	VWR International
23G needle	VWR International
Intravenous cannulation	VWR International
10ml syringe	VWR International
Syringe insulin 0,5ml	BD Micro-Fine+
PCR plates, qPCR	Biozym Scientific
Sealing foil, qPCR	Sigma-Aldrich
PVDF membrane	Life Science
4-15% MP TGX Gel	Bio Rad
Forceps	Fisher Scientific
Scissors	Fisher Scientific
Whatman blotting paper	GE Healthcare, Freiburg, Germany
OCT	CellPath
Cryostat	CryoStar

2.2 Cell culture methodology

2.2.1 Mouse primary Monocyte isolation

C57BL/6J mice, aged 8-10 weeks (Charles River), were sacrificed to extract femurs and tibiae. The separated bones were sterilized by briefly soaking in 75% alcohol, and the two ends of the bones were split with sterile forceps (Fisher Scientific 15307805) and scissors (Fisher Scientific 15654444) to form a through state. Bone marrow-derived cells were flushed out with 10 ml PBS (Life Technologies 5001223) through a syringe (VWR International 4617100V), and large tissue debris was removed through a 70 µm sterile filter (Falcon 352350). Bone marrow cells were obtained after centrifugation at 300g for 10 min (Eppendorf Rotina 420R), Red cell lysis solution (Miltenyi Biotec 130-094-183) was used for red blood cells clearing. Subsequently, primary monocytes were obtained using the Monocyte isolation kit (Miltenyi Biotec 130100629) and placed in a 37 °C incubator with 5% CO₂. RPMI 1640 (GIBCO 21875034) supplemented with 10% (v/v) FBS (Life Technologies 10500064), 20ng/ml GM-CSF (R and D Systems 415-ML-020/CF), 1% (v/v) Pen-strep (GIBCO 15140122), and 1% (v/v) sodium pyruvate (Sigma S8636) was used to culture the cells.

2.2.2 Macrophages differentiation and polarization

Primary monocytes were stimulated in the medium containing RPMI1640 (GIBCO 21875034), 10% heat-inactivated FBS (Life Technologies 10500064) and 20 ng/ml GM-CSF (R and D Systems 415-ML-020/CF). After 7 days cells were differentiated into adherent macrophages, replace the culture medium every other day. Adherent macrophages were divided into two groups, one group was treated with fresh medium consisting 100 ng/ml LPS (Sigma Aldrich L8274) and 50 ng/ml interferon-γ (IFNγ, PeproTech 315-05-100) for 24 hours to Classic activated Macrophages. Another group added the medium containing 50ng/ml M-CSF (PeproTech 315-02-10) and 20ng/ml Interleukin-4 (IL4, PeproTech 214-14-20) (Ying et al., 2013), then was cultured for 24 hours to obtain alternative activated Macrophages.

2.3 scRNA-seq data analysis

Scanpy50 were used to perform all the analyzes (Wolf et al., 2018). The matrices of each samples were combined, and quality control measures were implemented. Combat and cell cycle regression algorithms were implemented to address batch and cell cycle effects. The UMAP algorithm was chosen as the primary method for dimensional reduction.

Mouse IPF lung datasets were obtained from the Collaborative laboratory (GSE141259). Cell annotation was performed by iteratively increasing the threshold during ensuring that distinct cell clusters are preserved. During the subclustering of macrophage, naïve monocytes served as the control cluster. Genes markers of each cluster were ranked with the 'wilcoxon' assay and subsequently applied to gene ontology term overrepresentation analysis. The expression profiles of Macrophages were computed using the gene score function. The profibrotic Macrophages was defined by the Markers of Marco, Ctss, Chi3l3, Lyz2, Ccl6, Lgmn, Spp1, Cd163, Cd9, Tyrobp, Atp6v0d2, Psap, Lgals3, Ftl1, Lpl, Tmsb4x, Wfdcl7, Mrc1, Ear2, Fcerlg, Cyba, Cstb, Ctsl. For the Resolution macrophages profile, the markers Grn, C1qb, Ctss, Ctsb, C1qc, Ctsd, Mrc1, Lyz2, Apoe, C1qa, Tyrobp, Cd36, Fth1, Ctsl, Spp1, Lgmn, Fcer1g, Psap, Sepp1, Cst3, Ftl1, B2m, Cd68, Itm2b, Lgals3 were used.

Human lung IPF single cell data was acquired from the GEO repository (GSE128033). Human Macrophage clusters annotation was operated with scArches (Lotfollahi et al., 2022). Subsequently, the cells of human dataset were annotated. Parameters were applied following scArches optimization guidelines. Trajectories from two clusters of macrophages and from the naïve monocyte-to-resolution macrophage trajectory inference was performed using PAGA with RNA velocity directed edges and the scvelo toolkit. (Bergen et al., 2020; Wolf et al., 2019). Human trajectories, including those from the unbiased dataset and from the naïve monocyte-to-resolution macrophage trajectory clusters, were set by PAGA only, given the unmatched the human samples. The arrangement was conducted through diffusion pseudotime to substitute velocity pseudotime.

2.4 Precision-cut lung slices and in vitro culture

2.4.1 Precision-cut lung slices assay

According to the experimental methods in the reference literature (Akram et al., 2019; Lehmann et al., 2018; Uhl et al., 2015; Wu et al., 2019), with slight adjustments, C57BL/6J mice (Charles River) aged 6 to 12 weeks were deeply anesthetized by intraperitoneal injection of ketamine (100 mg/mL, Vetquinol) and xylazine (20 mg/mL, Sedaxylan). The abdominal cavity of the mice was opened with sterile scissors (Fisher Scientific 15654444), the abdominal aorta was incised and the mice were euthanized by bleeding. Open the chest with scissors (Fisher Scientific 15654444) upward and remove the chest walls on both sides. 10 ml PBS (Life Technologies 5001223) was perfused through the right ventricle of the heart towards the lung tissue through a 26G needle

(VWR International 02040676) to remove blood cells. Carefully remove the anterior chest wall to expose the trachea, pass forceps underneath the trachea, and take sterile medical thread to fix the needle as a backup. Precision ophthalmic scissors make a mini cut on the trachea below the cricoid cartilage. Insert the plastic tube wrapped with the intravenous cannulation (VWR International 4252110B) into the trachea, and tie it with a knot of medical thread. After intubation, 2% low melting point agarose (Sigma A9414) prepared with phenol red-free RPMI1640 medium (GIBCO 11835030) was injected into the trachea until both lungs were inflated. Wait for 1 minute, remove the intravenous cannulation (VWR International 4252110B) and tighten the fixation line, remove the lungs together with the heart and transfer them to pre-cooled medium, and place them on ice until they are completely solidified.

The left lung lobe was separated to remove the liquid on the surface of the lung lobe, and the lung surface was evenly coated with NHS-ester dye (Life Technologie A20000) for 1 min, and then the lung surface was rinsed with Tris-HCL solution to remove excess dye. The fluorescent dye-labeled lung lobes were transversely sectioned using a vibrotome (Zeiss Hyrax V55) at a thickness of 300µm per slice. The parameters were set to a speed of 10–12 µm/s, a frequency of 80Hz and the amplitude of 1 mm. PCLS was incubated for 2 hours at 37°C and washed twice with warm RPMI1640 (GIBCO 21875034). PCLS was cultured in the medium of RPMI 1640 (GIBCO 21875034) with 10% (v/v) FBS (Life Technologies 10500064), 2.5µg/mL (0.1%) amphotericin B (Sigma A2942) and 1% (v/v) Pen-strep (GIBCO 15140122), and then transferred to a 37 °C incubator with 5% CO₂.

2.4.2 PCLS Coculture with immune cells

3D lung sections with fluorescent labeling in the pleural layer were co-cultured with 2x10⁵ mouse primary monocytes, 2x10⁵ differentiated adherent macrophages M0, 2x10⁵ LPS/ IFNγ activated macrophages and 2x10⁵ IL4/M-CSF Macrophages in 24-well plates separately, adding medium RPMI 1640 (GIBCO 21875034) medium supplemented with 10% (v/v) FBS (Life Technologies 10500064), 2.5μg/mL (0.1%) amphotericin B (Sigma A2942) and 1% (v/v) Pen-strep (GIBCO 15140122), and then cultured in a 37 °C incubator with 5% CO₂. The control group was set to an equal volume of culture medium, and each group of samples was set to 4 replicates. The fluorescence distribution of lung slices was recorded with fluorescence microscope using a compiled zoom of 10x at timepoint of d0, d3, d5, and the medium was changed every other day.

A dual factor experiment was used to verify macrophages' function. Labeled PCLS was firstly co-cultured with 2x10⁵ LPS/ IFNγ-activated macrophages for three days, and then 2x10⁵ mouse primary monocytes, 2x10⁵ differentiated adherent macrophages M0 and 2x10⁵ IL4/M-CSF polarized macrophages were added in 24-well plates separately, with 4 sample replicates in each group. The control group was a group without adding cells and a group with 2x10⁵ macrophages activated by LPS/IFNγ. The fluorescence distribution of each lung slice was recorded with the fluorescence microscope on d0, d3, and d5. The medium was changed every other day. Culture conditions were using medium RPMI 1640 (GIBCO 21875034) containing with 10% (v/v) FBS (Life Technologies 10500064), 2.5μg/mL (0.1%) amphotericin B (Sigma A2942) and 1% (v/v) Pen-strep (GIBCO 15140122). Then samples were transferred to a 37 °C incubator with 5% CO₂.

2.4.3 PCLS Coculture with Chemicals

Screening of differentially expressed genes between two types of macrophages based on comparison of single cell data, including potential macrophage targets MMP7, MMPs, SLAMF5, CD47, Progranulin, and CD36. Also listed are NF-kB signaling pathway targets related to inflammation and perlecan functional structural targets differentially expressed in lung disease tissues. The *in vitro* PCLS fibrosis model was used to verify the role of inhibitors or recombinant proteins of relevant targets in the fibrosis process. In the same way, based on the co-culture experiment of cells and PCLS, chemicals were added to treat each target, and the role of the target was verified by tracking the trajectory of labeled ECM movement. We set the groups as Control +DMSO, LPS/ IFNγ-activated macrophages, LPS/ IFNγ-activated macrophages+ Chemical, IL4/ M-CSF induced macrophages, IL4/ M-CSF induced macrophages (first 3 days)+ IL4/ M-CSF induced macrophages.

Table 8 Chemicals for the targets

Targets	Chemicals	Manufacturer	Ref No.
Perlecan	Heparan Sulfate	Medchemexpress	HY-101916
Perlecan	Chlorate	Sigma-Aldrich	403016
CD47	Anti-CD47 Blocking Antibody	Biozol Diagnostica	BXC-BE0283
CD36	Sulfosuccinimidyl oleate	Santa Cruz	sc-208408B

Progranulin	Recombinant Progranulin protein	Bio-Techne	AF2557
Progranulin	Vorinostat	Biomol	LC-V-8477
Progranulin	D(+)-Trehalose	Carl Roth	5151.2
MMP7	Isofraxidin	Sigma-Aldrich	PHL89229
MMPs	GM6001	Sigma-Aldrich	CC1100
SLAMF5	CD84 protein	Biozol Diagnostica	BLD-326002
legumain	RR-11a	Biozol Diagnostica	ADQ-A19852-1
NF-kB	Gliotoxin	Biomol	Cay11433-1
Phagocytosis	Cytochalasin D	Th Geyer.	10838343
Lung fibrosis	Nintedanib esylate	Santa Cruz	sc-396761B
Lung fibrosis	Pirfenidone	Santa Cruz	sc-203663

2.5 Animal experiments

2.5.1 Approval of animal experiments

All experiments adhered strictly to the guidelines set forth by the ethics committee of the Helmholtz Zentrum Munich and were duly approved by the regional council of Upper Bavaria Germany (Project ROB-55.2-2532.Vet_02-19-101). To induce experimental fibrotic phenotype , added 50 μ L Bleomycin (2 U/kg, Bleomycin sulfate, dissolved in DPBS) was administered intratracheally by an intravenous cannula (VWR International 4252110B). Control mice were treated with 50 μ L DPBS (Life Technologies 5001223).

2.5.2 Lung bleomycin animal Model

10-12 weeks C57BL/6J female mice ordered from Charles River (Sulzfeld, Germany) were applied for lung bleomycin model. Non-toxic fluorochrome-conjugated NHS-Ester (Life Technologie A20000) was intrapleural injected (50 microliters of 10 mg /ml) 2 days before bleomycin instillation. At the day of bleomycin instillation, mice are anesthetized with MMF (Medetomidine at 500 μg/kg, Midazolam at 5mg/kg and Fentanyl at 50 μg/kg body weight). The eyes of the mice were protected with ointment (Bayer, 0010087848). Then Bleomycin was in-fused at a concentration of 2 U/kg. The control group was set up in PBS. The experiments were then terminated and specimens collected at either 7, 14, 21, 28, 45 days (Izbicki et al., 2002; Peng et al., 2013; Ruscitti et al., 2017; Schiller et al.,

2015) after instillation depending on the experiment described below. Progranulin administration experiments were set up on bleomycin model. Progranulin was intrapleural injected twice, the first injection was with bleomycin instillation and the second was added on day7. The lung samples were collected on day7, day14, day 21, day28 comparing the histological features with control and bleomycin group. Each group had 6 mice for replication.

2.6 RNA analysis

2.6.1 RNA extraction and cDNA synthesis

2x10⁵ Primary macrophages (M0) were seeded into 12 well plates within the medium containing different chemicals. The groups were set up with 20 mU/ml bleomycin (Sigma-Aldrich B5507), 100 ng/ml LPS (Sigma Aldrich L8274) + 50 ng/ml interferon-γ (IFNγ, PeproTech 315-05-100), 100 ng/ml LPS (Sigma Aldrich L8274) + 50 ng/ml interferon-γ (IFNγ, PeproTech 315-05-100)+ 50ng/ml Progranulin, 100 ng/ml LPS (Sigma Aldrich L8274) + 50 ng/ml interferon-γ (IFNγ, PeproTech 315-05-100)+ 10 μm Isofraxidin (MCE HY-N0774), 50ng/ml M-CSF (PeproTech 315-02-10) + 20ng/ml Interleukin-4 (IL4, PeproTech 214-14-20), and PBS as control. The RNA was extracted by using the RNeasy kit (Qiagen 74104). The concentration and quality was quantified through a NanoDrop1000(PeqLab). Then cDNA was synthesized via reverse transcription kit. The process involved incubation for 10 minutes at 20°C, Then an annealing cycle was set for 75 minutes at 43°C and an extension for 5 minutes at 99°C. The reaction was then cooled to 4°C for storage.

2.6.2 Quantitative real-time PCR

The mRNA levels of the specific genes were assessed by SYBR Green (Roche) and an LC480 Light Cycler (Roche), with normalization against the reference gene GAPDH. The Primers were diluted to a final concentration of 500 nM with RNase/DNase-free water. The qPCR system were carried out: starting denaturation was 5 minutes at 95°C, then 45 cycles of denaturation for 5 seconds at 95°C, annealing for 5 seconds at 59°C, and elongation for 10 seconds at 72°C. Subsequently, a melting curve analysis was performed to characterize the dissociation features of dsDNA, involving denaturation for 5 seconds at 95°C, annealing for 1 minute at 60°C, and continuous acquisition was set from 60°C to 95°C. The reaction concluded with a final cooling step at 4°C. The level of relative transcript expression were determined by calculating the difference between cycle threshold values (ΔCt).

2.7 Histology

2.7.1 Immunofluorescence

Lung samples from animal experiments underwent fixation with 4% paraformaldehyde O/N (PFA, VWR 43368.9), followed by three washes with clean DPBS and subsequent processing for sectioning with OCT infiltration. The slides were then cleaned 3 times with 0.05% PBST to remove the OCT and blocked for 1 hour with 10% donkey serum in PBST at RT. Subsequently, the solution were changed with primary antibody in blocking buffer at 4°C O/N. Afterward, Slides were washed 3 times with PBST and then incubated with secondary antibody for 1 hour at RT. After that, sections underwent 3 rinses in PBST and were mounted with mounting media containing DAPI.

PCLS 3D-staining, fixed PCLS slides (approximately 1 cm²) were treated PBSGT for 1 day. Solution was changed with the primary antibody in PBSGT for 48 hours at RT. Then samples were washed 3 times for 3hours, following dipping in the solution of secondary antibody in PBSGT for 48 hours. Primary antibodies used: a-SMA (Abcam ab21027, 1:150), CD206 (R und D Systems AF2535 1:500), CD80 (Abcam ab134120 1:200), GRN (Bio-Techne AF2557 1:500), MMP7 (Proteintech 10374-2-AP 1:200), Col1 (Biomol E-AB-36387.20 1:200), Col4 (Abcam ab6586 1:200), LGMN (Tebu-Bio 126144-61944-100 1:200), MARCO (Abcam ab259264 1:200), perlecan (A76, Abcam ab26265 1:500), perlecan (7B5, Life Technologies 134400 1:500), perlecan (A74, Abcam ab23418 1:500), perlecan (5D7-2E4, Life Technologies MABT12 1:500), perlecan (A7L6, Abcam ab2501 1:500).

2.7.2 Masson-trichrome stain

Trichrome staining (Masson) (Sigma Aldrich HT15) was conducted utilizing a common kit. The slides were imaged using a ZEISS AxioImager.Z2m microscopy with a 20× objective. The sample under microscope showed collagen fibers were blue, muscle fibers were red, red blood cells were orange, and cell nuclei were gray-black.

2.7.3 Image Analysis

Histological images were analyzed using Fiji (v.1.53c). In order to quantify the movement trajectory of labeled pleural layer ECM in in vivo slices and in vitro 3D lung tissue experiments, we measured the pleural layer thickness at different time points. Each sample took measurement data from four different areas, and each group ensured four sample repetitions. We compared the data from the fibrosis group with the results from the

healthy group to draw conclusions. Immunofluorescence staining results analysis Positive cell rate, the staining cells numbers in same size of area was caculated by combining double-positive signals in DAPI and labeled antibody channels. By quantifying the fluorescence intensity of labeled matrix antibodies, their average fluorescence intensity was measured in lung sections of the same size, and then the data were compared between healthy and disease groups. Fractal analysis was based on the ImageJ plugin "FracLac" 29, applied the same parameters and preprocessing (Correa-Gallegos et al., 2019; Correa-Gallegos et al., 2023).

2.8 Protein analysis

2.8.1 Mass spectrometry data analysis

Eleven human lung health and Idiopathic Pulmonary Fibrosis (IPF) samples were sourced from the proteomecentral public database (dataset ID PXD011116). Raw data underwent analysis through MaxQuant. The software allowed for two missing cleavage sites (Tyanova et al., 2016). Carbamidomethylation of cysteine served as a fixed modify command. The bait database was constructed by upending the previous sequence to enhance the reliability of peptide and protein identifications.

The "proteome" MaxQuant output file facilitated quantification of protein. Subsequent data preprocessing was conducted using Perseus86 software. Contaminants and proteins identified solely or the decoy database were filtered out. The lowest threshold was established for protein detection of 6 valid values. LFQ values of protein abundances were subjected to a comprehensive data analysis pipeline comprising sample normalization, technical replicate averaging, noise level estimation, and fold change evaluation. Robust quantile normalization was applied to the LFQ values, particularly suitable for heavy-tailed distributions. The resulting protein peptide intensities were normalized to account for systematic changes in data distribution between samples. Significance of fold change between conditions was determined by the t-statistic model. The P value <0.01 and missing values <50% were deemed significantly altered.

2.8.2 ELISA assay

Supernatants of PCLS after treatments were analyzed using ELISA Kits for mouse perlecan (Biozol BYT-ORB780077), Progranulin (Life technologies EMGRN) according to the instructions. The concentrations were calculated and analyzed by GraphPad Prism 9.0 using the protein standard included in the ELISA kits.

2.9 Statistical analysis

All Data were recorded and analyzed with GraphPad Prism 9.0. The analysis was operated using one-way ANOVA, t-test, two-tailed paired t-test. Data are shown as means \pm SEMs and were considered statistically significant when p \leq 0.05.

3. Results

3.1 Fibrotic macromolecules accrule inward from the pleural ECM

3.1.1 Inward egress of fibrotic macromolecules in animal models of fibrosis

To reveal the dynamic involvement of lung pleura extracellular matrix (ECM) during lung injury, we used NHS-easter dye to label the pleural layer of lung ECM, then traced the dynamic changes of labeled ECM proteins in a bleomycin model of lung fibrosis (Fig. 3.1a). The resulting NHS-ester dye tags ECM with FITC+ signal. We then performed bleomycin intratracheal instillation in mouse lungs, and we quantified the depth of matrix movement, as well as performed fractal analysis of ECM fibers at Day 14 post Bleomycin (Fig. 3.1b). FITC+ labeled proteins appeared in the bleomycin group within deep lung tissue, and its statistical depth was approximately 5 times the thickness of the labeled pleural layer as compared to control groups. Fractal dimension was used to analyze the structural complexity of the green fluorescent fiber based on its distribution and folding degree. The results showed that the bleomycin group was 1.5 times that of the control group. Transverse slices were used to obtain the overall signal distribution level of the plane. It was found that the green signal in the bleomycin group could diffuse throughout the entire lung plane on day 21, while in the control group, the signal clearly remained only in the pleural layer.

Immunofluorescence staining of markers related to fibrosis found that the aSMA⁺ cell rate in the bleomycin group accounted for 40% of the cells in the area, and the Col1⁺ cell rate accounted for 75% of the cells in the area. Both groups of fibrosis marker-positive cells were much higher than those in the control group (Fig. 3.1c), and the structure of the green labeled macromolecules is spatially associated with fibrosis markers. This proves that green labeled ECM protein may be involved in the process of pulmonary fibrosis, and this green label can track the dynamic changes of pulmonary fibrosis.

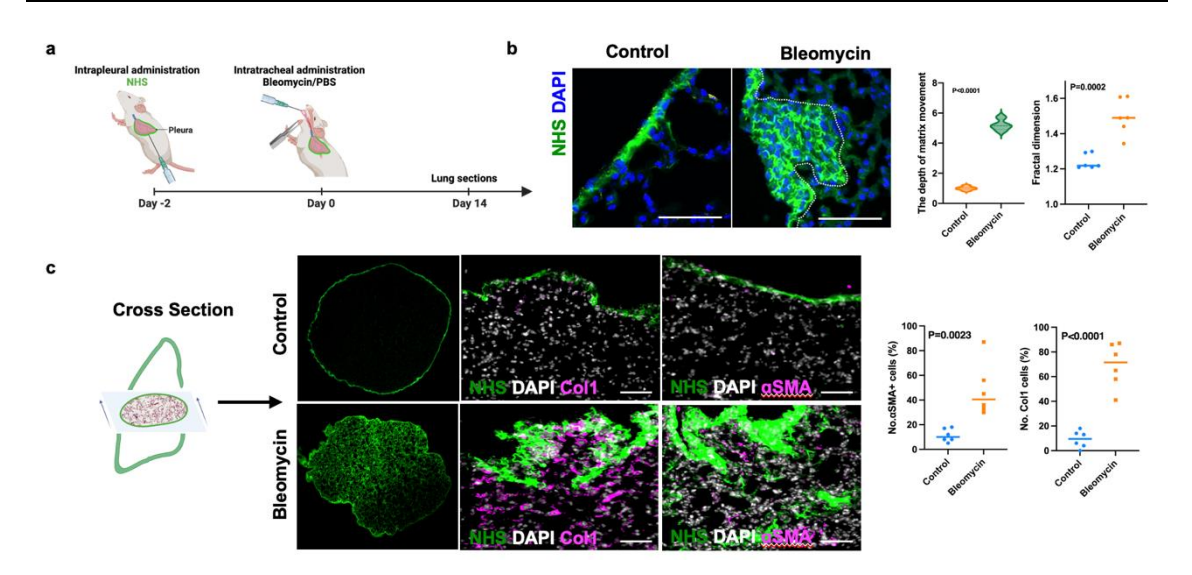


Figure 3.1 Pleural layer ECM is accompanied by inward movement of fibrosis.

a. Scheme of bleomycin animal model, NHS-easter dye marks the pleural layer ECM in advance. b. Tissue sections show that the day14 sample has shown a movement trend, statistical analysis of the depth of ECM influx (left) and the complexity of fiber dimension analysis (right). c. Observe the degree of fiber diffusion of the marker in the pleural layer on day 21 on the cross section. The fluorescent image shows the marker (Green) and fibrosis marker (magenta), and the positive rate of the fibrosis marker is counted. Scale bar is $100 \ \mu m$ (b, c).

3.1.2 Inward egress of fibrotic proteins in ex vivo models

In order to simplify animal experiments and facilitate subsequent large-scale drug screening experiments, we designed *ex vivo* tissue explant culture experiments. Low melting point agarose gel was perfused into mouse lungs, and NHS-ester dye was used to label the ECM protein of the lung pleural layer, and then vibratome was used to slice the lungs into uniformly 300micron thick lung sections. We treated lung slices with bleomycin for 7 days *ex vivo* and tracked the changes in NHS-labeled pleural layer ECM. The results showed that the labeled thickening of the bleomycin group was 1.915 times that of the control, and the fiber structure and dimensional complexity was higher than that of the control group, indicative of fibrosis development (Fig3.2).

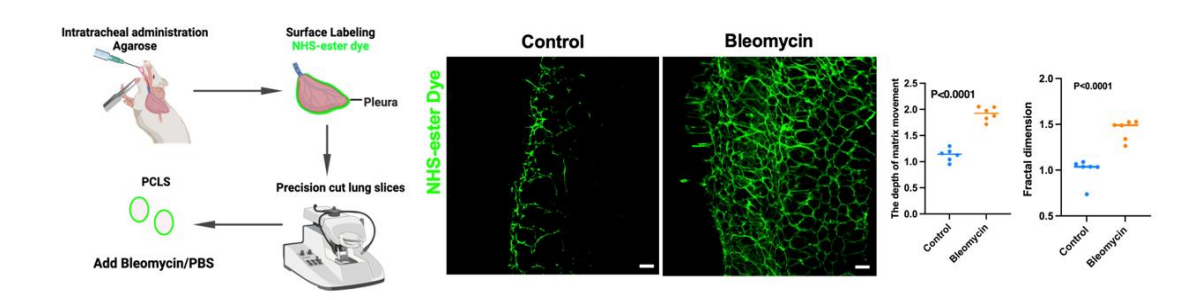


Figure 3.2 In vitro pulmonary fibrotic 3D model.

Schematic flow chart of lung slices *in vitro* (left) and fluorescence images of the fibrosis group and control group labeled with ECM in the pleural layer (right), with statistics on changes in ECM movement depth and fibrosis dimension. The scale scale is 0.2mm.

Labeled lung sections showed the phenotype of the control group on day0 (left), and on day 7 of bleomycin stimulation, lung sections showed an inward influx of green fluorescent fibers and a decrease in the central black area (right). We tested the fibrosis-associated markers aSMA and Col1 by immunofluorescence staining, and found that cells positive for both were highly expressed in the bleomycin group. Furthermore, we captured the signal of second harmonic generation (SHG) overlapping with the labeled area using a multi-photon microscope, thus demonstrating that the movable FITC+ material are strongly associated with fibrosis.

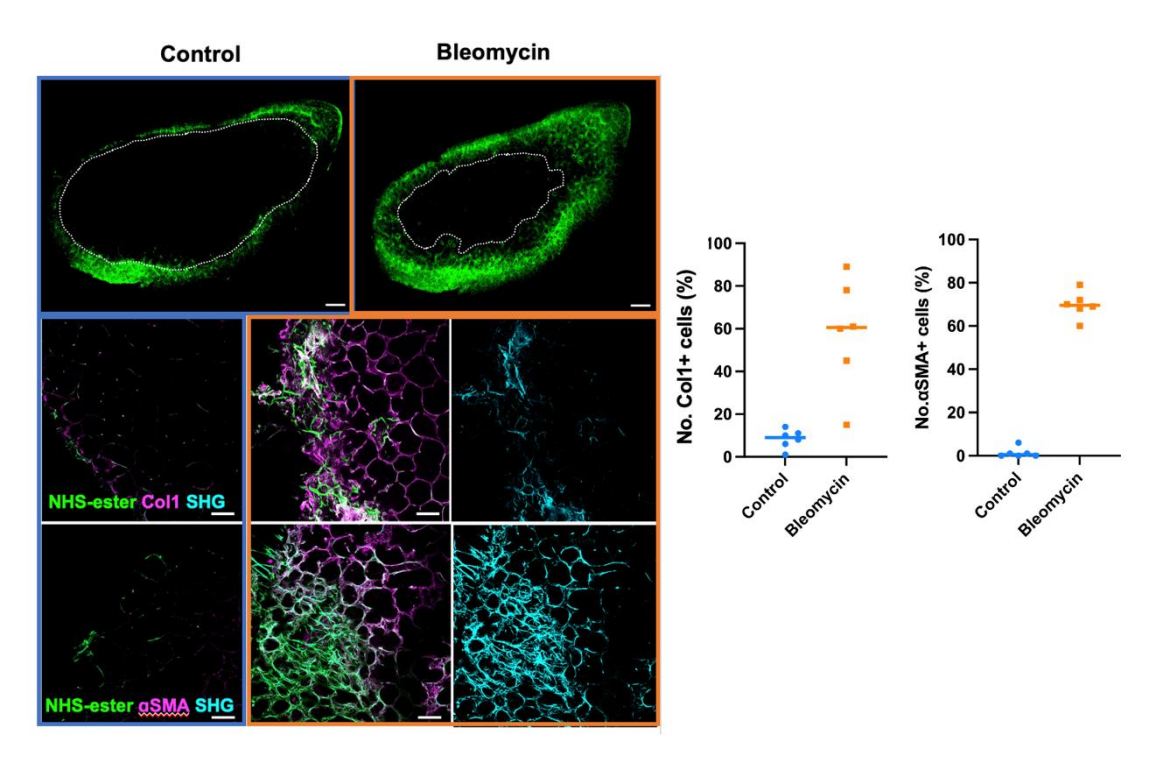


Figure 3.3 fibrotic markers signature in PCLS model.

The fluorescence results show the labeled pleural layer ECM (green), fibrotic marker (magenta) and Second harmonic signal (cyan). The statistical results show the positive rate of fibrotic marker cells. Scale bar is 2mm (top), 0.2mm (bottom).

3.2 Monocyte-derived macrophages adopt distinct responses signature in severe bleomycin model

3.2.1 Different clusters of lung macrophages

To investigate the function of distinct macrophage clusters during pulmonary fibrosis, we defined different cell populations by single-cell RNA sequencing methods. The database contains seven time points from day0, day3, day7, day10, day14, day21 and day28. These time points contain the initial stages of inflammation, the stage of fibrosis onset and the stage of fibrosis resolution. We detected two distinct macrophages clusters (Fig. 3.4a). Cluster 1 was defined as profibrotic macrophages, marked by Marco, Lgmn and Cd163. Cluster 2 scored highest for resolution macrophages, marked by Grn, Ctsb and Mrc1. To trace the number of distinct macrophages among the 7 timepoints, we recorded the percentage of cells, which showed that monocyte numbers were highest at day0 and continued to decline thereafter. Profibrotic macrophages started at less than 20%, peaked at 65% on day21, and then declined in number. Resolution-type macrophages remained low until day21, and then began to rise rapidly after day21, outnumbering profibrotic macrophages on day28 (Fig.3.4c). Our investigation revealed distinct expression patterns of markers MARCO and GRN, associated with profibrotic macrophages and resolution macrophages, respectively. To further validate these findings, we assessed the expression of activated macrophages in vitro.

Comparative analysis demonstrated that MARCO exhibited heightened expression levels in macrophages activated by LPS/IFNy, in contrast to unstimulated macrophages. Conversely, GRN demonstrated relatively elevated expression in macrophages stimulated by IL4/M-CSF (Fig.3.4d). These observations suggest that the macrophage subclusters identified from single-cell sequencing results can be recapitulated *in vitro* through these two treatment modalities.

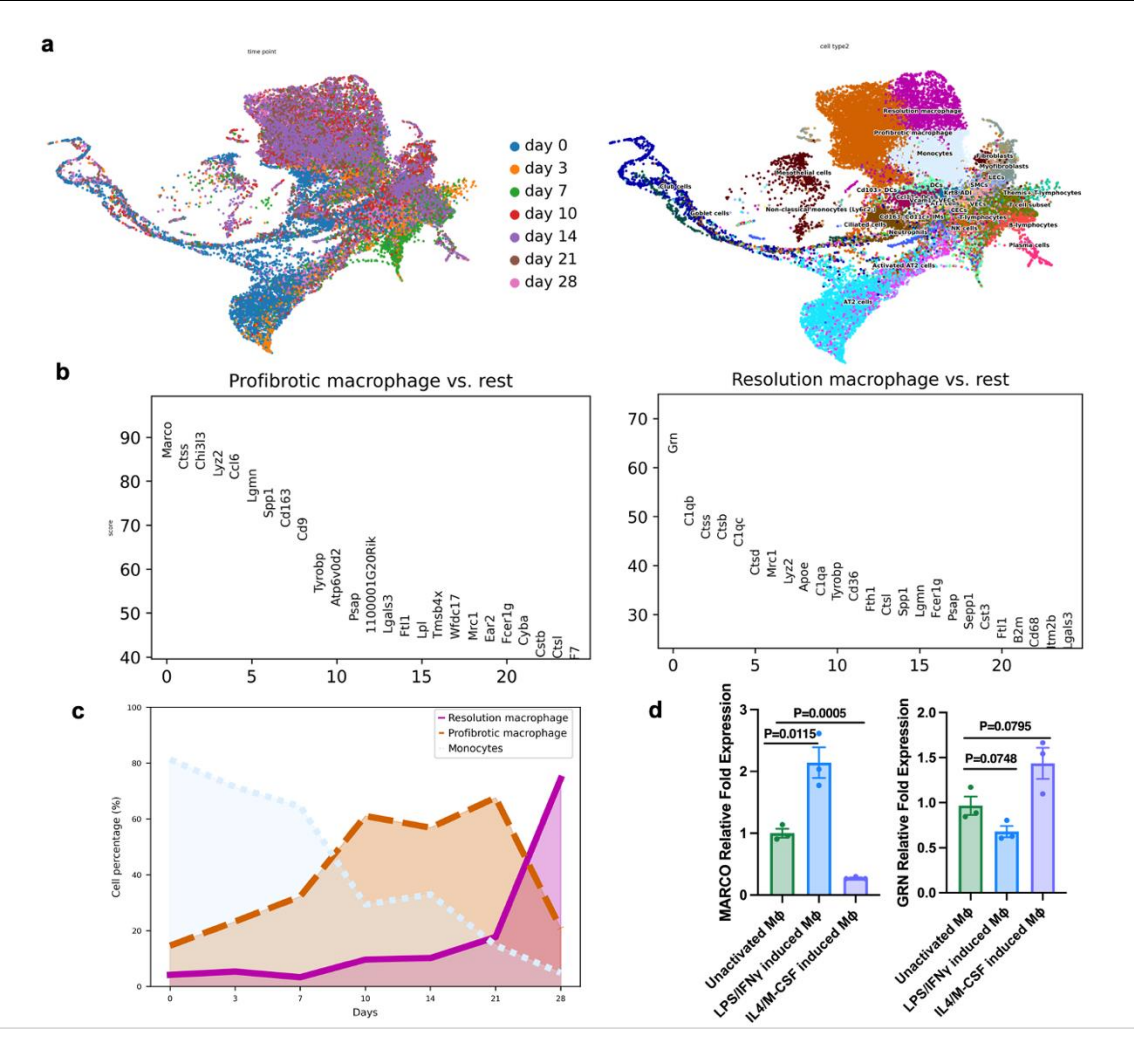


Figure 3.4 two macrophages subcluster in mouse IPF scRNA-seq.

a.All cell populations at 7 time points of single cell data, including two types of macrophage subpopulations. b. profibrotic and resolution macrophages' gene marker. c. Track the differential changes in the cell proportions of two macrophage subpopulations at different time points. d. qPCR results show the relative expression of two high-confidence markers in the Macrophages samples with different treatment.

3.2.2 Aggregation of macrophage subpopulations during different stages

Due to the limitation of single-cell RNA sequencing time points, we were unable to analyze the macrophage expression and distribution that tracked the subsequent day45 time points. Therefore we collected sections from lung bleomycin experiments at six time points to count the distribution of NHS-labeled signals and changes in the number of the two types of macrophages. The results of the sections showed that the green fluorescent protein signal began to egress inward after day0 and reached a maximum of 60% on day21, while it began to resolve on day28 and finally fell to 20%. Whereas the trend of

profibrotic macrophages was similar to that of labeled signals, which continued to rise during the early immunization phase (day7-day14), reaching a peak of 37% at day21 and dropping to 5% at day28. In contrast, resolution macrophages rose from day14 and remained at high expression levels on day45. These results implie that different macrophages exercise their specific functions in the inflammatory and repair phases, respectively.

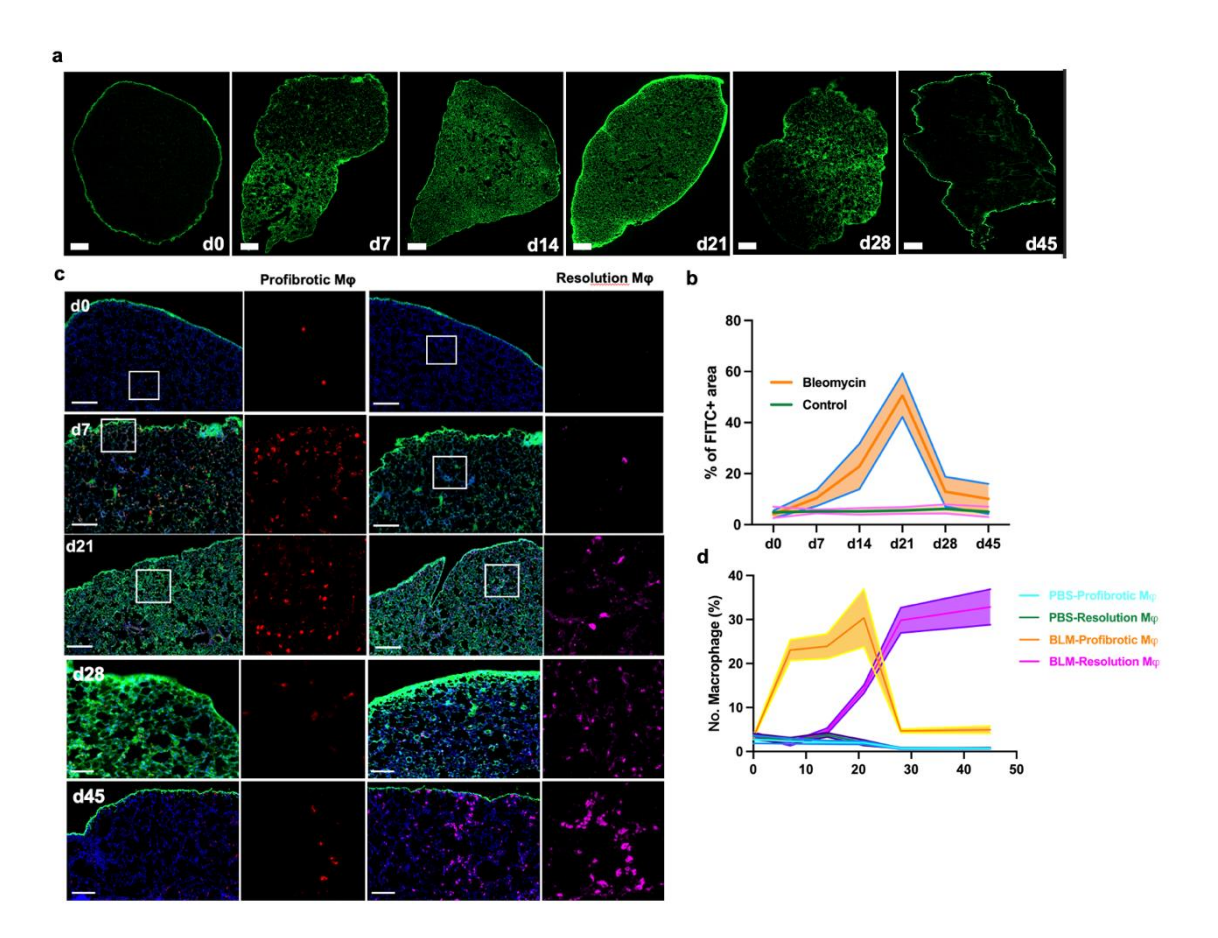


Figure 3.5 Profibrotic and resolution macrophage stages in the fibrosis process.

a. The fluorescence image shows the degree of diffuse inward movement of ECM in the pleural layer marked at different time points. b. Statistically analyze the average fluorescence intensity of the labeled protein (green) in the fluorescence photos at different time points. c. Changes in cell proportions of profibrotic (red) and resolution macrophage (magenta) at key time points. Scale bar is $100 \ \mu m$.

3.3 IPF triggers fibrosis-related profiles in macrophages

3.3.1 LPS/IFNy induces macrophages to promote the diffusion of labeled fibrotic macromolecules

According to the literature, LPS/IFNγ and IL4/M-CSF stimulation can differentiate macrophages into different activation states. here, we respectively added monocytes, inactive macrophages (M0), LPS/IFNγ induced macrophages (M1-like) and IL4/M-CSF stimulated macrophages (M2-like) onto PCLS lung explants, tracking changes in the thickness of NHS markers from day0, day3 to day5. The results showed that LPS/IFNγ induced macrophages showed fibrosis-promoting motility. We then co-cultured PCLS with M1-like for 3 days, after which we added separately monocytes, inactive macro-phage (M0), and IL4/M-CSF stimulated macrophages (M2-like). Tracing the NHS-labeled signals, it was found that the fibrosis moved inward when M1-like was added first for 3 days of co-culture, but the movement was suppressed after the addition of IL4/M-CSF-stimulated macrophages (M2-like) (Fig 3.6a). This result demonstrates that LPS/IFNγ-induced macrophages have the function of promoting the movement of fibrosis, while IL4/M-CSF-stimulated macrophages (M2-like) may exercise the opposite role.

To further explore the function of LPS/IFNy-induced macrophages, we screened potential targets such as Perlecan, MMPs, CD47, SLAMF5, CD36, and Progranulin based on single-cell sequencing results comparing the differentially expressed genes of probiotic macrophages and resolution macrophages. Specific inhibitors were added with to PCLS-macrophage co-cultures. Signal dynamic changes according to NHS labeling showed that the profibrotic macrophage group (F) was higher enrichment of fibrosis than the control group, and the amplitude of ECM movement was elevated by the addition of two inhibitors of Perlecan (heparan and chlorate). Whereas the addition of GM6001 and Isofraxidin inhibited inward fiber movement, which are inhibitors of MMPs and specific MMP7, respectively. Similarly, the addition of SLAMF5 inhibitor, CD47 inhibitor, and Progranulin recombinant protein inhibited the function of profibrotic macrophages. The difference in effect was not significant with the addition of SR-B3 inhibitor (Fig 3.6b). According to the group with the most statistically significant differences, profibrotic macrophage function was effected strongly by MMP7 and Perlecan, alluding to their mechanism of action.

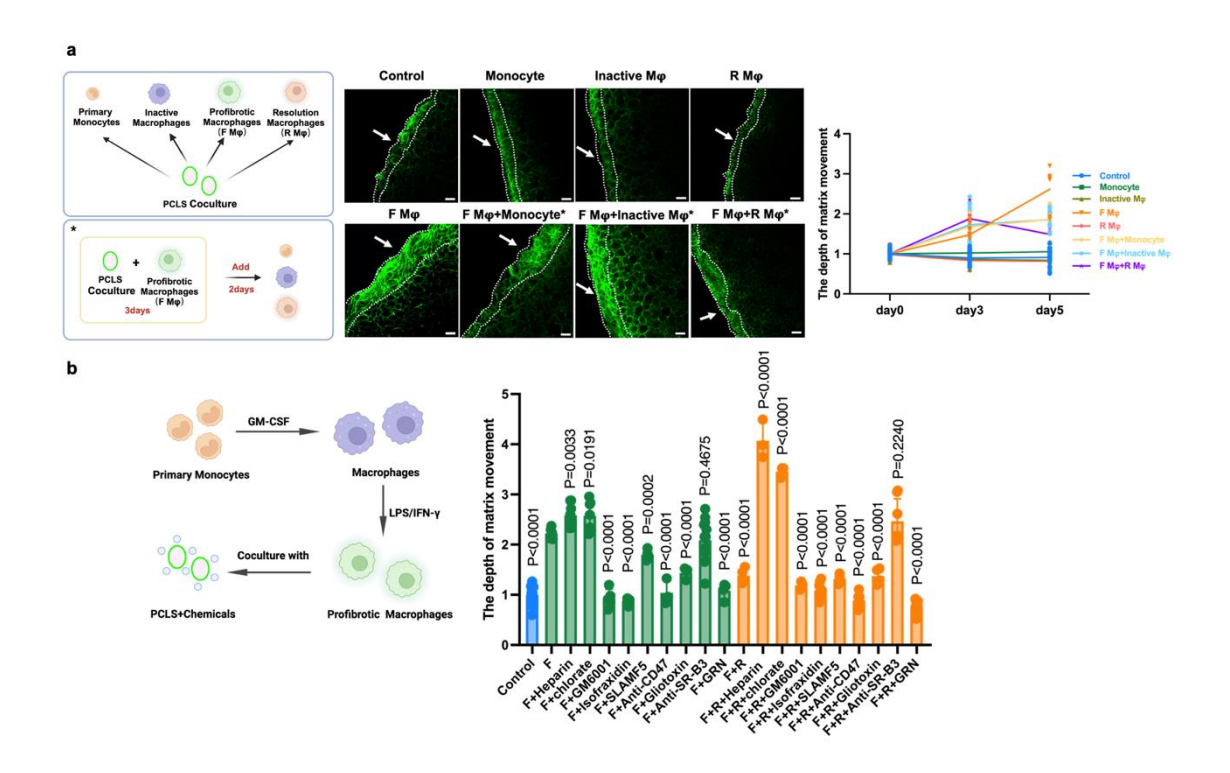


Figure 3.6 LPS/IFNγ-induced and IL4/M-CSF activated macrophages play different role in fibrotic matrix movement.

a.PCLS and cell co-culture experiment, the fluorescence image shows the changes in the pleural layer after single factors are added to cells and PCLS culture (upper layer 1 -5), two-factor analysis adds M1 group first and then other cell groups. Statistical analysis of changes in pleural layer thickness at different time points. b. Profibrotic macrophages differentiation method, drug-treated cell targets are co-cultured with PCLS, and matrix movement changes are counted. Scale bar is 0.2mm.

3.3.2 Profibrotic macrophage disrupts ECM structure through Perlecan and MMP7

According to the differential expression heat map of macrophages, profibrotic macrophages highly expressed MMP7. Based on the drug screen assay, Isofraxidin, specifically inhibits the expression of MMP7, which significantly impeded the function of profibrotic macrophage. Therefore we verified the effect of this drug by using *in vitro* bleomycin model. The results showed that inhibition of MMP7 secretion directly blocked the development of fibrosis stimulated by bleomycin (Fig 3.7a). We also verified that Perlecan is one of the important components of the lung basement membrane, which contains five functional structural domains, and we examined the distribution of different structural domains in healthy and diseased states. and the immunofluorescence staining

images verified that the distribution and expression of domain3 and domain5 was much higher in the bleomycin samples than in the control groups. This result implies that the two structural domains may be potential targets of action (Fig 3.7b). We co-localized MMP7 and the two key structural domains by immunofluorescence staining, and found that MMP7 and the two structural domains were highly expressed and nearly distributed in the bleomycin group (Fig 3.7c).

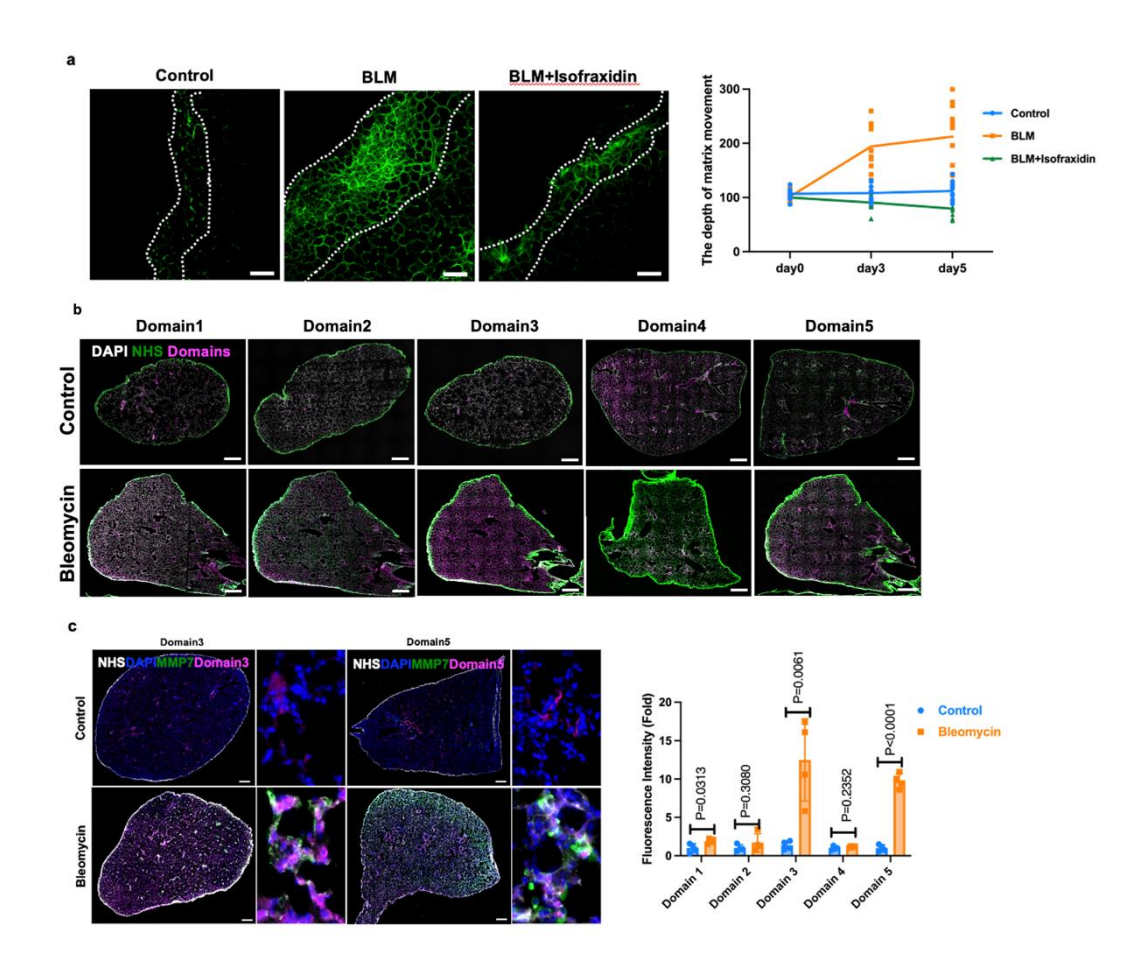


Figure 3.7 Effect of Profibrotic macrophage on lung perlecan.

a. Fluorescence photos show the results of treatment of fibrotic PCLS with the MMP7 inhibitor isofraxidin. Statistically track the movement changes of the matrix at different time points. b. Immunofluorescence shows the protein expression of the five domains of perlecan in the bleomycin sections and the control sections, and the average fluorescence intensity of the five domains in the sample was calculated. c. Fluorescence colocalization of MMP7 and two differentially accumulated domains. Scale bar is 10 mm.

3.4 IPF triggers self-repair regulators in macrophages

3.4.1 Resolution macrophages regulate affinity for ECM and phagocytosis through secretion of Progranulin

Based on our PCLS model of fibrosis, we added macrophages (R) activated by IL4/M-CSF alone to co-cultures with PCLS, which showed no significant difference from control. Subsequent addition of various inhibitor treatments was also not significant, except for the addition of the phagocytosis-associated inhibitor of SR-B3 which appeared to be significantly different. Addition of blocking CD47 antibody group and addition of Progranulin recombinant protein group showed enhanced inhibition of fibrosis spreading. Subsequently, a similar trend of results was observed in the group with resolution macrophage and various chemicals after 3 days of pretreatment with profibrotic macrophage (Fig. 3.8a). We thus hypothesized that the function exercised by resolution macrophage might be related to the phagocytic mechanism.

Based on the comparison of the significance of differences in the drug screening assay, the group with the addition of Progranulin showed enhanced repair function of resolution macrophages. Based on the differential gene expression, we found that resolution macrophages highly expressed Progranulin, so we verified the function of Progranulin in our PCLS fibrosis model. The results recorded that the spread of fibrosis was significantly inhibited by adding Progranulin recombinant protein to the bleomycin group. Statistical parallel comparison of the treatment effect with existing antifibrotic drugs Pirfenidone, Nintedanib and macrophage scavenger Chlodronate liposomes showed that the antifibrotic effect of Progranulin was significant (Fig3.8b).

ELISA comparing the difference in protein expression levels of Progranulin in different treatment groups showed that the highest expression was found in the group of macrophages activated by the addition of IL4/M-CSF to PCLS (Fig3.8c). To further validate the function of resolution macrophages, we designed cellular experiments in which Perlecan purified proteins were co-incubated with beads with FITC fluorescent signals, followed by addition of the beads to co-culture with IL4/M-CSF-activated macrophages. The control group was blank co-incubated with fluorescent beads, and fluorescent photographs showed that Perlecan protein-incubated bead group presented a stronger affinity to macrophages, and a greater number of beads were phagocytosed into the cells (Fig3.8d). From this, it can be inferred that resolution macrophages highly express Progranulin along with higher phagocytosis and affinity for Perlecan.

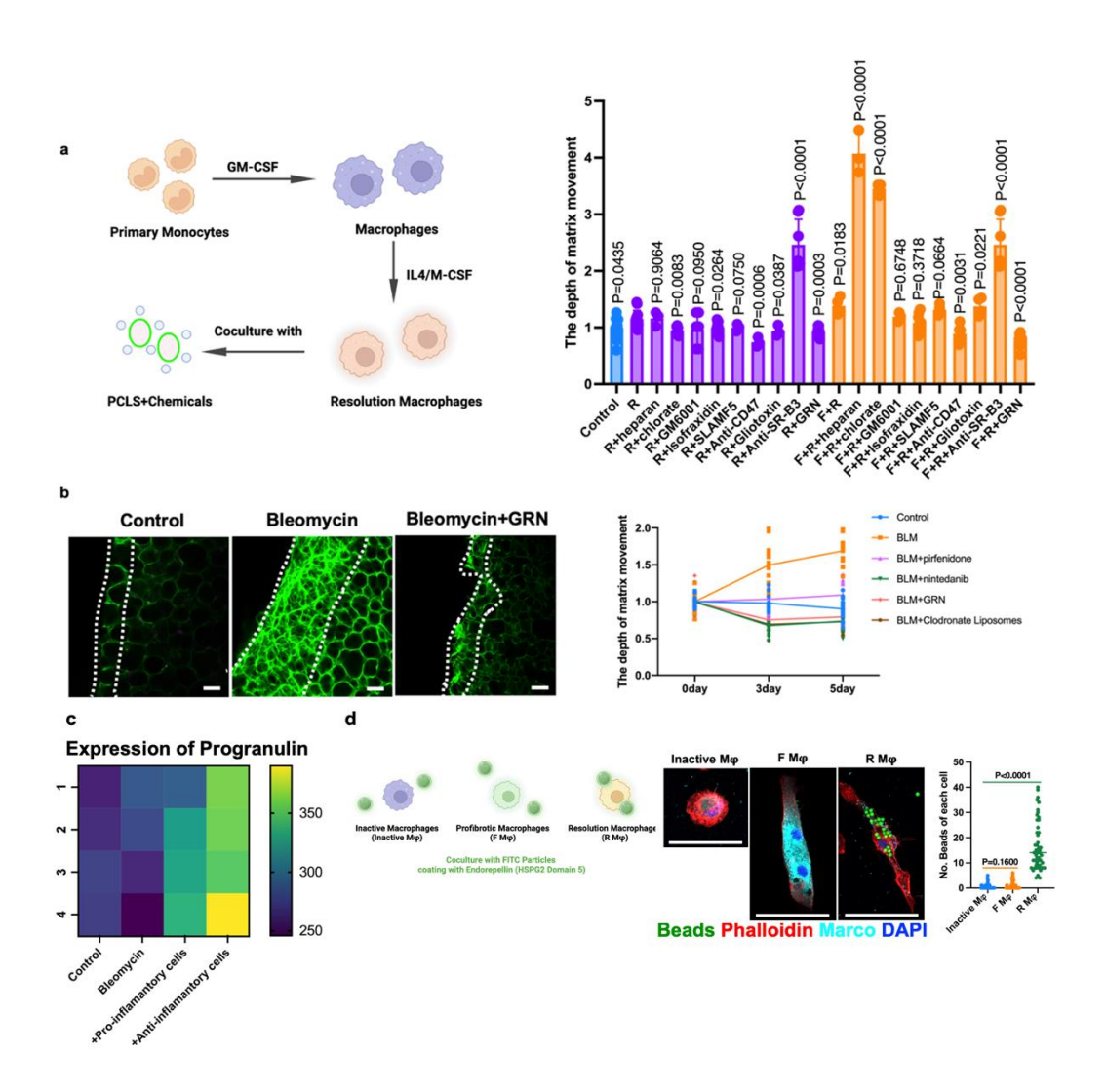


Figure 3.8 The role of resolution macrophages in pulmonary fibrosis.

a. Resolution macrophages differentiation process. Drug-treated macrophage targets were co-cultured with PCLS, and matrix movement distances were statistically compared. b. Fluorescence results show that GRN recombinant protein repairs fibrotic PCLS, and the data changes of each group at different time points are counted. Scale bar is 0.2 mm. c. ELISA test to compare the protein levels of GRN under different culture conditions of PCLS. d. The domain V domain protein of perlecan is wrapped with fluorescent beads and then incubated with resolution macrophages. The phagocytosis ability is detected by fluorescence microscopy, and the number of beads contained in each cell is counted. Scale bar is 2 μ m.

3.4.2 Prograunlin is a repair factor in the early fibrosis process

In order to verify the role of progranulin recombinant protein in the mouse *in vivo* model, we added Progranulin recombinant protein in the bleomycin experimental group twice via intratracheal instillation at day0 and day7 time points. We collected samples for sectioning to observe the lung fibrosis phenotypes at day21. The results showed that the level of lung fibrosis in mice after instilment of Progranulin recombinant protein was significantly lower than that in the group with Bleomycin alone (Fig3.9a), and the same result was verified by the Masson staining structure. We recorded the body weight of the mice daily from day0 to day21, and the Bleomycin group lost up to 10% of their body weight, while the Bleomycin plus Progranulin recombinant protein group lost up to 2% of their body weight (Fig3.9b). Combined with the statistics of assessing the level of pulmonary fibrosis in the sections, the level of fibrosis in the Progranulin plus Progranulin recombinant protein samples were dramaticly lower than that in the Bleomycin samples. This shows that early addition of Progranulin significantly inhibited fibrosis development.

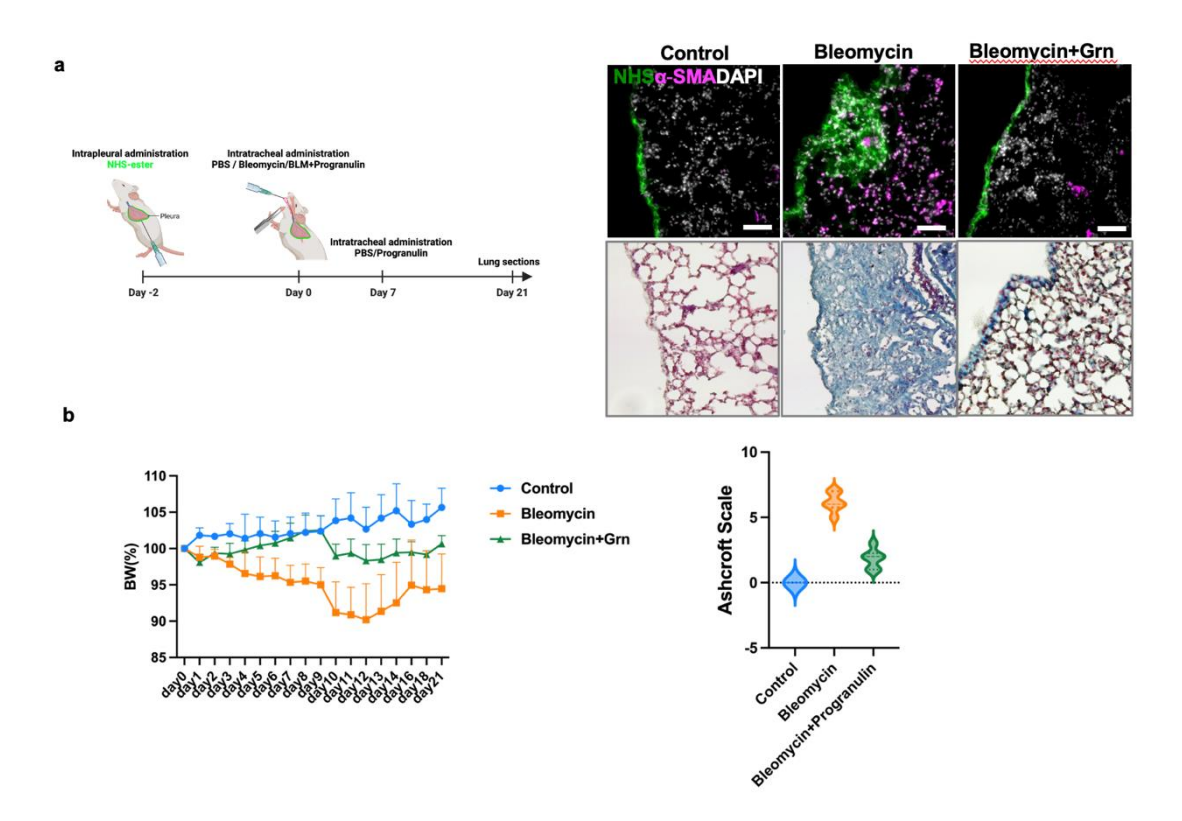


Figure 3.9 Progranulin regulates early pulmonary fibrosis levels.

a. Animal pulmonary fibrosis model, progranulin was perfused on day0 and day7 respectively. Staining of day21 sample sections shows the level of fibrosis. b. Record the weight changes of mice in each group from day 0 to day 21, and evaluate the fibrosis level of each group based on the Masson staining results. Scale bar is 100 µm.

3.5 Resolution macrophages in human IPF and ILD

3.5.1 Human Macrophages clusters in scRNA-seq

Comparing the single cell data of lung tissue in human IPF and non-lesional areas, and combining the distribution of the two types of samples, we divided four macrophage sub-populations, among which Progranulin showed higher expression in healthy lung tissue, while MMP7 was expressed in healthy lung tissue. High expression in IPF samples was mainly concentrated in large cluster 1 macrophages (Fig. 3.10). This result laid the foundation for subsequent in-depth exploration of Progranulin and MMP7.

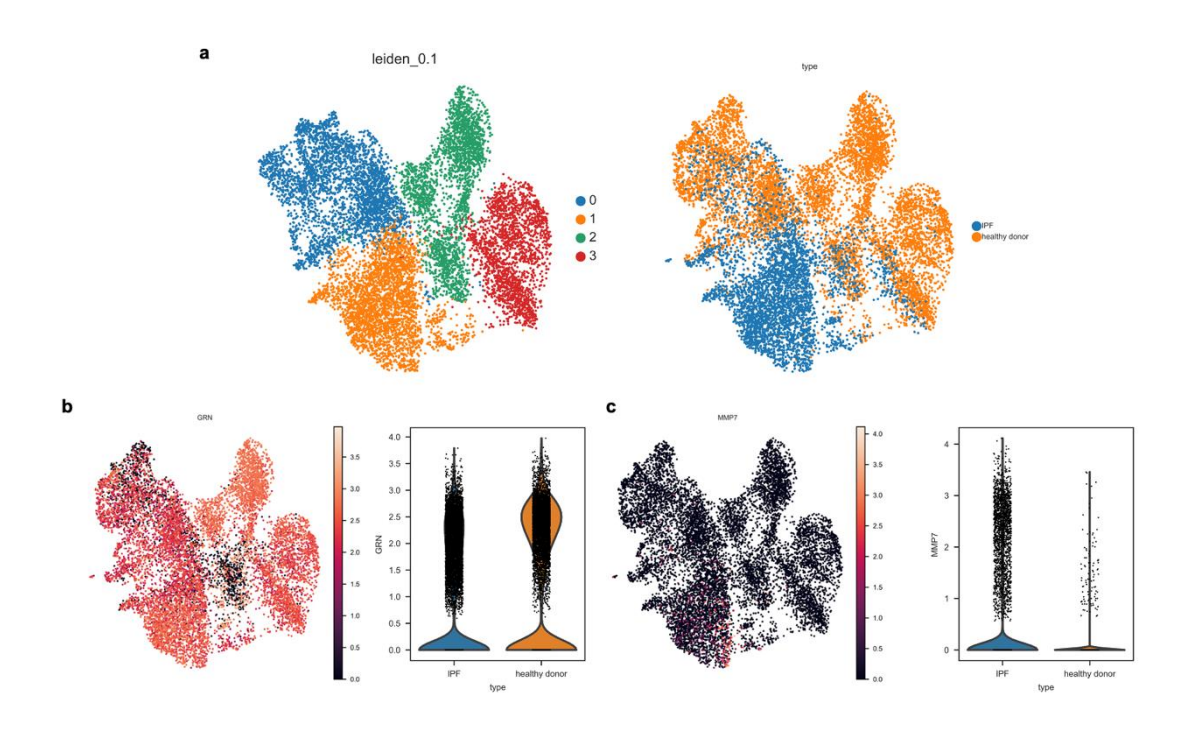


Figure 3.10 Macrophage population in human IPF.

a. Comparison of macrophage populations in human lung IPF and healthy samples. b. Progranulin expression in IPF and non-lesional lung tissue. c. Expression of MMP7 in IPF and non-lesional lung tissue.

3.5.2 Distribution of human lung fibrosis and proteomic differential phenotypes

According to the results of Masson's trichrome staining, the lung tissue of human IPF patients showed a thickening of the pleural layer, with blue collagen extending inward and connecting to fibrotic patches in deep lung interstitium (Fig3.10a). This part of the diseased tissue was significantly different from the healthy lung tissue. We analyzed the

proteomes of 11 human IPF lung samples and 11 healthy human lung samples, focusing on the cumulative abundance of peptides in the different structural domains of Perlecan and the statistics of the shear sites. We found that domain1, domain3 and domain5 of Perlecan were highly enriched in the bleomycin samples instead of healthy one (Fig3.10a). And the shear sites of domain3 and domain5 were more in the Bleomycin group. This result also implies that the structural changes of Perlecan are one of potential targets to regulate pulmonary fibrosis.

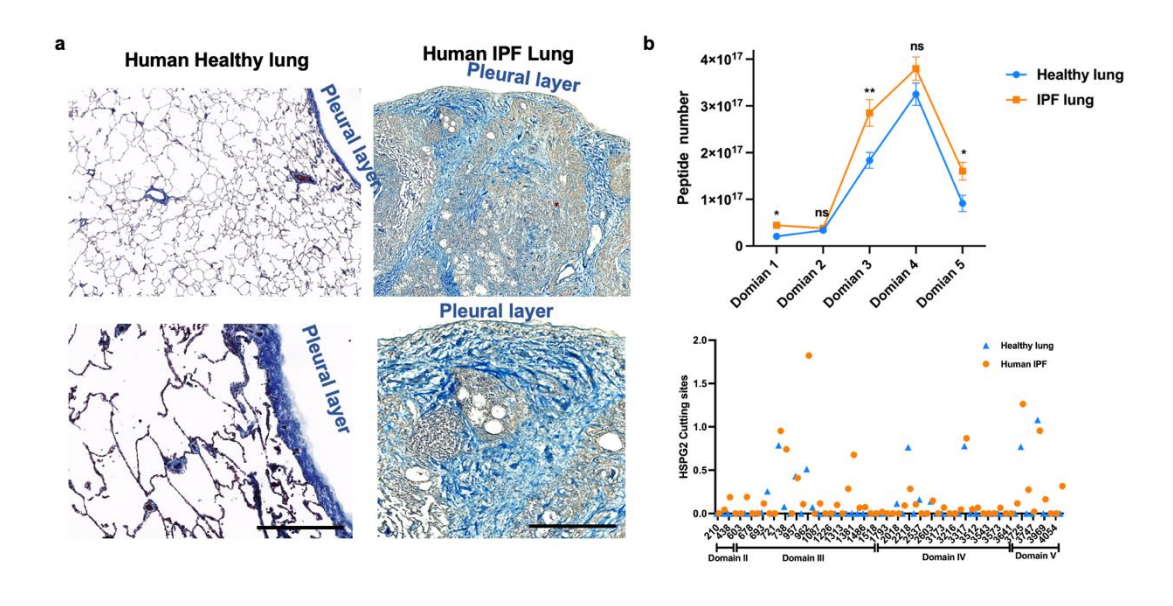


Figure 3.11 Distribution of human pleural layer ECM in IPF lesions.

a.Masson staining shows differences in collagen deposition in healthy and IPF lung tissue. b. Statistics on the accumulation of peptide abundances of the five domains of human perlecan and the differences in the number of cleavage sites in different domains. Scale bar is $200 \ \mu m$.

3.5.3 Distribution of Profibrotic macrophages and resolution macrophages in human IPF samples

To explore whether the two clusters of macrophages with different functions defined in the mouse model are compatible and applicable to the human lung tissue microenvironment, we traced the distribution of the two classes of macrophages by immunofluorescence staining in human healthy and diseased samples. Perlecan is an important component of the basement membrane in the human lung tissue but it is locally overexpressed in a group of human IPF samples. Profibrotic macrophages were highly expressed in its periphery, and the expression of this cell population was higher than in the

present disease samples. The resolution macrophages, on the other hand, highly express Progranulin, which is expressed in the healthy group and also in the IPF tissue, and tightly associated with areas rich in Perlecan protein expression. Immunolocalization of Progranulin and CD206 in IPF samples showed high co-expression of positive cells.

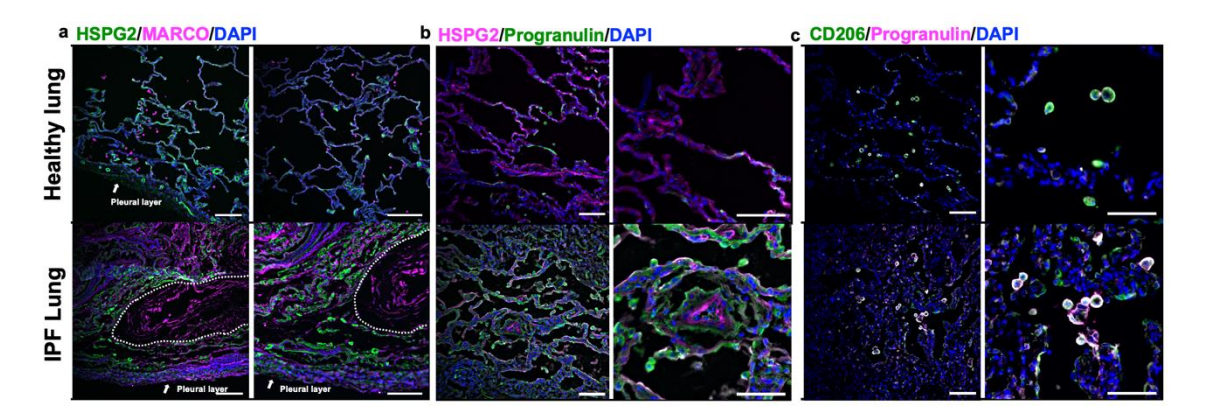


Figure 3.11 marker signals in human IPF.

a. Immunofluorescence photo showing co-localization of Perlecan/HSPG2 and profibrotic macrophage marker. b. Immunofluorescence results show co-localization of Perlecan/HSPG2 and resolution macrophage. c. Immunofluorescence resolution macrophage and CD206 marker co-localize. Scale bar is 100 µm.

4. Discussion

Lung structure injury and excessive deposition of collagen are common lesions in mouse and human lung fibrosis, and this pathological feature is often found in the later stages of the disease. According to our experimental design, the ECM structural proteins of the lung were labeled at the pleural surface, and coupled with the fibrosis stimulator Bleomycin, we observed that the fibrous components of the pleural layer also participated in and formed part of the pulmonary fibrosis lesions. According to the results, the labeled ECM in the pleural layer gradually accumulates inward along with the process of fibrosis. This phenomenon has an important impact on exploring the formation of fibrosis symptoms. This also confirms that the lesions in patients with pulmonary fibrosis are always related to the pleural layer (Lynch et al., 2018; Martinez et al., 2017). Previous studies by our group have found, in other tissue models of scars and fibrosis, that ECM movements are directly involved in repair and influx into the lesion in skin wound models and peritoneal adhesion models (Correa-Gallegos et al., 2019; Correa-Gallegos et al., 2023; Fischer et al., 2022). This study reveals the impact and role of dynamic changes in ECM based on the pleural layer on the lung microenvironment, which has clinical significance for the research and diagnosis of pulmonary fibrosis.

We found that macrophages are closely involved in the regulation of pulmonary fibrosis, and this refined classification based on their functions has an important impact on tracking the accumulation of their cell populations at different stages. Our data shows that two types of macrophage subpopulations have direct effects on lung pleura ECM structure, thereby participating in the regulation of pulmonary fibrosis. The root of this process is the multiple plasticity functions of macrophages, which form two types of distinct effects on the fibrosis process in the face of varying degrees of microenvironmental changes. Among them, a type of profibrotic macrophages can play a dominant role during inflammation. Profibrotic macrophages secrete pro-inflammatory factors, increase cell metabolism, secrete copious amounts of MMP7, which destroy the basic structure of the lung ECM, and lay the foundation for fiber movement. Previous studies have shown that MMP7 assists cancer cell invasion by cleaving Glycoslylated and basement membrane bound Perlecan, and the enriched domain IV fragment of Perlecan induces cancer cell aggregation (Grindel et al., 2014; Melrose, 2020). However, given that domain IV of Perlecan is also highly expressed in normal tissues, the difference between control and Bleomycin group in immunofluorescence staining results is not significant. But our singlecell sequencing and proteomic data show that Perlecan differentially accumulates in domain III and domain V in pulmonary fibrosis samples of mice and human. Domain III exhibits pro-angiogenic properties, contributing to extracellular matrix (ECM) organization. Moreover, the endogenous release of domain V by matrix metalloproteinases (MMPs) from full-length Perlecan facilitates tissue repair by engaging in angiogenic interactions with various element such as VEGF, VEGF-Receptor 2 (VEGF-R2), α2β1 integrin, ECM-1, and progranulin (Arikawa-Hirasawa, 2022; Hayes et al., 2022; Tanimoto et al., 2017; Wilson, 2022). Our results demonstrate that repair macrophages highly express Progranulin, and Progranulin administration in the early stages decreases pulmonary fibrosis in animal models, indicating the recombinant protein has a significant effect on inhibiting the level of fibrosis. Our results demonstrate that the function of this secreted protein is not only to regulate anti-inflammatory levels, but also to have high affinity for Domain V and promote the clearance of beads coated with Domain V protein, suggesting that repair macrophages regulate fibrotic microenvironment through Progranulin.

In human IPF single cell sequencing results and tissue section staining results, the expression of Progranulin in healthy tissues in non-lesion areas was higher than that in pulmonary fibrosis tissue areas. Studies have tracked the difference in Progranulin levels in the blood of IPF, ILD and healthy patients. The results show that the Progranulin levels in healthy and ILD patients are higher than those in IPF (Liu et al., 2021; Tanaka et al., 2015; Toth et al., 2023; Xie et al., 2021; Zhao et al., 2024). This result is consistent with our speculation. Progranulin is involved in regulating early pulmonary fibrosis levels and contributes by inhibiting the process of pulmonary fibrosis. Our results show that human healthy lung tissue and IPF tissue have differential accumulation of Domain III and Domain V of Perlecan, which is consistent with the results of the fibrosis model in mice. This suggests that mouse and human macrophages exert an identical molecular mechanism in pulmonary fibrosis.

An crucial consideration in this study is the limited number of biological replicates in our *in vivo* experiments. Nonetheless, despite this limitation, multiple results such as *ex vivo* PCLS fibrosis models, cell differentiation stimulation co-culture models, and support from single-cell sequencing and proteomic analysis, indicate the important role of both macrophage subsets in the process of pulmonary fibrosis. Although a large number of studies have classified M1 and M2 macrophage groups according to stimulus, the macrophages of those group still have different functional roles (Zhang et al., 2018). Our single-cell sequencing data indicates that resolution macrophages are directly differentiated from monocytes and are involved in regulating phagocytosis and anti-inflammatory levels.

Profibrotic macrophages differentiate from non-classical monocytes and participate in the regulation of metallopeptidase activity and heparin binding activity. Further, our data indicates that profibrotic macrophages directly destroy the Perlecan structure by secreting MMP7 and promoting the movement of cells and fiber structures from the pleural ECM. Differential accumulation domain V of Perlecan can enhance the binding effect of Progranulin. Resolution macrophages highly express Progranulin to regulate the immune level of the lung microenvironment. It can also enhance the affinity to Perlecan domain V, thereby riveting the broken ECM structure, and clearing the specific excessive accumulation of ECM components.

These results have important clinical implications because different subtypes of macrophages can directly determine the stage of pulmonary fibrosis progression and characterize the body's self-repair ability. In particular, both macrophages anchor a specific Perlecan structural component in the ECM that is abnormally accumulated not only in pulmonary fibrotic disease but also in human lung tumor samples. Pathological analysis of the differential accumulation of different structural domains of Perlecan can determine the stage of lung damage. Treatments tailored to modulate early stages of pulmonary fibrosis would be beneficial by directly stimulating repair macrophages to inhibit profibrotic development and early clear excess collagen deposition to prevent excessive damage to lung structures.

5. Conclusiones and Outlook

This thesis reveals that two types of macrophage subpopulations, profibrotic macrophages and resolution macrophages, can promote or inhibit the movement of pulmonary fibrosis by directly acting on the structural components of lung pleural ECM. This study demonstrates the strong plasticity of macrophages and defines their specific functions at different stages of fibrosis. Profibrotic macrophages destroy the Perlecan structure in the lung ECM by secreting MMP7 and promoting the influx of ECM fibers in the pleural layer to form a part of the fibrotic lesions. Resolution macrophages have a strong affinity for the conserved domain V of Perlecan by secreting Progranulin, which improves/activates its ability to phagocytose and clear specific ECM structures.

In human lung tissue, Progranulin was highly expressed in non-lesion lung tissue and in ILD patient lung tissue compared with IPF samples. This also implies that Progranulin is a potential target for self-repair. Based on the current understanding, we need to continue to verify the role of Progranulin and MMP7 in the fibrosis microenvironment of human lung tissue, compare the regulatory effects of Progranulin and MMP7 on fibrosis at different concentration levels, and explore more possibilities for macrophages to lung ECM direct effect.

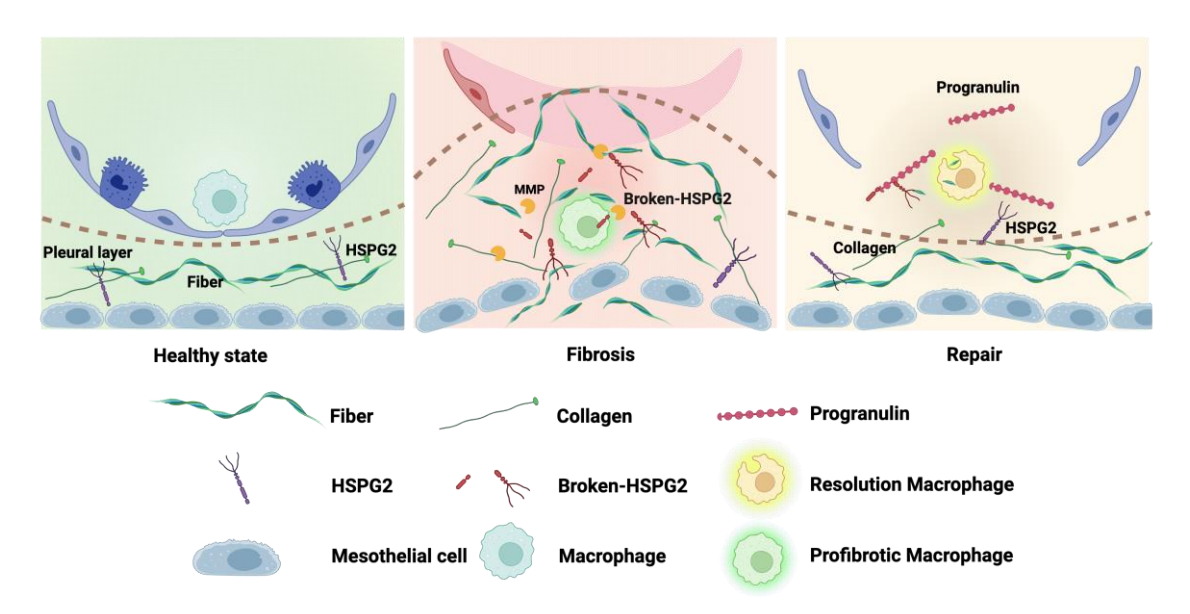


Figure 5.1 Revised model of pulmonary fibrosis.

Profibrotic macrophages directly destroy the lung ECM structure and promote inward migration of pleural fibers. Repair macrophages regulate the level of pneumonia by secreting progranulin and improve phagocytosis of ECM structures.

References

- Abdalhameid, E., Abd El-Haleim, E. A., Abdelsalam, R. M., Georgy, G. S., Fawzy, H. M., & Kenawy, S. A. (2023). Cinnamic acid mitigates methotrexate-induced lung fibrosis in rats: comparative study with pirfenidone. *Naunyn Schmiedebergs Arch Pharmacol*. https://doi.org/10.1007/s00210-023-02652-w
- Abuserewa, S. T., Duff, R., & Becker, G. (2021). Treatment of Idiopathic Pulmonary Fibrosis. *Cureus*, 13(5), e15360. https://doi.org/10.7759/cureus.15360
- Adams, S. J., Stone, E., Baldwin, D. R., Vliegenthart, R., Lee, P., & Fintelmann, F. J. (2023). Lung cancer screening. *Lancet*, 401(10374), 390-408. https://doi.org/10.1016/S0140-6736(22)01694-4
- Aegerter, H., Lambrecht, B. N., & Jakubzick, C. V. (2022). Biology of lung macrophages in health and disease. *Immunity*, *55*(9), 1564-1580. https://doi.org/10.1016/j.immuni.2022.08.010
- Agostini, C., & Gurrieri, C. (2006). Chemokine/cytokine cocktail in idiopathic pulmonary fibrosis. *Proc Am Thorac Soc*, *3*(4), 357-363. https://doi.org/10.1513/pats.200601-010TK
- Akram, K. M., Yates, L. L., Mongey, R., Rothery, S., Gaboriau, D. C. A., Sanderson, J., Hind, M., Griffiths, M., & Dean, C. H. (2019). Live imaging of alveologenesis in precision-cut lung slices reveals dynamic epithelial cell behaviour. *Nat Commun*, 10(1), 1178. https://doi.org/10.1038/s41467-019-09067-3
- Alsafadi, H. N., Staab-Weijnitz, C. A., Lehmann, M., Lindner, M., Peschel, B., Konigshoff, M., & Wagner, D. E. (2017). An ex vivo model to induce early fibrosis-like changes in human precision-cut lung slices. *Am J Physiol Lung Cell Mol Physiol*, 312(6), L896-L902. https://doi.org/10.1152/ajplung.00084.2017
- Arikawa-Hirasawa, E. (2022). Impact of the heparan sulfate proteoglycan perlecan on human disease and health. *Am J Physiol Cell Physiol*, 322(6), C1117-C1122. https://doi.org/10.1152/ajpcell.00113.2022
- Arora, S., Dev, K., Agarwal, B., Das, P., & Syed, M. A. (2018). Macrophages: Their role, activation and polarization in pulmonary diseases. *Immunobiology*, 223(4-5), 383-396. https://doi.org/10.1016/j.imbio.2017.11.001
- Bain, C. C., Bravo-Blas, A., Scott, C. L., Perdiguero, E. G., Geissmann, F., Henri, S., Malissen, B., Osborne, L. C., Artis, D., & Mowat, A. M. (2014). Constant replenishment from circulating monocytes maintains the macrophage pool in the intestine of adult mice. *Nat Immunol*, 15(10), 929-937. https://doi.org/10.1038/ni.2967
- Bain, C. C., & MacDonald, A. S. (2022). The impact of the lung environment on macrophage development, activation and function: diversity in the face of adversity. *Mucosal Immunol*, 15(2), 223-234. https://doi.org/10.1038/s41385-021-00480-w
- Bauer, Y., White, E. S., de Bernard, S., Cornelisse, P., Leconte, I., Morganti, A., Roux, S., & Nayler, O. (2017). MMP-7 is a predictive biomarker of disease progression in patients with idiopathic pulmonary fibrosis. *ERJ Open Res*, 3(1). https://doi.org/10.1183/23120541.00074-2016
- Bergen, V., Lange, M., Peidli, S., Wolf, F. A., & Theis, F. J. (2020). Generalizing RNA velocity to transient cell states through dynamical modeling. *Nat Biotechnol*, 38(12), 1408-1414. https://doi.org/10.1038/s41587-020-0591-3
- Biswas, S. K., & Mantovani, A. (2010). Macrophage plasticity and interaction with lymphocyte subsets: cancer as a paradigm. *Nat Immunol*, 11(10), 889-896. https://doi.org/10.1038/ni.1937
- Bosurgi, L., Cao, Y. G., Cabeza-Cabrerizo, M., Tucci, A., Hughes, L. D., Kong, Y., Weinstein, J. S., Licona-Limon, P., Schmid, E. T., Pelorosso, F., Gagliani, N., Craft, J. E., Flavell, R. A., Ghosh, S., & Rothlin, C. V. (2017). Macrophage function in tissue repair and remodeling requires IL-4 or IL-13 with apoptotic cells. *Science*, *356*(6342), 1072-1076. https://doi.org/10.1126/science.aai8132
- Cedilak, M., Banjanac, M., Belamaric, D., Paravic Radicevic, A., Faraho, I., Ilic, K., Cuzic, S., Glojnaric, I., Erakovic Haber, V., & Bosnar, M. (2019). Precision-cut lung slices from

- bleomycin treated animals as a model for testing potential therapies for idiopathic pulmonary fibrosis. *Pulm Pharmacol Ther*, *55*, 75-83. https://doi.org/10.1016/j.pupt.2019.02.005
- Chakarov, S., Lim, H. Y., Tan, L., Lim, S. Y., See, P., Lum, J., Zhang, X. M., Foo, S., Nakamizo, S., Duan, K., Kong, W. T., Gentek, R., Balachander, A., Carbajo, D., Bleriot, C., Malleret, B., Tam, J. K. C., Baig, S., Shabeer, M., . . . Ginhoux, F. (2019). Two distinct interstitial macrophage populations coexist across tissues in specific subtissular niches. *Science*, 363(6432). https://doi.org/10.1126/science.aau0964
- Chen, Y. Q., Wang, C. J., Xie, K., Lei, M., Chai, Y. S., Xu, F., & Lin, S. H. (2020). Progranulin Improves Acute Lung Injury through Regulating the Differentiation of Regulatory T Cells and Interleukin-10 Immunomodulation to Promote Macrophage Polarization. *Mediators Inflamm*, 2020, 9704327. https://doi.org/10.1155/2020/9704327
- Christenson, S. A., Smith, B. M., Bafadhel, M., & Putcha, N. (2022). Chronic obstructive pulmonary disease. *Lancet*, 399(10342), 2227-2242. https://doi.org/10.1016/S0140-6736(22)00470-6
- Correa-Gallegos, D., Jiang, D., Christ, S., Ramesh, P., Ye, H., Wannemacher, J., Kalgudde Gopal, S., Yu, Q., Aichler, M., Walch, A., Mirastschijski, U., Volz, T., & Rinkevich, Y. (2019). Patch repair of deep wounds by mobilized fascia. *nature*, *576*(7786), 287-292. https://doi.org/10.1038/s41586-019-1794-y
- Correa-Gallegos, D., Ye, H., Dasgupta, B., Sardogan, A., Kadri, S., Kandi, R., Dai, R., Lin, Y., Kopplin, R., Shenai, D. S., Wannemacher, J., Ichijo, R., Jiang, D., Strunz, M., Ansari, M., Angelidis, I., Schiller, H. B., Volz, T., Machens, H. G., & Rinkevich, Y. (2023). CD201(+) fascia progenitors choreograph injury repair. *nature*, *623*(7988), 792-802. https://doi.org/10.1038/s41586-023-06725-x
- Curran, C. S., Bolig, T., & Torabi-Parizi, P. (2018). Mechanisms and Targeted Therapies for Pseudomonas aeruginosa Lung Infection. *Am J Respir Crit Care Med*, 197(6), 708-727. https://doi.org/10.1164/rccm.201705-1043SO
- Della Latta, V., Cecchettini, A., Del Ry, S., & Morales, M. A. (2015). Bleomycin in the setting of lung fibrosis induction: From biological mechanisms to counteractions. *Pharmacol Res*, 97, 122-130. https://doi.org/10.1016/j.phrs.2015.04.012
- Desch, A. N., Gibbings, S. L., Goyal, R., Kolde, R., Bednarek, J., Bruno, T., Slansky, J. E., Jacobelli, J., Mason, R., Ito, Y., Messier, E., Randolph, G. J., Prabagar, M., Atif, S. M., Segura, E., Xavier, R. J., Bratton, D. L., Janssen, W. J., Henson, P. M., & Jakubzick, C. V. (2016). Flow Cytometric Analysis of Mononuclear Phagocytes in Nondiseased Human Lung and Lung-Draining Lymph Nodes. *Am J Respir Crit Care Med*, *193*(6), 614-626. https://doi.org/10.1164/rccm.201507-1376OC
- Dharmarajan, K., Wang, Y., Lin, Z., Normand, S. T., Ross, J. S., Horwitz, L. I., Desai, N. R., Suter, L. G., Drye, E. E., Bernheim, S. M., & Krumholz, H. M. (2017). Association of Changing Hospital Readmission Rates With Mortality Rates After Hospital Discharge. *JAMA*, 318(3), 270-278. https://doi.org/10.1001/jama.2017.8444
- Di Martino, E., Provenzani, A., Vitulo, P., & Polidori, P. (2021). Systematic Review and Metaanalysis of Pirfenidone, Nintedanib, and Pamrevlumab for the Treatment of Idiopathic Pulmonary Fibrosis. *Ann Pharmacother*, *55*(6), 723-731. https://doi.org/10.1177/1060028020964451
- Dick, S. A., Wong, A., Hamidzada, H., Nejat, S., Nechanitzky, R., Vohra, S., Mueller, B., Zaman, R., Kantores, C., Aronoff, L., Momen, A., Nechanitzky, D., Li, W. Y., Ramachandran, P., Crome, S. Q., Becher, B., Cybulsky, M. I., Billia, F., Keshavjee, S., . . . Epelman, S. (2022). Three tissue resident macrophage subsets coexist across organs with conserved origins and life cycles. *Sci Immunol*, 7(67), eabf7777. https://doi.org/10.1126/sciimmunol.abf7777
- DuFort, C. C., Paszek, M. J., & Weaver, V. M. (2011). Balancing forces: architectural control of mechanotransduction. *Nat Rev Mol Cell Biol*, 12(5), 308-319. https://doi.org/10.1038/nrm3112
- Duitman JanWillem, 2,* Cong Lin,3 Sophie Moog,1,2 Madeleine Jaillet,1,2 Yves Castier,4 Aurélie Cazes,4 Keren S. Borensztajn,5 Bruno Crestani,1,2,4 and C. Arnold Spek3. (2018).

- CCAAT/enhancer binding protein delta (C/EBPδ) deficiency does not affect bleomycininduced pulmonary fibrosis. *J Clin Transl Res.*
- Duscher, D., Maan, Z. N., Wong, V. W., Rennert, R. C., Januszyk, M., Rodrigues, M., Hu, M., Whitmore, A. J., Whittam, A. J., Longaker, M. T., & Gurtner, G. C. (2014). Mechanotransduction and fibrosis. *J Biomech*, 47(9), 1997-2005. https://doi.org/10.1016/j.jbiomech.2014.03.031
- Eaton, T., Lewis, C., Young, P., Kennedy, Y., Garrett, J. E., & Kolbe, J. (2004). Long-term oxygen therapy improves health-related quality of life. *Respir Med*, *98*(4), 285-293. https://doi.org/10.1016/j.rmed.2003.10.008
- Epelman, S., Lavine, K. J., Beaudin, A. E., Sojka, D. K., Carrero, J. A., Calderon, B., Brija, T., Gautier, E. L., Ivanov, S., Satpathy, A. T., Schilling, J. D., Schwendener, R., Sergin, I., Razani, B., Forsberg, E. C., Yokoyama, W. M., Unanue, E. R., Colonna, M., Randolph, G. J., & Mann, D. L. (2014). Embryonic and adult-derived resident cardiac macrophages are maintained through distinct mechanisms at steady state and during inflammation. *Immunity*, *40*(1), 91-104. https://doi.org/10.1016/j.immuni.2013.11.019
- Epelman, S., Lavine, K. J., & Randolph, G. J. (2014). Origin and functions of tissue macrophages. *Immunity*, 41(1), 21-35. https://doi.org/10.1016/j.immuni.2014.06.013
- Fischer, A., Wannemacher, J., Christ, S., Koopmans, T., Kadri, S., Zhao, J., Gouda, M., Ye, H., Muck-Hausl, M., Krenn, P. W., Machens, H. G., Fassler, R., Neumann, P. A., Hauck, S. M., & Rinkevich, Y. (2022). Neutrophils direct preexisting matrix to initiate repair in damaged tissues. *Nat Immunol*, 23(4), 518-531. https://doi.org/10.1038/s41590-022-01166-6
- Flaherty, K. R., Fell, C. D., Huggins, J. T., Nunes, H., Sussman, R., Valenzuela, C., Petzinger, U., Stauffer, J. L., Gilberg, F., Bengus, M., & Wijsenbeek, M. (2018). Safety of nintedanib added to pirfenidone treatment for idiopathic pulmonary fibrosis. *Eur Respir J*, *52*(2). https://doi.org/10.1183/13993003.00230-2018
- Fragoulis, G. E., Nikiphorou, E., Larsen, J., Korsten, P., & Conway, R. (2019). Methotrexate-Associated Pneumonitis and Rheumatoid Arthritis-Interstitial Lung Disease: Current Concepts for the Diagnosis and Treatment. *Front Med (Lausanne)*, *6*, 238. https://doi.org/10.3389/fmed.2019.00238
- Francois, A., Gombault, A., Villeret, B., Alsaleh, G., Fanny, M., Gasse, P., Adam, S. M., Crestani, B., Sibilia, J., Schneider, P., Bahram, S., Quesniaux, V., Ryffel, B., Wachsmann, D., Gottenberg, J. E., & Couillin, I. (2015). B cell activating factor is central to bleomycin- and IL-17-mediated experimental pulmonary fibrosis. *J Autoimmun*, *56*, 1-11. https://doi.org/10.1016/j.jaut.2014.08.003
- Ginhoux, F., Greter, M., Leboeuf, M., Nandi, S., See, P., Gokhan, S., Mehler, M. F., Conway, S. J., Ng, L. G., Stanley, E. R., Samokhvalov, I. M., & Merad, M. (2010). Fate mapping analysis reveals that adult microglia derive from primitive macrophages. *Science*, 330(6005), 841-845. https://doi.org/10.1126/science.1194637
- Gomez Perdiguero, E., Klapproth, K., Schulz, C., Busch, K., Azzoni, E., Crozet, L., Garner, H., Trouillet, C., de Bruijn, M. F., Geissmann, F., & Rodewald, H. R. (2015). Tissue-resident macrophages originate from yolk-sac-derived erythro-myeloid progenitors. *nature*, 518(7540), 547-551. https://doi.org/10.1038/nature13989
- Gordon, S. (2003). Alternative activation of macrophages. *Nat Rev Immunol*, 3(1), 23-35. https://doi.org/10.1038/nri978
- Grindel, B. J., Martinez, J. R., Pennington, C. L., Muldoon, M., Stave, J., Chung, L. W., & Farach-Carson, M. C. (2014). Matrilysin/matrix metalloproteinase-7(MMP7) cleavage of perlecan/HSPG2 creates a molecular switch to alter prostate cancer cell behavior. *Matrix Biol*, 36, 64-76. https://doi.org/10.1016/j.matbio.2014.04.005
- Gubbiotti, M. A., Neill, T., & Iozzo, R. V. (2017). A current view of perlecan in physiology and pathology: A mosaic of functions. *Matrix Biol*, *57-58*, 285-298. https://doi.org/10.1016/j.matbio.2016.09.003
- Guha, M., & Mackman, N. (2001). LPS induction of gene expression in human monocytes. *Cell Signal*, *13*(2), 85-94. https://doi.org/10.1016/s0898-6568(00)00149-2

- Guilliams, M., De Kleer, I., Henri, S., Post, S., Vanhoutte, L., De Prijck, S., Deswarte, K., Malissen, B., Hammad, H., & Lambrecht, B. N. (2013). Alveolar macrophages develop from fetal monocytes that differentiate into long-lived cells in the first week of life via GM-CSF. *J Exp Med*, 210(10), 1977-1992. https://doi.org/10.1084/jem.20131199
- Hanson, R. R., & Kasik, J. E. (1977). The pneumoconioses. *Heart Lung*, *6*(4), 646-652. https://www.ncbi.nlm.nih.gov/pubmed/586217
- Hayes, A. J., Farrugia, B. L., Biose, I. J., Bix, G. J., & Melrose, J. (2022). Perlecan, A Multi-Functional, Cell-Instructive, Matrix-Stabilizing Proteoglycan With Roles in Tissue Development Has Relevance to Connective Tissue Repair and Regeneration. Front Cell Dev Biol, 10, 856261. https://doi.org/10.3389/fcell.2022.856261
- Henjakovic, M., Martin, C., Hoymann, H. G., Sewald, K., Ressmeyer, A. R., Dassow, C., Pohlmann, G., Krug, N., Uhlig, S., & Braun, A. (2008). Ex vivo lung function measurements in precision-cut lung slices (PCLS) from chemical allergen-sensitized mice represent a suitable alternative to in vivo studies. *Toxicol Sci*, 106(2), 444-453. https://doi.org/10.1093/toxsci/kfn178
- Hoeffel, G., Wang, Y., Greter, M., See, P., Teo, P., Malleret, B., Leboeuf, M., Low, D., Oller, G., Almeida, F., Choy, S. H., Grisotto, M., Renia, L., Conway, S. J., Stanley, E. R., Chan, J. K., Ng, L. G., Samokhvalov, I. M., Merad, M., & Ginhoux, F. (2012). Adult Langerhans cells derive predominantly from embryonic fetal liver monocytes with a minor contribution of yolk sac-derived macrophages. *J Exp Med*, 209(6), 1167-1181. https://doi.org/10.1084/jem.20120340
- Hong, J. Y., Chung, Y., Steenrod, J., Chen, Q., Lei, J., Comstock, A. T., Goldsmith, A. M., Bentley, J. K., Sajjan, U. S., & Hershenson, M. B. (2014). Macrophage activation state determines the response to rhinovirus infection in a mouse model of allergic asthma. *Respir Res*, 15(1), 63. https://doi.org/10.1186/1465-9921-15-63
- Hou, W., Hu, S., Li, C., Ma, H., Wang, Q., Meng, G., Guo, T., & Zhang, J. (2019). Cigarette Smoke Induced Lung Barrier Dysfunction, EMT, and Tissue Remodeling: A Possible Link between COPD and Lung Cancer. *Biomed Res Int*, 2019, 2025636. https://doi.org/10.1155/2019/2025636
- Initiative, C.-H. G. (2023). A second update on mapping the human genetic architecture of COVID-19. *nature*, 621(7977), E7-E26. https://doi.org/10.1038/s41586-023-06355-3
- Izbicki, G., Segel, M. J., Christensen, T. G., Conner, M. W., & Breuer, R. (2002). Time course of bleomycin-induced lung fibrosis. *Int J Exp Pathol*, 83(3), 111-119. https://doi.org/10.1046/j.1365-2613.2002.00220.x
- Jenkins, R. G., Moore, B. B., Chambers, R. C., Eickelberg, O., Konigshoff, M., Kolb, M., Laurent, G. J., Nanthakumar, C. B., Olman, M. A., Pardo, A., Selman, M., Sheppard, D., Sime, P. J., Tager, A. M., Tatler, A. L., Thannickal, V. J., White, E. S., Cell, A. T. S. A. o. R., & Molecular, B. (2017). An Official American Thoracic Society Workshop Report: Use of Animal Models for the Preclinical Assessment of Potential Therapies for Pulmonary Fibrosis. Am J Respir Cell Mol Biol, 56(5), 667-679. https://doi.org/10.1165/rcmb.2017-0096ST
- Jenkins, S. J., & Allen, J. E. (2021). The expanding world of tissue-resident macrophages. Eur J Immunol, 51(8), 1882-1896. https://doi.org/10.1002/eji.202048881
- Kalchiem-Dekel, O., Galvin, J. R., Burke, A. P., Atamas, S. P., & Todd, N. W. (2018). Interstitial Lung Disease and Pulmonary Fibrosis: A Practical Approach for General Medicine Physicians with Focus on the Medical History. *J Clin Med*, 7(12). https://doi.org/10.3390/jcm7120476
- Kim, W., Khan, S. K., Gvozdenovic-Jeremic, J., Kim, Y., Dahlman, J., Kim, H., Park, O., Ishitani, T., Jho, E. H., Gao, B., & Yang, Y. (2017). Hippo signaling interactions with Wnt/beta-catenin and Notch signaling repress liver tumorigenesis. *J Clin Invest*, *127*(1), 137-152. https://doi.org/10.1172/JCI88486
- King, T. E., Jr., Pardo, A., & Selman, M. (2011). Idiopathic pulmonary fibrosis. *Lancet*, 378(9807), 1949-1961. https://doi.org/10.1016/S0140-6736(11)60052-4

- Lahmar, Q., Keirsse, J., Laoui, D., Movahedi, K., Van Overmeire, E., & Van Ginderachter, J. A. (2016). Tissue-resident versus monocyte-derived macrophages in the tumor microenvironment. *Biochim Biophys Acta*, 1865(1), 23-34. https://doi.org/10.1016/j.bbcan.2015.06.009
- Lancaster, L. H., de Andrade, J. A., Zibrak, J. D., Padilla, M. L., Albera, C., Nathan, S. D., Wijsenbeek, M. S., Stauffer, J. L., Kirchgaessler, K. U., & Costabel, U. (2017). Pirfenidone safety and adverse event management in idiopathic pulmonary fibrosis. *Eur Respir Rev*, 26(146). https://doi.org/10.1183/16000617.0057-2017
- Lauenstein, L., Switalla, S., Prenzler, F., Seehase, S., Pfennig, O., Forster, C., Fieguth, H., Braun, A., & Sewald, K. (2014). Assessment of immunotoxicity induced by chemicals in human precision-cut lung slices (PCLS). *Toxicol In Vitro*, *28*(4), 588-599. https://doi.org/10.1016/j.tiv.2013.12.016
- Lehmann, M., Buhl, L., Alsafadi, H. N., Klee, S., Hermann, S., Mutze, K., Ota, C., Lindner, M., Behr, J., Hilgendorff, A., Wagner, D. E., & Konigshoff, M. (2018). Differential effects of Nintedanib and Pirfenidone on lung alveolar epithelial cell function in ex vivo murine and human lung tissue cultures of pulmonary fibrosis. *Respir Res*, 19(1), 175. https://doi.org/10.1186/s12931-018-0876-y
- Ley, B., Brown, K. K., & Collard, H. R. (2014). Molecular biomarkers in idiopathic pulmonary fibrosis. *Am J Physiol Lung Cell Mol Physiol*, 307(9), L681-691. https://doi.org/10.1152/ajplung.00014.2014
- Li, S., Shi, J., & Tang, H. (2022). Animal models of drug-induced pulmonary fibrosis: an overview of molecular mechanisms and characteristics. *Cell Biol Toxicol*, *38*(5), 699-723. https://doi.org/10.1007/s10565-021-09676-z
- Liu, M., Shan, M., Zhang, Y., & Guo, Z. (2021). Progranulin Protects Against Airway Remodeling Through the Modulation of Autophagy via HMGB1 Suppression in House Dust Mite-Induced Chronic Asthma. *J Inflamm Res*, 14, 3891-3904. https://doi.org/10.2147/JIR.S322724
- Liu, T., De Los Santos, F. G., & Phan, S. H. (2017). The Bleomycin Model of Pulmonary Fibrosis. *Methods Mol Biol*, *16*27, 27-42. https://doi.org/10.1007/978-1-4939-7113-8 2
- Liu, Z., Gu, Y., Chakarov, S., Bleriot, C., Kwok, I., Chen, X., Shin, A., Huang, W., Dress, R. J., Dutertre, C. A., Schlitzer, A., Chen, J., Ng, L. G., Wang, H., Liu, Z., Su, B., & Ginhoux, F. (2019). Fate Mapping via Ms4a3-Expression History Traces Monocyte-Derived Cells. *Cell*, 178(6), 1509-1525 e1519. https://doi.org/10.1016/j.cell.2019.08.009
- Lord, M. S., Tang, F., Rnjak-Kovacina, J., Smith, J. G. W., Melrose, J., & Whitelock, J. M. (2018). The multifaceted roles of perlecan in fibrosis. *Matrix Biol*, 68-69, 150-166. https://doi.org/10.1016/j.matbio.2018.02.013
- Lotfollahi, M., Naghipourfar, M., Luecken, M. D., Khajavi, M., Buttner, M., Wagenstetter, M., Avsec, Z., Gayoso, A., Yosef, N., Interlandi, M., Rybakov, S., Misharin, A. V., & Theis, F. J. (2022). Mapping single-cell data to reference atlases by transfer learning. *Nat Biotechnol*, *40*(1), 121-130. https://doi.org/10.1038/s41587-021-01001-7
- Lugg, S. T., Scott, A., Parekh, D., Naidu, B., & Thickett, D. R. (2022). Cigarette smoke exposure and alveolar macrophages: mechanisms for lung disease. *Thorax*, 77(1), 94-101. https://doi.org/10.1136/thoraxjnl-2020-216296
- Lynch, D. A., Sverzellati, N., Travis, W. D., Brown, K. K., Colby, T. V., Galvin, J. R., Goldin, J. G., Hansell, D. M., Inoue, Y., Johkoh, T., Nicholson, A. G., Knight, S. L., Raoof, S., Richeldi, L., Ryerson, C. J., Ryu, J. H., & Wells, A. U. (2018). Diagnostic criteria for idiopathic pulmonary fibrosis: a Fleischner Society White Paper. *Lancet Respir Med*, *6*(2), 138-153. https://doi.org/10.1016/S2213-2600(17)30433-2
- Malhotra, J., Malvezzi, M., Negri, E., La Vecchia, C., & Boffetta, P. (2016). Risk factors for lung cancer worldwide. *Eur Respir J*, *48*(3), 889-902. https://doi.org/10.1183/13993003.00359-2016
- Martinez, F. J., Collard, H. R., Pardo, A., Raghu, G., Richeldi, L., Selman, M., Swigris, J. J., Taniguchi, H., & Wells, A. U. (2017). Idiopathic pulmonary fibrosis. *Nat Rev Dis Primers*, 3, 17074. https://doi.org/10.1038/nrdp.2017.74

- Martinez, J. R., Grindel, B. J., Hubka, K. M., Dodge, G. R., & Farach-Carson, M. C. (2019). Perlecan/HSPG2: Signaling role of domain IV in chondrocyte clustering with implications for Schwartz-Jampel Syndrome. *J Cell Biochem*, 120(2), 2138-2150. https://doi.org/10.1002/jcb.27521
- Mass, E., Ballesteros, I., Farlik, M., Halbritter, F., Gunther, P., Crozet, L., Jacome-Galarza, C. E., Handler, K., Klughammer, J., Kobayashi, Y., Gomez-Perdiguero, E., Schultze, J. L., Beyer, M., Bock, C., & Geissmann, F. (2016). Specification of tissue-resident macrophages during organogenesis. *Science*, 353(6304). https://doi.org/10.1126/science.aaf4238
- Mass, E., Nimmerjahn, F., Kierdorf, K., & Schlitzer, A. (2023). Tissue-specific macrophages: how they develop and choreograph tissue biology. *Nat Rev Immunol*, 23(9), 563-579. https://doi.org/10.1038/s41577-023-00848-y
- Mei, Q., Liu, Z., Zuo, H., Yang, Z., & Qu, J. (2021). Idiopathic Pulmonary Fibrosis: An Update on Pathogenesis. Front Pharmacol, 12, 797292. https://doi.org/10.3389/fphar.2021.797292
- Melrose, J. (2020). Perlecan, a modular instructive proteoglycan with diverse functional properties. Int J Biochem Cell Biol, 128, 105849. https://doi.org/10.1016/j.biocel.2020.105849
- Molawi, K., Wolf, Y., Kandalla, P. K., Favret, J., Hagemeyer, N., Frenzel, K., Pinto, A. R., Klapproth, K., Henri, S., Malissen, B., Rodewald, H. R., Rosenthal, N. A., Bajenoff, M., Prinz, M., Jung, S., & Sieweke, M. H. (2014). Progressive replacement of embryo-derived cardiac macrophages with age. *J Exp Med*, 211(11), 2151-2158. https://doi.org/10.1084/jem.20140639
- Mongiat, M., Taylor, K., Otto, J., Aho, S., Uitto, J., Whitelock, J. M., & Iozzo, R. V. (2000). The protein core of the proteoglycan perlecan binds specifically to fibroblast growth factor-7. *J Biol Chem*, 275(10), 7095-7100. https://doi.org/10.1074/jbc.275.10.7095
- Mulugeta, S., Nureki, S., & Beers, M. F. (2015). Lost after translation: insights from pulmonary surfactant for understanding the role of alveolar epithelial dysfunction and cellular quality control in fibrotic lung disease. *Am J Physiol Lung Cell Mol Physiol*, 309(6), L507-525. https://doi.org/10.1152/ajplung.00139.2015
- Murray, J. F. (2010). The structure and function of the lung. *Int J Tuberc Lung Dis*, *14*(4), 391-396. https://www.ncbi.nlm.nih.gov/pubmed/20202294
- Murray, L. A., Chen, Q., Kramer, M. S., Hesson, D. P., Argentieri, R. L., Peng, X., Gulati, M., Homer, R. J., Russell, T., van Rooijen, N., Elias, J. A., Hogaboam, C. M., & Herzog, E. L. (2011). TGF-beta driven lung fibrosis is macrophage dependent and blocked by Serum amyloid P. *Int J Biochem Cell Biol*, 43(1), 154-162. https://doi.org/10.1016/j.biocel.2010.10.013
- Murray, P. J., Allen, J. E., Biswas, S. K., Fisher, E. A., Gilroy, D. W., Goerdt, S., Gordon, S., Hamilton, J. A., Ivashkiv, L. B., Lawrence, T., Locati, M., Mantovani, A., Martinez, F. O., Mege, J. L., Mosser, D. M., Natoli, G., Saeij, J. P., Schultze, J. L., Shirey, K. A., . . . Wynn, T. A. (2014). Macrophage activation and polarization: nomenclature and experimental guidelines. *Immunity*, *41*(1), 14-20. https://doi.org/10.1016/j.immuni.2014.06.008
- Nagao, S., Taguchi, K., Sakai, H., Tanaka, R., Horinouchi, H., Watanabe, H., Kobayashi, K., Otagiri, M., & Maruyama, T. (2014). Carbon monoxide-bound hemoglobin-vesicles for the treatment of bleomycin-induced pulmonary fibrosis. *Biomaterials*, *35*(24), 6553-6562. https://doi.org/10.1016/j.biomaterials.2014.04.049
- Natsuizaka, M., Chiba, H., Kuronuma, K., Otsuka, M., Kudo, K., Mori, M., Bando, M., Sugiyama, Y., & Takahashi, H. (2014). Epidemiologic survey of Japanese patients with idiopathic pulmonary fibrosis and investigation of ethnic differences. *Am J Respir Crit Care Med*, 190(7), 773-779. https://doi.org/10.1164/rccm.201403-0566OC
- O'Shea, J. J., & Paul, W. E. (2010). Mechanisms underlying lineage commitment and plasticity of helper CD4+ T cells. *Science*, 327(5969), 1098-1102. https://doi.org/10.1126/science.1178334
- Peng, R., Sridhar, S., Tyagi, G., Phillips, J. E., Garrido, R., Harris, P., Burns, L., Renteria, L., Woods, J., Chen, L., Allard, J., Ravindran, P., Bitter, H., Liang, Z., Hogaboam, C. M., Kitson, C., Budd, D. C., Fine, J. S., Bauer, C. M., & Stevenson, C. S. (2013). Bleomycin

- induces molecular changes directly relevant to idiopathic pulmonary fibrosis: a model for "active" disease. *PLoS One*, 8(4), e59348. https://doi.org/10.1371/journal.pone.0059348
- Perdiguero, E. G., & Geissmann, F. (2016). The development and maintenance of resident macrophages. *Nat Immunol*, 17(1), 2-8. https://doi.org/10.1038/ni.3341
- Qi, X. M., Luo, Y., Song, M. Y., Liu, Y., Shu, T., Liu, Y., Pang, J. L., Wang, J., & Wang, C. (2021). Pneumoconiosis: current status and future prospects. *Chin Med J (Engl)*, 134(8), 898-907. https://doi.org/10.1097/CM9.0000000000001461
- Raes, G., De Baetselier, P., Noel, W., Beschin, A., Brombacher, F., & Hassanzadeh Gh, G. (2002). Differential expression of FIZZ1 and Ym1 in alternatively versus classically activated macrophages. *J Leukoc Biol*, 71(4), 597-602. https://www.ncbi.nlm.nih.gov/pubmed/11927645
- Raghu, G., van den Blink, B., Hamblin, M. J., Brown, A. W., Golden, J. A., Ho, L. A., Wijsenbeek, M. S., Vasakova, M., Pesci, A., Antin-Ozerkis, D. E., Meyer, K. C., Kreuter, M., Santin-Janin, H., Mulder, G. J., Bartholmai, B., Gupta, R., & Richeldi, L. (2018). Effect of Recombinant Human Pentraxin 2 vs Placebo on Change in Forced Vital Capacity in Patients With Idiopathic Pulmonary Fibrosis: A Randomized Clinical Trial. *JAMA*, 319(22), 2299-2307. https://doi.org/10.1001/jama.2018.6129
- Richeldi, L., Collard, H. R., & Jones, M. G. (2017). Idiopathic pulmonary fibrosis. *Lancet*, 389(10082), 1941-1952. https://doi.org/10.1016/S0140-6736(17)30866-8
- Richeldi, L., Cottin, V., Flaherty, K. R., Kolb, M., Inoue, Y., Raghu, G., Taniguchi, H., Hansell, D. M., Nicholson, A. G., Le Maulf, F., Stowasser, S., & Collard, H. R. (2014). Design of the INPULSIS trials: two phase 3 trials of nintedanib in patients with idiopathic pulmonary fibrosis. *Respir Med*, 108(7), 1023-1030. https://doi.org/10.1016/j.rmed.2014.04.011
- Ruscitti, F., Ravanetti, F., Essers, J., Ridwan, Y., Belenkov, S., Vos, W., Ferreira, F., KleinJan, A., van Heijningen, P., Van Holsbeke, C., Cacchioli, A., Villetti, G., & Stellari, F. F. (2017). Longitudinal assessment of bleomycin-induced lung fibrosis by Micro-CT correlates with histological evaluation in mice. *Multidiscip Respir Med*, 12, 8. https://doi.org/10.1186/s40248-017-0089-0
- Saarialho-Kere, U., Kerkela, E., Jeskanen, L., Hasan, T., Pierce, R., Starcher, B., Raudasoja, R., Ranki, A., Oikarinen, A., & Vaalamo, M. (1999). Accumulation of matrilysin (MMP-7) and macrophage metalloelastase (MMP-12) in actinic damage. *J Invest Dermatol*, 113(4), 664-672. https://doi.org/10.1046/j.1523-1747.1999.00731.x
- Schiller, H. B., Fernandez, I. E., Burgstaller, G., Schaab, C., Scheltema, R. A., Schwarzmayr, T., Strom, T. M., Eickelberg, O., & Mann, M. (2015). Time- and compartment-resolved proteome profiling of the extracellular niche in lung injury and repair. *Mol Syst Biol*, *11*(7), 819. https://doi.org/10.15252/msb.20156123
- Schulz, C., Gomez Perdiguero, E., Chorro, L., Szabo-Rogers, H., Cagnard, N., Kierdorf, K., Prinz, M., Wu, B., Jacobsen, S. E., Pollard, J. W., Frampton, J., Liu, K. J., & Geissmann, F. (2012). A lineage of myeloid cells independent of Myb and hematopoietic stem cells. Science, 336(6077), 86-90. https://doi.org/10.1126/science.1219179
- Sefik, E., Qu, R., Junqueira, C., Kaffe, E., Mirza, H., Zhao, J., Brewer, J. R., Han, A., Steach, H. R., Israelow, B., Blackburn, H. N., Velazquez, S. E., Chen, Y. G., Halene, S., Iwasaki, A., Meffre, E., Nussenzweig, M., Lieberman, J., Wilen, C. B., . . . Flavell, R. A. (2022). Inflammasome activation in infected macrophages drives COVID-19 pathology. *nature*, 606(7914), 585-593. https://doi.org/10.1038/s41586-022-04802-1
- Senga, T., Iwamoto, T., Kitamura, T., Miyake, Y., & Hamaguchi, M. (2001). JAK/STAT3-dependent activation of the RalGDS/Ral pathway in M1 mouse myeloid leukemia cells. *J Biol Chem*, 276(35), 32678-32681. https://doi.org/10.1074/jbc.M105749200
- Senior, R. M., Bielefeld, D. R., & Abensohn, M. K. (1975). The effects of proteolytic enzymes on the tensile strength of human lung. *Am Rev Respir Dis*, 111(2), 184-188. https://doi.org/10.1164/arrd.1975.111.2.184
- Shifren, A., & Mecham, R. P. (2006). The stumbling block in lung repair of emphysema: elastic fiber assembly. *Proc Am Thorac Soc*, *3*(5), 428-433. https://doi.org/10.1513/pats.200601-009AW

- Smith, S. M., West, L. A., & Hassell, J. R. (2007). The core protein of growth plate perlecan binds FGF-18 and alters its mitogenic effect on chondrocytes. *Arch Biochem Biophys*, *468*(2), 244-251. https://doi.org/10.1016/j.abb.2007.10.006
- Solomon, J. J., Danoff, S. K., Woodhead, F. A., Hurwitz, S., Maurer, R., Glaspole, I., Dellaripa, P. F., Gooptu, B., Vassallo, R., Cox, P. G., Flaherty, K. R., Adamali, H. I., Gibbons, M. A., Troy, L., Forrest, I. A., Lasky, J. A., Spencer, L. G., Golden, J., Scholand, M. B., . . . Investigators, T. N. (2023). Safety, tolerability, and efficacy of pirfenidone in patients with rheumatoid arthritis-associated interstitial lung disease: a randomised, double-blind, placebo-controlled, phase 2 study. Lancet Respir Med, 11(1), 87-96. https://doi.org/10.1016/S2213-2600(22)00260-0
- Stout, R. D., & Suttles, J. (2005). Immunosenescence and macrophage functional plasticity: dysregulation of macrophage function by age-associated microenvironmental changes. *Immunol Rev*, 205, 60-71. https://doi.org/10.1111/j.0105-2896.2005.00260.x
- Tanaka, A., Tsukamoto, H., Mitoma, H., Kiyohara, C., Ueda, N., Ayano, M., Ohta, S., Kimoto, Y., Akahoshi, M., Arinobu, Y., Niiro, H., Tada, Y., Horiuchi, T., & Akashi, K. (2015). Serum progranulin levels are elevated in dermatomyositis patients with acute interstitial lung disease, predicting prognosis. *Arthritis Res Ther*, 17(1), 27. https://doi.org/10.1186/s13075-015-0547-z
- Tanimoto, R., Palladino, C., Xu, S. Q., Buraschi, S., Neill, T., Gomella, L. G., Peiper, S. C., Belfiore, A., Iozzo, R. V., & Morrione, A. (2017). The perlecan-interacting growth factor progranulin regulates ubiquitination, sorting, and lysosomal degradation of sortilin. *Matrix Biol*, *64*, 27-39. https://doi.org/10.1016/j.matbio.2017.04.001
- Tarique, A. A., Logan, J., Thomas, E., Holt, P. G., Sly, P. D., & Fantino, E. (2015). Phenotypic, functional, and plasticity features of classical and alternatively activated human macrophages. *Am J Respir Cell Mol Biol*, *53*(5), 676-688. https://doi.org/10.1165/rcmb.2015-0012OC
- Thiessen, R. D., Fenwick, J. L., & Lynch, D. A. (2019). Advances in CT Diagnosis of UIP and IPF. Semin Roentgenol, 54(1), 6-14. https://doi.org/10.1053/j.ro.2018.12.001
- Toth, N. M., Muller, V., Nagy, T., Polivka, L., Horvath, P., Bohacs, A., & Eszes, N. (2023). Serum Progranulin Level Might Differentiate Non-IPF ILD from IPF. *Int J Mol Sci*, 24(11). https://doi.org/10.3390/ijms24119178
- Tyanova, S., Temu, T., & Cox, J. (2016). The MaxQuant computational platform for mass spectrometry-based shotgun proteomics. *Nat Protoc*, 11(12), 2301-2319. https://doi.org/10.1038/nprot.2016.136
- Uhl, F. E., Vierkotten, S., Wagner, D. E., Burgstaller, G., Costa, R., Koch, I., Lindner, M., Meiners, S., Eickelberg, O., & Konigshoff, M. (2015). Preclinical validation and imaging of Wnt-induced repair in human 3D lung tissue cultures. *Eur Respir J*, 46(4), 1150-1166. https://doi.org/10.1183/09031936.00183214
- Upagupta, C., Shimbori, C., Alsilmi, R., & Kolb, M. (2018). Matrix abnormalities in pulmonary fibrosis. *Eur Respir Rev*, 27(148). https://doi.org/10.1183/16000617.0033-2018
- Ural, B. B., Yeung, S. T., Damani-Yokota, P., Devlin, J. C., de Vries, M., Vera-Licona, P., Samji, T., Sawai, C. M., Jang, G., Perez, O. A., Pham, Q., Maher, L., Loke, P., Dittmann, M., Reizis, B., & Khanna, K. M. (2020). Identification of a nerve-associated, lung-resident interstitial macrophage subset with distinct localization and immunoregulatory properties. *Sci Immunol*, *5*(45). https://doi.org/10.1126/sciimmunol.aax8756
- Vancheri, C., Kreuter, M., Richeldi, L., Ryerson, C. J., Valeyre, D., Grutters, J. C., Wiebe, S., Stansen, W., Quaresma, M., Stowasser, S., Wuyts, W. A., & Investigators, I. T. (2018). Nintedanib with Add-on Pirfenidone in Idiopathic Pulmonary Fibrosis. Results of the INJOURNEY Trial. *Am J Respir Crit Care Med*, 197(3), 356-363. https://doi.org/10.1164/rccm.201706-1301OC
- Vandenbroucke, R. E., Vanlaere, I., Van Hauwermeiren, F., Van Wonterghem, E., Wilson, C., & Libert, C. (2014). Pro-inflammatory effects of matrix metalloproteinase 7 in acute inflammation. *Mucosal Immunol*, 7(3), 579-588. https://doi.org/10.1038/mi.2013.76

- Varin, A., & Gordon, S. (2009). Alternative activation of macrophages: immune function and cellular biology. *Immunobiology*, 214(7), 630-641. https://doi.org/10.1016/j.imbio.2008.11.009
- Watson, C. K., Schloesser, D., Fundel-Clemens, K., Lerner, C., Gabler, S., Baskaran, P., Wohnhaas, C. T., Dichtl, S., Huber, H. J., Ask, K., Gantner, F., Viollet, C., Thomas, M. J., Ramirez, F., Murray, P. J., & El Kasmi, K. C. (2023). Antifibrotic Drug Nintedanib Inhibits CSF1R to Promote IL-4-associated Tissue Repair Macrophages. *Am J Respir Cell Mol Biol*, 68(4), 366-380. https://doi.org/10.1165/rcmb.2022-0021OC
- Weibel, E. R. (2009). What makes a good lung? *Swiss Med Wkly*, 139(27-28), 375-386. https://doi.org/10.4414/smw.2009.12270
- Weibel, E. R. (2017). Lung morphometry: the link between structure and function. *Cell Tissue Res*, 367(3), 413-426. https://doi.org/10.1007/s00441-016-2541-4
- White, E. S. (2015). Lung extracellular matrix and fibroblast function. *Ann Am Thorac Soc*, 12 Suppl 1(Suppl 1), S30-33. https://doi.org/10.1513/AnnalsATS.201406-240MG
- Whitelock, J. M., Melrose, J., & Iozzo, R. V. (2008). Diverse cell signaling events modulated by perlecan. *Biochemistry*, 47(43), 11174-11183. https://doi.org/10.1021/bi8013938
- Wilson, S. E. (2022). Defective perlecan-associated basement membrane regeneration and altered modulation of transforming growth factor beta in corneal fibrosis. *Cell Mol Life Sci*, 79(3), 144. https://doi.org/10.1007/s00018-022-04184-7
- Wolf, F. A., Angerer, P., & Theis, F. J. (2018). SCANPY: large-scale single-cell gene expression data analysis. *Genome Biol*, 19(1), 15. https://doi.org/10.1186/s13059-017-1382-0
- Wolf, F. A., Hamey, F. K., Plass, M., Solana, J., Dahlin, J. S., Göttgens, B., Rajewsky, N., Simon, L., & Theis, F. J. (2019). PAGA: graph abstraction reconciles clustering with trajectory inference through a topology preserving map of single cells. *Genome biology*, 20, 1-9.
- Wollin, L., Wex, E., Pautsch, A., Schnapp, G., Hostettler, K. E., Stowasser, S., & Kolb, M. (2015). Mode of action of nintedanib in the treatment of idiopathic pulmonary fibrosis. *Eur Respir J*, 45(5), 1434-1445. https://doi.org/10.1183/09031936.00174914
- Wu, X., van Dijk, E. M., Ng-Blichfeldt, J. P., Bos, I. S. T., Ciminieri, C., Konigshoff, M., Kistemaker, L. E. M., & Gosens, R. (2019). Mesenchymal WNT-5A/5B Signaling Represses Lung Alveolar Epithelial Progenitors. Cells, 8(10). https://doi.org/10.3390/cells8101147
- Xiao, Y., Lian, H., Zhong, X. S., Krishnachaitanya, S. S., Cong, Y., Dashwood, R. H., Savidge, T. C., Powell, D. W., Liu, X., & Li, Q. (2022). Matrix metalloproteinase 7 contributes to intestinal barrier dysfunction by degrading tight junction protein Claudin-7. *Front Immunol*, 13, 1020902. https://doi.org/10.3389/fimmu.2022.1020902
- Xie, T., Han, L., Chen, Y., & Wu, H. (2021). Progranulin and Activin A Concentrations are Elevated in Serum from Patients with Acute Exacerbations of Idiopathic Pulmonary Fibrosis. *Lung*, 199(5), 467-473. https://doi.org/10.1007/s00408-021-00470-6
- Yang, Y., Ma, L., Wang, C., Song, M., Li, C., Chen, M., Zhou, J., & Mei, C. (2020). Matrix metalloproteinase-7 in platelet-activated macrophages accounts for cardiac remodeling in uremic mice. *Basic Res Cardiol*, 115(3), 30. https://doi.org/10.1007/s00395-020-0789-2
- Ying, W., Cheruku, P. S., Bazer, F. W., Safe, S. H., & Zhou, B. (2013). Investigation of macrophage polarization using bone marrow derived macrophages. *J Vis Exp*(76). https://doi.org/10.3791/50323
- Yona, S., Kim, K. W., Wolf, Y., Mildner, A., Varol, D., Breker, M., Strauss-Ayali, D., Viukov, S., Guilliams, M., Misharin, A., Hume, D. A., Perlman, H., Malissen, B., Zelzer, E., & Jung, S. (2013). Fate mapping reveals origins and dynamics of monocytes and tissue macrophages under homeostasis. *Immunity*, 38(1), 79-91. https://doi.org/10.1016/j.immuni.2012.12.001
- Yu, W. H., & Woessner, J. F., Jr. (2000). Heparan sulfate proteoglycans as extracellular docking molecules for matrilysin (matrix metalloproteinase 7). *J Biol Chem*, 275(6), 4183-4191. https://doi.org/10.1074/jbc.275.6.4183

References

- Zhang, L., Wang, Y., Wu, G., Xiong, W., Gu, W., & Wang, C. Y. (2018). Macrophages: friend or foe in idiopathic pulmonary fibrosis? *Respir Res*, 19(1), 170. https://doi.org/10.1186/s12931-018-0864-2
- Zhao, M., Wang, M., Chen, X., Gao, Y., Chen, Q., Wang, L., Bao, Q., Sun, D., Du, W., Xu, Y., Xie, L., Jiang, X., Zhang, L., Peng, L., Zhang, B., & Yao, Y. (2024). Targeting progranulin alleviated silica particles-induced pulmonary inflammation and fibrosis via decreasing II-6 and Tgf-beta1/Smad. *J Hazard Mater*, 465, 133199. https://doi.org/10.1016/j.jhazmat.2023.133199
- Zhou, B., Shao, J., Schaefbauer, K. J., Egan, A. M., Carmona, E. M., Limper, A. H., & Zhang, X. (2021). Grading Bleomycin-Induced Pulmonary Fibrosis in ex vivo Mouse Lungs Using Ultrasound Image Analysis. *J Ultrasound Med*, 40(4), 763-770. https://doi.org/10.1002/jum.15448

Acknowledgements

Embarking on this journey has been both wonderful and fascinating. I have always held the belief that life's shortcomings are enriched through the passage of time, and this rings true in the culmination of our endeavors.

I am deeply appreciative of the encounter that transpired three years ago. It is remarkable to reflect on how a simple email forged a connection spanning approximately 12,458 kilometers, linking Munich, Germany, to Guangzhou, China. As the old Chinese proverb goes, "It is better to travel thousands of miles than to read thousands of books." This memorable experience serves as invaluable wealth in my life journey.

My profound gratitude extends to my mentor, Dr. Yuval Rinkevich, whose guidance and unwavering support have been instrumental throughout my three-year journey. Your generosity in providing me with invaluable opportunities and selfless assistance has profoundly impacted my academic and personal growth. Whenever uncertainties arose, your patient guidance and use of pen and paper to illuminate the path of correct thinking have been invaluable. Your dedication to scientific research and your unwavering spirit of exploration and inquiry serve as inspiring examples that I continually strive to emulate and uphold.

I would also like to express my heartfelt appreciation to Prof. Dr. Jürgen Behr and Prof. Dr. rer. nat. Markus Rehberg, both esteemed members of the Thesis Advisory Committee (TAC), for their invaluable advice and unwavering support. Your wisdom and guidance have been indispensable at every stage of my journey, and I am profoundly grateful for the privilege of learning from you.

I consider myself immensely fortunate to have crossed paths with each of you during my academic pursuits. Your contributions have been instrumental in shaping my research endeavors and personal development, and for that, I am deeply thankful.

I extend my heartfelt appreciation to Prof. Dongsheng Jiang, whose profound knowledge and unwavering support have been invaluable to my journey. Your patient guidance and willingness to share your expertise have enriched my understanding and shaped my growth as a scientist. I am also deeply grateful to Dr. Mahesh Gouda for his multifaceted

expertise and creative insights. Your selfless mentorship in experimental skills and lifework balance has been truly inspiring. Special thanks to Dr. Adrian Fischer for imparting invaluable animal experimentation skills and offering guidance on various subjects. Your mentorship has been instrumental in my development. I am immensely thankful to Dr. Safouane Kadri for your unwavering support and assistance in data analysis. Your willingness to help, regardless of the challenges, has been greatly appreciated. Gratitude also goes to Natalja Ring for her boundless positive energy and sense of responsibility in nurturing and caring for our team. I would like to express my appreciation to Dr. Martin Mück-Häusl for your constant support and cheerful demeanor. Lastly, I am indebted to Dr. Donovan Correa Gallegos for your outstanding example and role-modeling, which have been a source of inspiration for us all.

I would also like to thank my lovely colleagues, who have created a lot of happiness to my study and life. Thanks to Ruoxuan Dai, Ruiji Guo, Xiangyu Zhang, Meng Liu, Shaoping Hu, Wei Han, Jiakuan Zhao, Shaohua Zhu, Haifeng Ye, Jiazheng Lai, George Vogelaar, Christoph Deisenhofer, Fanzhu Zeng, Xu Jin, Aydan Sardogan, Bikram Dasgupta, Subhasree Dutta, Andy Qarri, Ravinder Kandi and Ryo Ichijo.

In addition to studying in the laboratory, I also learned a lot of knowledge at CPC lung research school, from basic introduction to follow-up abstracts, grant writing and reporting. This is an advanced learning class full of love and encouragement. Special thanks to Dr. Melanie Penning and PD Dr. Claudia Staab-Weijnitz. It is your precious efforts that has benefited us a lot.

Regarding microscope photography technology, I am very grateful to PD Dr. Steffen Dietzel and Mariano Gonzalez Pisfil from the Core Facility Bioimaging at the Biomedical Center of LMU. You not only provided me with a two-week course of study, but also patiently guided me in using multiple microscopes. Regarding flow cytometry, I would like to thank Dr. Theodoros Kapellos and Jiakuan, I really appreciate your help. Regarding the analysis of proteomics, I would like to thank Christoph Deisenhofer, the master of proteomics. You are a partner who is always trustworthy.

I extend my heartfelt gratitude to Dr. Ruoxuan Dai and Ruiji Guo for their unwavering encouragement and steadfast support, both in action and spirit. Your companionship during numerous rainy and snowy days on the way to the animal house has been a

source of immense comfort and camaraderie. Moreover, I deeply appreciate your invaluable assistance amidst the hustle and bustle of laboratory work. It is my profound fortune to have crossed paths with both of you in this shared pursuit.

Finally, I would like to thank my husband, Xiaoqi Ji, for always encouraging and loving me during my most difficult times. You are the best life partner worthy of praise. Thanks to my parents and family for eternal spiritual and material support. Thanks to my puppy Lucky, I hope you haven't forgotten me after not seeing me for so many years.

Thank you for the time, thank you for the fate.

Affidavit



place, date

LUDWIG-MAXIMILIANS-UNIVERSITÄT MÜNCHEN





Signature doctoral candidate

Affidavit				
Lin Yue				
Surname, first name				
Max-Lebsche-Platz 31				
Street	-			
81377, Munich, Germany				
Zip code, town, country	-			
I hereby declare, that the submitted thesis entitled:				
Mechanisms of macrophage-driven fibrosis and its resolution				
is my own work. I have only used the sources indicated and have services of a third party. Where the work of others has been quo always given.				
I further declare that the dissertation presented here has not been form to any other institution for the purpose of obtaining an acade				
02.02.2024	Yue Lin			

Confirmation of congruency



LUDWIG-MAXIMILIANS-UNIVERSITÄT MÜNCHEN

Promotionsbüro Medizinische Fakultät





Confirmation of congruency between printed and electronic version of the doctoral thesis

Lin Yue	
Surname, first name	
Max-Lebsche-Platz 31	
Street	-
81377, Munich, Germany	
Zip code, town, country	-
I hereby declare, that the submitted thesis entitled:	
Mechanisms of macrophage-driven fibrosis and its resolution	
is congruent with the printed version both in content and format.	
02.02.2024	Yue Lin
place, date	Signature doctoral candidate

List of publications

Phagocyte Transcriptomic Analysis Reveals Focal Adhesion Kinase (FAK) and Heparan Sulfate Proteoglycans (HSPGs) as Major Regulators in Anti-bacterial Defense of Crassostrea hongkongensis

Yue Lin, Fan Mao, Yang Zhang, Ziniu Yu, et al

Frontiers in immunology (2020) DOI:10.3389/fimmu.2020.00416

TRAF suppresses the apoptosis of hemocytes by activating Pellino in Crassostrea hongkongensis.

Yue Lin, Fan Mao, Yang Zhang, Ziniu Yu, et al.

Dev. Comp.Immunol (2019) DOI:10.1016/j.dci.2019.103501

Wound infiltrating adipocytes are not myofibroblasts.

Kalgudde Gopal, S., Dai, R., Stefanska, A. M., Ansari, M., Zhao, J., Ramesh, P., Lin Y.,

... & Rinkevich, Y. (2023). Nature Communications.

Spatiotemporal differentiation of CD201-expressing fascia progenitors choreographs injury repair

Correa-Gallegos, D., Ye, H., Dasgupta, B., Sardogan, A., Ichijo, R., Dai, R., Lin, Y.,...

Machens, H. G& Rinkevich, Y. Nature (2023).

Organ dependency on fascia connective tissue.

Lin Y, Dai R, Vogelaar G, Rinkevich Y. (2024) Am J Physiol Cell Physiol.